https://ntrs.nasa.gov/search.jsp?R=19700011455 2020-03-12T01:17:39+00:00Z

General Disclaimer

One or more of the Following Statements may affect this Document

- This document has been reproduced from the best copy furnished by the organizational source. It is being released in the interest of making available as much information as possible.
- This document may contain data, which exceeds the sheet parameters. It was furnished in this condition by the organizational source and is the best copy available.
- This document may contain tone-on-tone or color graphs, charts and/or pictures, which have been reproduced in black and white.
- This document is paginated as submitted by the original source.
- Portions of this document are not fully legible due to the historical nature of some of the material. However, it is the best reproduction available from the original submission.

Produced by the NASA Center for Aerospace Information (CASI)

CR-102504

A THEORETICAL AND EXPERIMENTAL INVESTIGATION OF ACOUSTIC POINT SOURCE RADIATION IN THE PRESENCE OF A REFLECTING AND REFRACTING PLANE

By

John C. Corbin

Final Technical Report
Contract NAS8-21414

August 1969

Prepared for
George C. Marshall Space Flight Center
Marshall Space Flight Center, Alabama 35812

Prepared by
National Scientific Laboratories, Inc.
Westgate Research Park
McLean, Virginia 22101

FACILITY FORM 602
N70-20760
(ACCESSION NUMBER)
179
(PAGES)
NASA-CR-102504
(NASA CR OR TMX OR AD NUMBER)
1
(THRU)
(CODE)
23
(CATEGORY)

A THEORETICAL AND EXPERIMENTAL INVESTIGATION OF ACOUSTIC POINT SOURCE RADIATION IN THE PRESENCE OF A REFLECTING AND REFRACTING PLANE

By

John C. Corbin

Final Technical Report
Contract NAS8-21414

August 1969

Prepared for
George C. Marshall Space Flight Center
Marshall Space Flight Center, Alabama 35812

Prepared by
National Scientific Laboratories, Inc.
Westgate Research Park
McLean, Virginia 22101

CR - 102504
8/68 - 7/69

PRECEDING PAGE BLANK NOT FILMED.

ABSTRACT

This Final Technical Report by National Scientific Laboratories, Inc., was prepared for the National Aeronautics and Space Administration, George C. Marshall Space Flight Center, Marshall Space Flight Center, Alabama under Contract No. NAS8-21414. This document delineates the theoretical and experimental techniques applied to the problem of acoustic point source radiation in the presence of a reflecting and refracting half-space.

The study is concerned with the ultimate application of far-field data to the study of the dynamic environment of rocket engines, in particular, those of the Saturn V launch vehicle.

The work reported herein was performed at the laboratory facilities of National Scientific Laboratories, Inc., in the Westgate Research Park, McLean, Virginia during the period of August 1968 through July 1969.

PRECEDING PAGE BLANK NOT FILMED.

TABLE OF CONTENTS

TABLE OF CONTENTS (Cont'd)

LIST OF ILLUSTRATIONS

LIST OF ILLUSTRATIONS (Cont'd)

LIST OF TABLES

1. Introduction

This report, representing the end-item of Contract NAS8-21414, delineates the theoretical and experimental techniques applied to the problem of acoustic point source radiation in the presence of a reflecting and refracting half-space.

The primary reason for this study is concerned with the ultimate application of far-field data to the study of the dynamic environment of rocket engines, in particular, those of the Saturn V launch vehicle.*

A considerable acoustic output is associated with this environment to the extent that it dictates structural and electronic design considerations. In addition, the acoustic field dictates the minimum safe distance between unprotected personnel and the Saturn V under launch conditions.

This suggests a further application of the results of this study. Namely, the selection of ground covers to optimize noise abatement to reduce the required perimeter for rocket launch areas and for airports.

In view of the similarity between rocket and jet engines, application of the acoustic analysis can be extended to studies in the latter area.

This report is grouped into three basic areas, namely, theoretical, experimental, and conclusions.

---

*Reference 27 and 33. (All references given in Bibliography)

The theoretical investigation describes the derivation of a three-term asymptotic series to describe the velocity potential field in the neighborhood of the interface. A simpler expression, based on ray theory, is introduced to account for the remaining upper half-space.

Unfortunately, all data was derived on the basis of the latter formula since funds were not available to write a complete computer program for the interface formulation. Some intuitive arguments concerning the terms of the series indicate a basis for agreement between experiment and theory.

The experimental program served to confirm the existence of attenuation rates in excess of 6 dB per doubling of distance. Operation at inadequate power levels prevented accurate measurements at 1000 feet. It was determined that, of the three materials investigated, concrete, asphalt, and grass, that grass exhibited the most pronounced attenuation rates.

It was also determined that present methods of _in situ_ impedance measurements were wholly inadequate. Further, methods of determining the propagation constant on an _in situ_ basis are only sparsely documented.

Finally, conclusions are drawn relevant to the experimental and theoretical data, and recommended corrections to the deficiencies of this program are described.

2. Theoretical Analysis

The theoretical analysis that follows uses the Green's function technique where advantage is taken of obvious cylindrical symmetry peculiar to this problem.

Specifically, the radiated or incident spherical wave is represented as an integral superposition of infinitely many cylindrical waves each of which interacts with the plane surface through a factor that is identical to that encountered in plane waves.*

Thus, there are ostensibly two waves scattered from the surfaces: a reflected wave returning to the source or first medium, and a transmitted wave penetrating into the second medium. We will later see that the former wave is further analyzed into a reflected ray, and refracted ray(s), and that the latter are considerably affected by the location of (a) first order pole(s) in the complex plane of integration.

2.1 Table of Symbols

$A(\kappa^2)$	=	coefficient of γ_1 dependent part of M_{11}.
$Am(z)$	$\rightarrow$	Amplitude of $z = \lvert z \rvert$ is understood.
$Arg(z)$	$\rightarrow$	angular argument of z is understood.
$B(\kappa^2)$	=	γ_1 independent part of M_{11}.
$c_i=(ik_i r)^{-\frac{1}{2}}$	=	distance factor. Subscript is sometimes dropped.

---
*References 1,7,8,15,23,28,29.

$D(\kappa^2)$ = characteristic denominator in raw form.

$D_r(\kappa^2)$ = characteristic denominator in rationalized form.

$D_r^o(\kappa^2)$ = rationalized denominator with zero, κ_o, removed.

d_k = $ik_k g_k$

$F^{(2)}(g_1;r)$, $F_0^{(2)}(g_2)$, $F_k^{(2)}(g_1, g_2)$ = expansion coefficients for $V^{(2)}$ in two fluids model.

f = frequency, in Hertz.

$G^{(1)}(g_1, g_2; r)$, $G_k^{(1)}(g_1, g_2)$ = expansion coefficients for $V^{(1)}$ with first order pole subtracted.

g_k = vertical height argument for k^{th}- mode wave.

$H_0^1(z)$ = Hankel function of first kind, order 0, and argument, z.

h = vertical (z direction) height of generator.

$I = I(r,z;0,h) = I(g,k;r)$ velocity potential kernel due to interaction with surface.

$Im(z)$ $\rightarrow$ Imaginary part of the complex variable, z, is understood.

i = $\sqrt{-1}$

i = integer subscript corresponding to branch cut and conformal transformation under investigation.

$J_0(z)$ = Bessel function of order 0 and argument, z.

$J_1(z)$ = Bessel function of order 1 and argument, z.

j = integer subscript, $j \neq i$.

K = $K(g_1, ----, g_n; r) = K(g_k; r)$ = fundamental integral.

$K,_k$ = $\dfrac{\partial}{\partial g_k} K$

$K,_o$ = $\dfrac{1}{r}\dfrac{\partial}{\partial r}\left(r \dfrac{\partial}{\partial r} K\right)$

$K^{(i)}$ = fundamental integral conformally transformed to i^{th} branch point.

K_p = contribution from one first order pole to the fundamental integral.

$K_r = K_r(g_1, ----, g_N; r) = K_r(g_k; r)$ = pole residue.

$K_r^{(k)}$ = pole residue of k^{th} 1^{st}-order pole.

K_s = fundamental integral with 1^{st}-order pole subtracted.

k, l, m, n = integer subscripts.

k = propagation constant, general case.

k_k = propagation constant, k^{th} mode.

M = number of first order poles.

$\mathbf{M}$ = scattering matrix.

M_{ij} = scalar matrix element of $\mathbf{M}$ corresponding to conversion from the j^{th} incident to the i^{th} transmitted wave mode.

m = $(1 - n^2)^{\frac{1}{2}}$

N = number of wave propagation modes.

n = n_{12}

$N(\kappa^2)$ = numerator of M_{11}

$n_{k\ell} = \frac{k_\ell}{k_k}$ = complex index of refraction.

Q = simple source magnitude for velocity potential.

R = $\left[r^2 + (z - h)^2\right]^{\frac{1}{2}}$

R' = $\left[r^2 + (z + h)^2\right]^{\frac{1}{2}}$

$Re(z)$ $\longrightarrow$ Real part of the complex variable, z, is understood.

r = radial separation cylindrical coordinate.

$V = V(g_1, ----, g_N; r) = V(g_i; r)$ = general plane interaction kernel

$V^{(i)}$ = kernel evaluated around the i^{th} branch cut.

V_p = contribution from one first order pole to the two fluids kernel.

V_s = two fluids kernel with first order pole subtracted.

X = conformal transformation variable.

X_o = transform variable with κ evaluated at κ_o.

Y = transformation variable for integral representation of Hankel function.

z = vertical cylindrical coordinate.

γ = z-component of propagation constant, general case.

γ_k = z-component of propagation constant, k^{th} mode.

ζ = complex specific acoustic impedance ratio, referred to air

ζ_k = ζ of k^{th} medium or wave mode.

η = $\mathrm{Im}(\kappa)$

θ_c = critical angle

θ_k = angle of incidence, k^{th} wave mode.

θ = angle of incidence, general case.

κ = tangential propagation component.

κ_o = κ evaluated at pole to be subtracted or evaluated for residue.

κ_i = zeros of polynomial $D_r(\kappa^2)$

λ = wavelength

$\nu = \dfrac{\rho_1}{\rho_2}$ = complex density ratio.

ξ = $\mathrm{Re}(\kappa)$

ρ_k = mass density of k^{th} medium, $k = 1, 2$.

$\Phi(X, Y)$ = integrand obtained in transformation to X-Y variables and having a double saddle point at X & Y = 0.

$\psi(r,z;0,h)$ = velocity potential observed at r, z, due to a point source at 0, h.

$\omega = 2\pi f$ = frequency, radians per second.

2.2 Fundamental Integral Forms

Based on the qualitative description of the previous paragraph and the geometry of Figure 2.1, the pressure field in

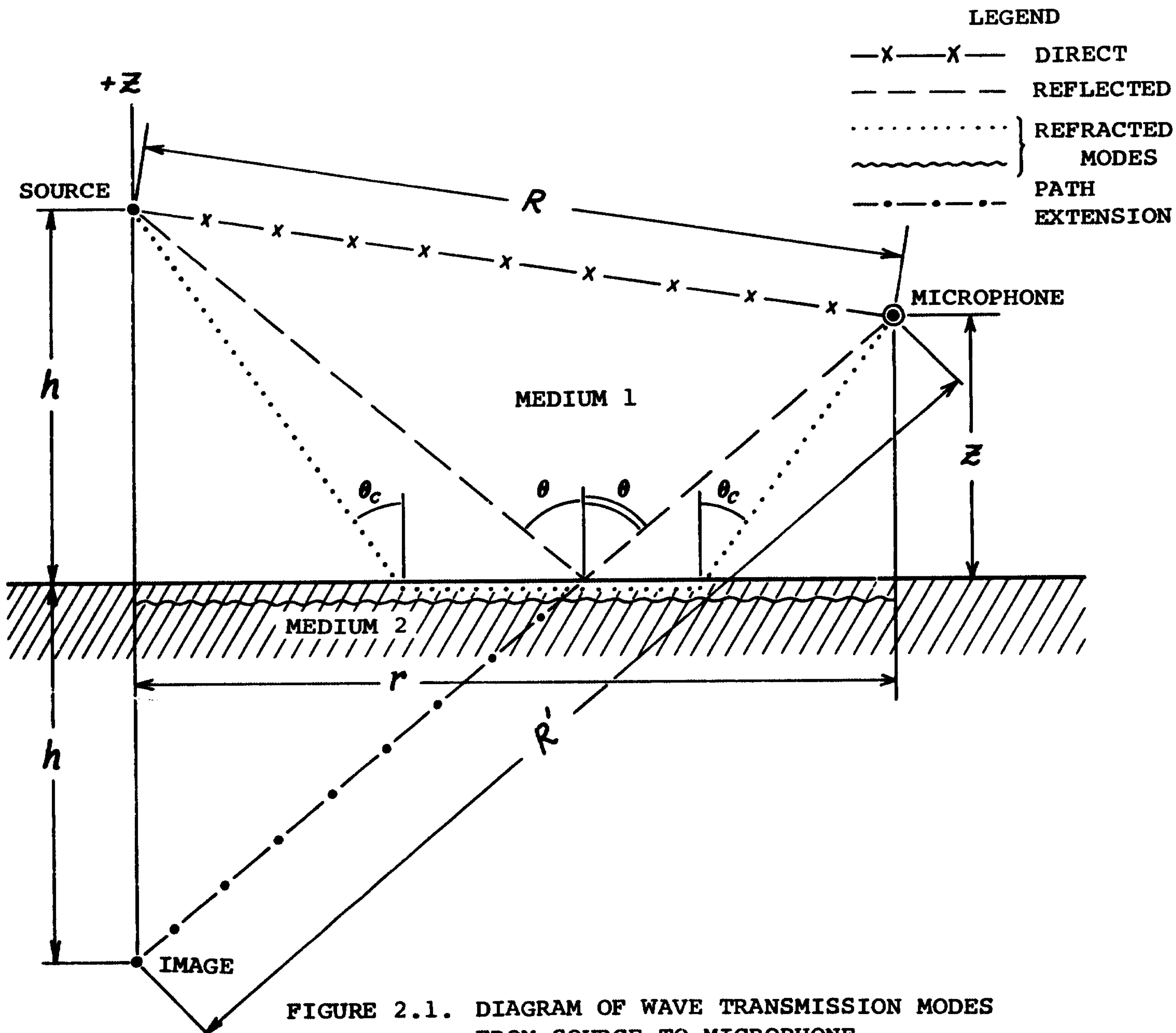

FIGURE 2.1. DIAGRAM OF WAVE TRANSMISSION MODES FROM SOURCE TO MICROPHONE.

medium 1, the region of greatest interest, is given by

$$\psi(r,z;0,h) = \frac{Q}{4\pi}\left[\frac{e^{ik_1R}}{R} + I(r,z;0,h)\right] \tag{2.1}$$

Evaluation of I is accomplished by noting that

$$\frac{e^{ik_1R}}{R} = \int_0^\infty \frac{1}{\gamma_1} \, e^{-\gamma_1|z-h|} \, J_0(\kappa r)\,\kappa d\kappa \tag{2.2}$$

If M_{11} is the scattering coefficient for the interaction of a type 1 radiation to a type 1 radiation in the same medium, then

$$I = \int_0^\infty \frac{1}{\gamma_1} \, M_{11} \, e^{-\gamma_1(z+h)} \, J_0(\kappa r)\,\kappa d\kappa \tag{2.3}$$

It further happens in the acoustic case that

$$\left.\begin{aligned} M_{11} &= \frac{N(\kappa^2)}{D(\kappa^2)} = -\frac{\gamma_1 A(\kappa^2) - B(\kappa^2)}{\gamma_1 A(\kappa^2) + B(\kappa^2)} \\ &= -1 + 2\,\gamma_1 \frac{A(\kappa^2)}{D(\kappa^2)} \end{aligned}\right\} \tag{2.4}$$

Hence, it is possible to obtain the following form for I,

$$I = -\frac{e^{ik_1R'}}{R'} + V(z+h,\,0,---,0;\,r) \tag{2.5}$$

where the generalized form

$$V(g_i;\,r) = V(g_1,\,g_2,---,g_N;\,r)$$

$$
\left.\begin{aligned}
&= 2\int_0^{\infty} \frac{A(\kappa^2) \prod_{k=1}^{N} e^{-\gamma_k g_k} J_0(\kappa r)}{D(\kappa^2)} \kappa\, d\kappa \\
&= \int_{-\infty}^{\infty} \frac{A(\kappa^2) \prod_{k=1}^{N} e^{-\gamma_k g_k} H_0^1(\kappa r)}{D(\kappa^2)} \kappa\, d\kappa
\end{aligned}\right\} \qquad (2.6)
$$

Further reduction of the integral is expedited if we consider the following form:

$$
K(g_i;\, r) = \int_{-\infty}^{\infty} \frac{\prod_{k=1}^{N} e^{-\gamma_k g_k} H_0^1(\kappa r)}{\prod_{k=1}^{M} \left[\kappa^2 - \kappa_k{}^2\right]} \kappa\, d\kappa \qquad (2.7)
$$

which serves as a generating function for all fields associated with the two propagating media. The quantities, κ_k, are the zeros of the characteristic denominator after rationalization.

Note that the numerator of $V(g_k;r)$, is obtained by performing appropriate partial differential operations of the generating functions. For this, the following shorthand notation is adopted:

$$
\left.\begin{aligned}
K_{,k} &= \frac{\partial}{\partial g_k} K(g_\ell;\, r) \\
&= -\int_{-\infty}^{\infty} \gamma_i \frac{\prod_{k=1}^{N} e^{-\gamma_k g_k} H_0^1(\kappa r)}{\prod_{k=1}^{M} \left[\kappa^2 - \kappa_k{}^2\right]} \kappa\, d\kappa
\end{aligned}\right\} \qquad (2.8)
$$

$$K_{,o} = \frac{1}{r} \frac{\partial}{\partial r}\left[r \frac{\partial}{\partial r} K\,(g_i;\, r)\right]$$

$$\left.= - \int_{-\infty}^{\infty} \kappa^2 \frac{\prod_{k=1}^{N} e^{-\gamma_k g_k} H_0^1\,(\kappa\, r)}{\prod_{k=1}^{M} \left[\kappa^2 - \kappa_k{}^2\right]} \kappa\, d\kappa \right\} \quad (2.9)$$

2.2.1 Additional Symbols

A_k = expansion coefficient for h(X).

A_k^ℓ = expansion coefficient for Φ (X, Y)

a_k = expansion coefficient for $D_r(\kappa^2)$

B_k^ℓ = expansion coefficient for g(X, Y)

C_k = expansion coefficient for $\frac{1}{2}\left[G(\xi) - G(-\xi)\right]$

D_k = expansion coefficient for f(X)

D_r = $D_r(\kappa^2)$ evaluated for $\kappa = k_i$

D_r', D_r'' = derivatives of $D_r(\kappa^2)$ evaluated for $\kappa = k_i$.

$E(g_k;\, r)$, $E_\ell\,(g_k)$ = expansion coefficients in asymptotic series for $K(g_k;\, r)$

$F(\kappa^2)$ = purely algebraic function of κ^2 appearing in I, e.g.

$$\frac{1}{\gamma_1} \frac{N(\kappa^2)}{D(\kappa^2)}$$

$f(X) \;\; = c^{-1} f(\xi)$

$f(\xi) \;\; = c\left[G(\xi) - G(-\xi)\right](1-\tfrac{1}{2}\xi^2)\,\xi$

$G(\xi) \;\; = \exp\left[\sum_{k=1}^{4} \gamma_k g_k\right]$

$g(X, Y)$ = part of $\Phi(X, Y)$ obtained from integral representation of Hankel function.

$h(X)$ = X-dependent part of $\Phi(X, Y)$ obtained from transformation of exponential function and rationalized denominator.

h^o = expansion factor

$m_{k\ell} = (1 - n_{k\ell}{}^2)^{\frac{1}{2}}$

N' = upper counting limit for terms of asymptotic series.

P_k = expansion coefficients for sinh $(-d_i p_i)$

$p_i(\xi) = p_i = \xi$ -representation of γ_i

Q_k = expansion coefficients for the product of exponential functions, Exp$(-d_j q_j)$

$Q_k^{(j)}$ = expansion coefficients for exp $(-d_j p_j)$

$q_j(\xi) = q_j = \xi$ -representation of γ_j

R_k = series coefficients in expansion of rationalized denominator, $D_r^{-1}(\kappa^2)$

$R_{N'}$ = remainder after N' terms of asymptotic series have been taken.

Ξ → original path of integration.

Ξ_i → branch cut indentations for completed contour.

ξ = conformal transformation variable, $c\xi = X$ except when specific reference is made to κ-plane and $Re(\kappa)$.

$\Phi^{(n)}$ = grouping of terms for asymptotic expansion.

2.2.2 Analysis of the Integrand

A cursory examination of the integral expressions of equation (2.6) or (2.7) is sufficient to verify that the existance of a closed form evaluation solution does not exist. In fact, the oscillatory behavior of the integrand precludes accurate evaluation using direct application of series or numerical techniques, especially when the g_i are small compared to r.*

One solution to this problem consists of extending the path of integration so that a closed loop obtains in the upper half κ-plane and the method of residues can be used. Application of this technique requires the introduction of the Hankel function as was done in equation (2.6).

Before proceeding further, it is necessary to investigate some of the topological features of the integrand components consisting of:

---

* It will be seen that this condition corresponds to examination of wave phenomena in the neighborhood of the interface, the region of greatest interest.

a) $e^{i\gamma_k g_k}$ products. γ_k is a double-valued function given by

$$\gamma_k = \pm \left[\kappa^2 - k_k^2\right]^{\frac{1}{2}} \tag{2.10}$$

with branch points at $\pm k_k$. Two (2) Riemann surfaces are required for a complete mapping of γ_k. Further, each pair of branch points must be joined by a branch cut.*

b) A purely algebraic expression involving powers of κ^2 and possibly γ_k. In addition to the γ_k branch cuts, this component may exhibit zeros and poles on various surfaces of the κ-plane. These are all of finite order, and may exist at infinity.

c) $H_0^1(\kappa r)$ introduced to extend the range of integration of $J_0(\kappa r)$ along the entire real axis. It possesses a logarithmic branch point at the origin and at infinity. This is not problematic since we are free to choose this along the $-\eta$ - axis. Aside from this, $H_0^1(\kappa r)$ should introduce no difficulties since it replaces the otherwise well behaved $J_0(\kappa r)$.

Taking these observations into account, it is expected that the desired closed path becomesthat shown in Figure 2.2 when two γ_k are assumed, i.e., $N = 2$. Note that the γ_k branch cuts pass through the point at infinity since analyticity must be preserved along the original path of integration. This requires that the integrals along the paths Ξ_i be evaluated.

*Reference 18, pp. 398-404.

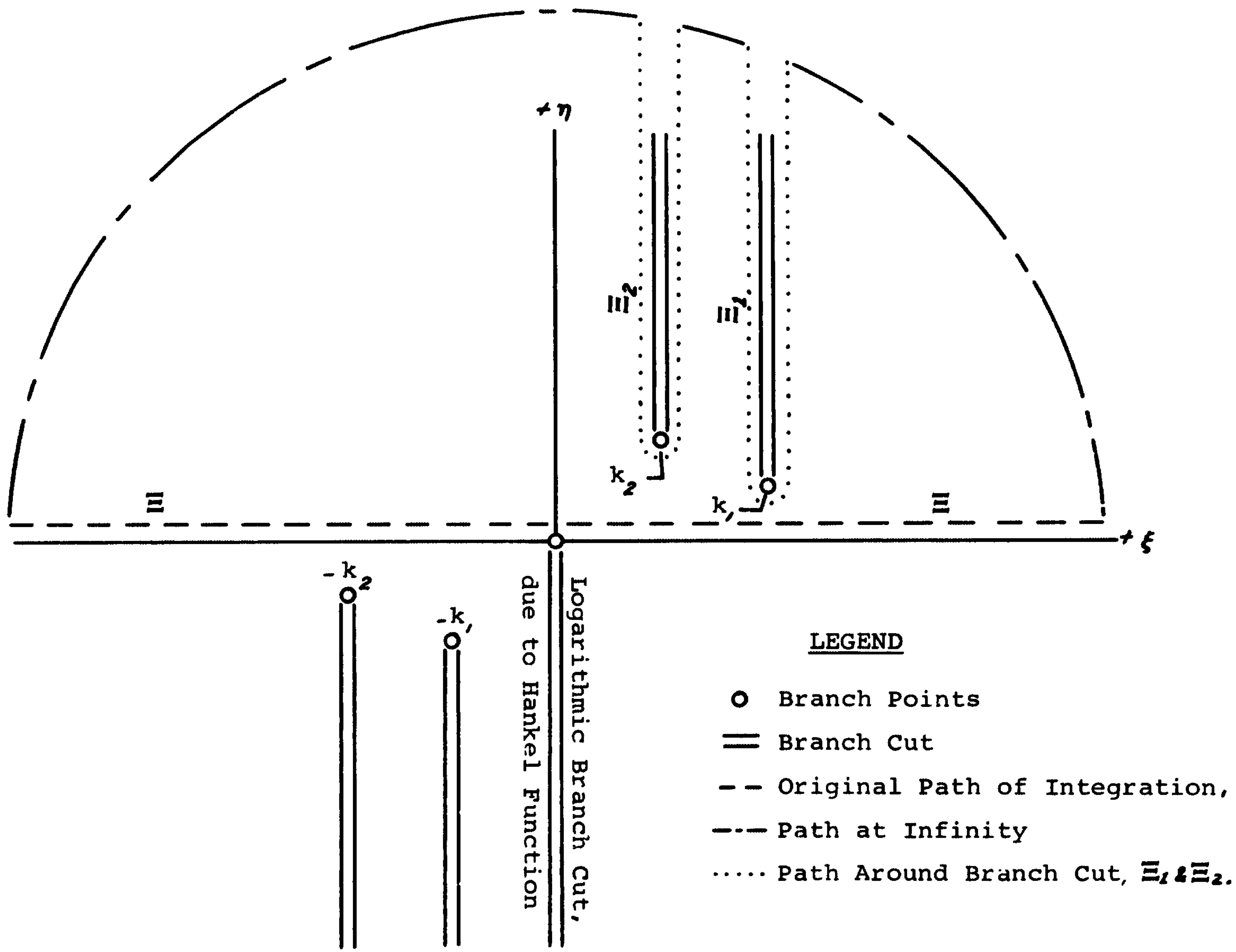

FIGURE 2.2. MAP OF κ PLANE BRANCH CUTS ASSOCIATED WITH $\pm\kappa_2$ AND $H_0^1(\kappa r)$ AND THE PATHS OF INTEGRATION.

Hence schematically

$$\int_{\Xi} = \int_{\Xi_1} + \int_{\Xi_2} + \frac{1}{2\pi i} \sum \begin{array}{l}\text{Applicable}\\ \text{Residues}\end{array} \tag{2.11}$$

Note that the arc at infinity does not contribute. In order to avoid difficulties with the essential singularity at infinity associated with the exponential functions it is necessary to choose that Riemann surface which satisfies

$$\mathrm{Re}(\gamma_k) > 0 \; ; \quad k = 1,\ 2,\ \text{---}\ N. \tag{2.12a}$$

Since the g_k are rigorously real and

$$g_k \geq 0 \tag{2.12b}$$

the exponential functions are well-behaved everywhere in the upper half κ-plane.

The Riemann surface for which these conditions are satisfied for all γ_k is defined as the first. The numbering scheme for other Riemann surfaces, in terms of the branch cut transitions, is shown in Figure 2.3 for N up to 4. It is evident that N functions of the form, γ_k, must require 2^N surfaces for a complete mapping.

Finally, it is not difficult to see that the essential singularity associated with the functions $e^{i\gamma_k g_k}$ will cancel any finite order pole arising from the purely algebraic part of

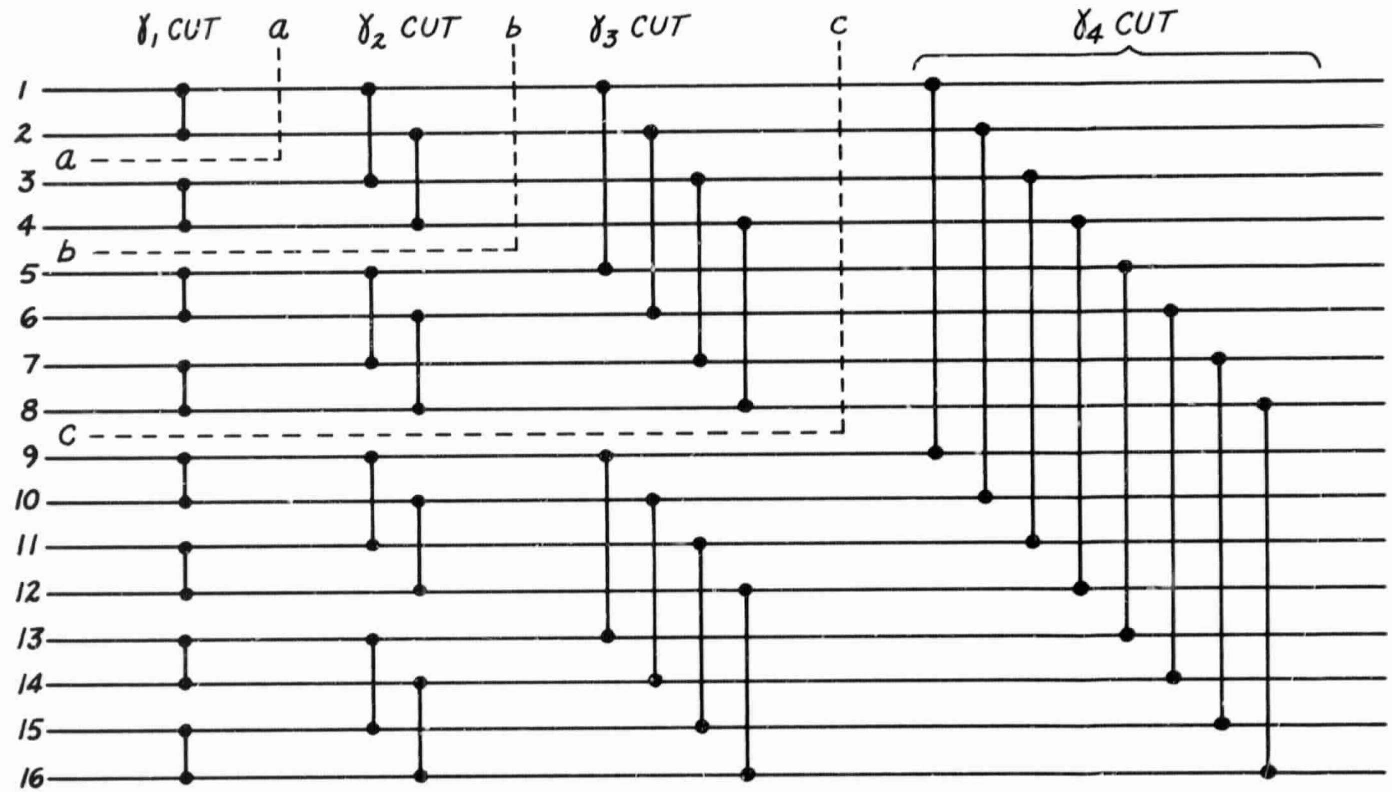

a-a - SINGLE BRANCH CUT (ONE DOUBLE-VALUED FUNCTION)

b-b - TWO BRANCH CUTS (TWO DOUBLE-VALUED FUNCTIONS)

c-c - THREE BRANCH CUTS (THREE DOUBLE-VALUED FUNCTIONS)

FIGURE 2.3 BRANCH CUT AND RIEMANN SURFACE DIAGRAM FOR UP TO FOUR DOUBLE VALUED FUNCTIONS, γ_k.

the integrand. Further, the Hankel function behaves like

$$\lim_{\kappa \to \infty} H_0^1(\kappa r) \sim \frac{1}{\kappa} e^{-\eta r} \tag{2.13}$$

so that equation (2.9) represents a valid alternate method of evaluating $\kappa(g_k ; r)$ without introducing convergence problems.

2.2.3 The Saddle Point Method of Integration

In analogy with equation (2.11) it is possible to write

$$K(g_k; r) = \sum_{\ell=1}^{N} K^{(\ell)}(g_k ; r) + \sum_{\ell=1}^{M}{}' K_r^{(\ell)}(g_k ; r) \tag{2.14}$$

where $\sum'$ indicates that a residue is to be included only if it is an actual pole on the first Riemann surface.

In evaluating the integral

$$I^{(k)} = \int_{\Xi_k} F(\kappa^2) \prod_{k=1}^{N} e^{-\gamma_k g_k} H_0^1(\kappa r) \kappa d\kappa \tag{2.15}$$

it is desired to perform a conformal transformation in which the new path of integration extends along the real axis, and where the origin of the new coordinate system represents a mini-max, or saddle point.

In fact, the actual method used turns out to be a double saddle point integral in X and Y, which is accomplished by using an integral representation for the Hankel function.*

*Reference 30, p 196.

As a consequence of applying this treatment, described in the following sections, a new integral representation of the form

$$K^{(k)} = -2\, k_k^{\,2}\, e^{\,ik_k r}\, \frac{2}{\pi} \int_0^{\infty}\!\!\int_0^{\infty} \Phi\,(X,\, Y)\, e^{-\frac{1}{2}(X^2 + Y^2)}\, dX dY \tag{2.16}$$

obtains.

This is optimally treated by expanding $\Phi\,(X,\, Y)$ in a power series and integrating term by term. Exact details of the saddle point method as applied to the general integral (2.15) are given in Banos.*

2.2.4 Series Expansion of Numerator Elements

It is now convenient to consider

$$K^{(i)}(g_k;\, r) = \int_{\Xi_i} \frac{\prod_{k=1}^{N} e^{-\gamma_k g_k}\, H_0^1\,(\kappa r)}{\prod_{k=1}^{M} \left[\kappa^2 - \kappa_k^{\,2}\right]}\, \kappa\, d\kappa \tag{2.17}$$

to which the conformal transformation

$$\tfrac{1}{2} X^2 = i\,(\,k_i - \kappa)\, r \tag{2.18}$$

is to be applied. Also the auxiliary variable

$$Y = c_i\, X\;;\quad c_i = (ik_i r)^{-\frac{1}{2}} \tag{2.19}$$

is introduced along with an index convention that :

*Reference 1 pp 63-81.

i assumes a value corresponding to the branch cut being considered. Hence, it prescribes the transformation relationships of Equations (2.18) and (2.19).

j assumes only values other than i .

Now, in analogy with Baños,* define the functions $p_i(\xi)$ and $q_j(\xi)$ such that

$$p_i \quad (\xi) = \xi \left\{ 1 - \frac{\xi^2}{8} - \frac{\xi^4}{128} - \frac{\xi^6}{1024} - \dots \right\}$$

$$|\xi| < 1 \tag{2.20}$$

$$q_i \quad (\xi) = \left[1 - n_{ji}{}^2 \right]^{\frac{1}{2}} \left\{ 1 + \frac{n_{ji}{}^2 \, \xi^2}{2 \, (1 - n_{ji}{}^2)} - \frac{n_{ji}{}^2 \, \xi^4}{8 \, (1 - n_{ji}{}^2)^2} + \frac{n_{ji}{}^4 \, \xi^6}{16 (1 - n_{ji}{}^2)^3} \dots \right\}$$

$$|\xi| < \left| 2 (1 - n_{ji}) / n_{ji} \right| \tag{2.21}$$

with

$$\sum_{k=1}^{N} \gamma_k \, g_k = d_i \, p_i \quad (\xi) + \sum_{j=1}^{N} d_j \, q_j \tag{2.22}$$

where

$$d_k = i \, k_k \, g_k \quad . \tag{2.23}$$

Further note that

$$\kappa d \kappa = - k_i{}^2 \; (1 - \tfrac{1}{2} \, \xi^2) \quad \xi \, d \, \xi \tag{2.24}$$

so that, it is possible to define

---

* Op cit, p. 87.

$$f(\xi) = \left[G(\xi) - G(-\xi)\right](1 - \tfrac{1}{2}\xi^2)\ \xi \tag{2.25}$$

$$G(\xi) = \exp\left[\sum_{k=1}^{4} \gamma_k\, g_k\right] \tag{2.26}$$

$$\tfrac{1}{2}\left[G(\xi) - G(-\xi)\right] = -\sinh\left[d_i\, p_i\right] \times \prod_{j=1}^{4} \exp\left[d_j\, q_j\right] \tag{2.27}$$

Next, the (exponential) and (hyperbolic sine) functions are expanded in a power series

$$e^{d_j q_j} = Q_0^{(j)}\left(1 + Q_2^{(j)}\xi^2 + Q_4^{(j)}\xi^4 + Q_6^{(j)}\xi^6 + \ldots\right),$$

$$|\xi|^2 < \left|\frac{2\,(1 - n_{ji})}{n_{ji}}\right| \tag{2.28}$$

$$-\sinh d_i p_i = P_1\,\xi\,(1 + P_2\xi^2 + P_4\xi^4 + P_6\xi^6 + \ldots),$$

$$|\xi|^2 < 4 \tag{2.29}$$

$$\left.\begin{aligned}
Q_0^{(j)} &= e^{d_j m_{ij}} \\
Q_2^{(j)} &= \frac{1}{2} d_j\, n_{ij}^2\, m_{ij}^{-1} \\
Q_4^{(j)} &= -\frac{1}{8} d_j n_{ji}^2\, m_{ji}^{-3} + \frac{1}{8} d_j^2\, n_{ji}^4\, m_{ji}^{-2} \\
Q_6^{(j)} &= \frac{1}{16} d_j n_{ji}^4\, m_{ji}^{-5} - \frac{1}{16} d_j^2 n_{ji}^4\, m_{ji}^{-4} \\
&\quad + \frac{1}{48} d_j^3\, n_{ji}^6\, m_{ji}^{-3}
\end{aligned}\right\} \tag{2.30}$$

with

$$m_{ij} = (1 - n_{ij})^{\frac{1}{2}} \tag{2.31}$$

and

$$\left.\begin{aligned} P_1 &= - d_i \\ P_2 &= - \frac{1}{3!} \left[\frac{3}{4} - d_i^{\,2} \right] \\ P_4 &= - \frac{1}{5!} \left[\frac{15}{16} + \frac{15}{2} d_i^{\,2} - d_i^{\,4} \right] \\ P_6 &= - \frac{1}{7!} \left[\frac{315}{64} - \frac{315}{16} d_i^{\,2} + \frac{105}{4} d_i^{\,2} - d_i^{\,6} \right] \end{aligned}\right\} \quad (2.32)$$

Next, note that

$$\prod_{j=1}^{4} \exp (d_j q_j) = Q_0 \ (1 + Q_2 \xi^2 + Q_4 \xi^4 + Q_6 \xi^6 + \ldots)$$

$$|\xi|^2 < \text{the smallest of } \left| \frac{2 \ (1 - n_{ji})}{n_{ji}} \right| \tag{2.33}$$

where

$$\left.\begin{aligned} Q_0 &= \prod_{j=1}^{4} Q_0^{(j)} \\ Q_2 &= \sum_{j=1}^{4} Q_2^{(j)} \\ Q_4 &= \sum_{j=1}^{4} \left\{ Q_4^{(j)} + \sum_{k>j}^{4} Q_2^{(j)} \ Q_2^{(k)} \right\} \\ Q_6 &= \sum_{j=1}^{4} \left\{ Q_6^{(j)} + \sum_{k>j}^{4} \left[Q_4^{(j)} Q_2^{(k)} \right.\right. \\ &\qquad \left.\left. + Q_2^{(j)} \ Q_4^{(k)} + \sum_{\ell>j}^{4} Q_2^{(j)} \ Q_2^{(k)} \ Q_2^{(\ell)} \right] \right\} \end{aligned}\right\} \quad (2.34)$$

and where it is understood that summations and products avoid index values of j, k, or ℓ = i in Equation (2.34).

At this point, the problem becomes identical to that discussed in Baños,* i.e.

$$\tfrac{1}{2}\Big[\, G(\xi) - G\ (\xi)\,\Big] = C_1\xi\,(1 + C_2\xi^2 + C_4\xi^4 + C_6\xi^6 + \ldots) \qquad (2.35)$$

with

$$\left.\begin{aligned} C_1 &= Q_o P_1 \\ C_2 &= Q_2 + P_2 \\ C_4 &= Q_4 + Q_2P_2 + P_4 \\ C_6 &= Q_6 + Q_4P_2 + Q_2P_4 + P_6 \end{aligned}\right\} \qquad (2.36)$$

Finally,

$$\left.\begin{aligned} f\ (X) &= 2\ c\ C_1\xi^2(1 - \tfrac{1}{2}\ \xi^2)(1 + C_2\xi^2 \\ &\qquad + C_4\xi^4 + C_6\ \xi^6 + \ldots) \\ &= D_2\ X^2 + D_4\ X^4 + D_6\ X^6 + D_8\ X^8 + \ldots \\ |X|^2 &< \begin{matrix}\text{least}\\ \text{of}\end{matrix} \left\{ \begin{matrix} 4\ k_2\ r \\ k_2\ r\ \left|\, 2\,(1 - n_{ji})/n_{ji} \,\right| \end{matrix} \right\} \end{aligned}\right\} \qquad (2.37)$$

where the i subscript is assumed, and

$$\left.\begin{aligned} D_2 &= 2c^3C_1 \\ D_4 &= 2c^5C_1(C_2 - \tfrac{1}{2}) \\ D_6 &= 2c^7C_1(C_4 - \tfrac{1}{2}C_2) \\ D_8 &= 2c^9C_1(C_6 - \tfrac{1}{2}C_4) \end{aligned}\right\} \qquad (2.38)$$

---

* _Op cit_, pp 88, 89.

Finally, an asymptotic expansion is substituted for the Hankel function. Hence

$$H_0^1(\kappa r) = \frac{4}{\pi} e^{-i\kappa r} \int_0^\infty (4i\kappa r - Y^2)^{-\frac{1}{2}} e^{-\frac{1}{2}Y^2} dY \qquad (2.39)$$

Substitution from equation (2.18) allows the identification and expansion of g (X, Y):

$$\begin{aligned} g(X, Y) &= \tfrac{1}{2}c_i \left[1 - \tfrac{1}{2} c_i^2 X^2 - \tfrac{1}{4} c_i^2 Y^2\right]^{-\frac{1}{2}} \\ &= \sum_{n=0}^{\infty} \sum_{m=0}^{n} B_{2(n-m)}^{2m} X^{2(n-m)} Y^{2m} \end{aligned} \qquad (2.40)$$

with

$$|X| < \left| 2 i k_i 4 - \tfrac{1}{2} Y^2 \right|^{\frac{1}{2}} \qquad (2.41)$$

Expanding the power series for g(X, Y) gives the following coefficients

$$B_0^0 = \frac{1}{2} c$$

$$B_2^0 = \frac{1}{8} c^3 \qquad B_0^2 = \frac{1}{16} c^3$$

$$B_4^0 = \frac{3}{64} c^5 \qquad B_2^2 = \frac{3}{64} c^5 \qquad B_0^4 = \frac{3}{256} c^5$$

$$B_6^0 = \frac{5}{256} c^7 \qquad B_2^2 = \frac{15}{512} c^7 \qquad B_2^4 = \frac{15}{1024} c^7 \qquad B_0^6 = \frac{5}{2048} c^7 \qquad (2.42)$$

2.2.5 Series Expansion of the Denominator

The denominator of equation (2.17) is best handled by considering individual expansions of $(\kappa^2 - \kappa_k^2)^{-1}$ or by direct expansion of the rationalized polynomial of order N in κ^2.

The former gives

$$\left(\kappa^2 - \kappa_k^2\right)^{-1} = \frac{1}{k_i^2 - \kappa_k^2} \left[1 + \frac{k_i^2}{k_i^2 - \kappa_k^2}\,\xi^2 + \frac{(3k_i^2 + \kappa_k^2)k_i^2}{4(k_i^2 - \kappa_k^2)^2}\,\xi^4 + \ldots\right]$$

$$|\xi^2| < \left| 2\,\frac{k_i - \kappa_k}{k_i} \right| \tag{2.43}$$

Alternatively, since the expansion coefficients of the rationalized denominator are known, one can expand directly from this rather than obtain the product of N series expansions such as equation (2.43).

Thus,

$$\prod_{k=1}^{M} \left[\kappa^2 - \kappa_k^2\right] = D_r\,(\kappa^2) \tag{2.44}$$

$$= \sum_{n=0}^{M} a_n \kappa^{2n}$$

Defining

$$\begin{aligned} D_r &= D_r(\kappa^2)\Big|_{\kappa = k_i} \\ D_r' &= \frac{\partial}{\partial \kappa} D_r\,(k^2)\Big|_{\kappa} \\ D_r'' &= \frac{\partial}{\partial \kappa^2} D_r\,(k^2)\Big|_{\kappa} \end{aligned} \tag{2.45}$$

it follows that

$$\frac{1}{D_r(\kappa^2)} = R_0 \left[1 + R_2 \xi^2 + R_4 \xi^4 + \ldots \right] \qquad (2.46)$$

where

$$R_0 = \frac{1}{D_r}$$

$$R_2 = \frac{1}{2} \frac{k_i c^2}{D_r} D_r' \qquad (2.47)$$

$$R_4 = \frac{1}{8} \frac{k_i{}^2 c^4}{D_r{}^2} (2D_r'^2 - D_r D_r'')$$

The radius of convergence for this series is given by the condition

$$\left| X^2 \right| < \text{the least of } 2r \left| k_i - \kappa_k \right| \qquad (2.48)$$

It should be quite evident from equation (2.48) that, unless the roots, κ_k, are far removed from all of the k_i, serious limitations will be imposed on the range of X. This problem will be discussed in paragraph 2.3.

2.2.6 Combination of Expansions

Recall that the integrand can be represented by

$$\Phi(X, Y) = h(X) g(X, Y) \qquad (2.49)$$

where g(X, Y) corresponds to the asymptotic expansion of the Hankel function. Introducing the series expansions

$$h(X) = \sum_{n=0}^{\infty} A_{2n} X^{2n} \tag{2.50}$$

$$g(X, Y) = \sum_{n=0}^{\infty} \sum_{m=0}^{n} B_{2(n-m)}^{2m} X^{2(n-m)} Y^{2m} \tag{2.51}$$

and

$$\Phi(X, Y) = \sum_{n=0}^{\infty} \sum_{m=0}^{n} A_{2(n-m)}^{2m} X^{2(n-m)} Y^{2m} \qquad (2.52$$

provided that

$$A_{2(n-m)}^{2m} = \sum_{\ell=0}^{n-m} A_{2\ell} B_{2(n-m+\ell)}^{2m} \tag{2.53}$$

$$A_{2\ell} = D_{2\ell} + \left[\sum_{k=1}^{\ell-1} D_{2k} R_{2(\ell-k)} \right] \tag{2.54}$$

It is desired to evaluate

$$\left.\begin{aligned} &\int_0^{\infty} \int_0^{\infty} \Phi(X, Y) \; e^{-\frac{1}{2}(X^2+Y^2)} dXdY \\ &\quad = \frac{\pi}{2} \left[\sum_{n=0}^{N} \Phi^{(n)} + R_N \right] \end{aligned}\right\} \tag{2.55}$$

where

$$\Phi^{(n)} = \sum_{m=0}^{n} \frac{(2m!)[2(n-m)]!}{2^n m!(n-m)!} A_{2(m-n)}^{2m} \tag{2.56}$$

and R_N is a remainder,

$$R_N \leq \Phi^{(N+1)} \tag{2.57}$$

Expanding the fundamental kernel

$$K^{(i)}(g_k;r) = \frac{E^{(i)}(g_k;r)}{(ik_i r)^2}\left[1 + \sum_{n=1}^{N} \frac{E_n^{(i)}(g_k)}{2^n n!\,(ik_i r)^n}\right] \tag{2.58}$$

It is possible to solve the $E_n^{(i)}$ in terms of the $\Phi^{(n)}$. It is typically unnecessary to go beyond $N = 2$.

Finally, the E functions are evaluated using the relationships developed throughout this section and listed for convenience in Tables 2.1 - 2.3.

$$E^{(i)}(g_k;r) = \frac{2\,k_i^2 d_i\, e^{ik_i r} \prod_{j=1}^{4} \exp\,(d_j m_j)}{D_r} \tag{2.59}$$

$$E_1^{(i)}(g_k) = -2 + 3\sum_{j=1}^{4} d_j n_{ji}^2 m_{ji}^{-1} + \tfrac{1}{4} d_i^2 + 3\,\frac{k_i D_r'}{D_r} \tag{2.60}$$

$$\left.\begin{aligned} E_2^{(i)}(g_k) = &- 21 \sum_{j=1}^{4} d_j n_{ji}^2 m_{ji}^{-1} - 15 \sum_{j=1}^{4} d_j n_{ji}^2 m_{ji}^{-3} \\ &- 12\, d_i^2 + 15\left(\sum_{j=1}^{4} d_j n_{ji}^2 m_{ji}^{-1}\right)^2 \\ &+ 10\, d_i^2 \sum_{j=1}^{4} d_j n_{ji}^2 m_{ji}^{-1} + d_i^4 \\ &- 21\,\frac{k_i D_r'}{D_r} + 30\,\frac{k_i D_r'}{D_r}\sum_{j=1}^{4} d_i n_{ji}^2 m_{ji}^{-1} \\ &+ 10\, d_i^2\,\frac{k_i D_r'}{D_r} + 30\,\frac{k_i^2 D_r'^2}{D_r^2} - 15\,\frac{k_i^2 D_r' D_r''}{D_r^2} \end{aligned}\right\} \tag{2.61*}$$

*There is a disagreement in sign for the term,

$10d_i^2 \sum_{j=1} d_i n_{ji}^2 m_{ji}^{-1}$, when a comparison is made between this equation and the corresponding results in Baños, i.e., Reference 1,p92 (Eqn. 4.48); p 115 (Eqn. 4.144); p 104 (Eqn. 4.96); and p 118 (Eqn. 4.157).

$$K^{(i)}(g_k;r) = \frac{E^{(i)}(g_k;r)}{(ik_i r)^2}\left[1 + \frac{E_1^{(i)}(g_k)}{2(ik_i r)} + \frac{E_2^{(i)}(g_k)}{8(ik_i r)^2} + \frac{E_3^{(i)}(g_k)}{48(ik_i r)^3} + \dots\right] \tag{2.58}$$

$$\int_0^\infty\int_0^\infty \Phi(X,Y)\, e^{-\frac{1}{2}(X^2+Y^2)}\, dX\, dY = \frac{\pi}{2}\left\{\sum_{n=0}^{N} \Phi^{(n)} + R_N\right\} \tag{2.54}$$

$$\Phi(X,Y) = g(X,Y)\; h(X) \quad \left\{\begin{array}{l} g(X,Y) = \displaystyle\sum_{n=0}^{\infty}\sum_{m=0}^{n} B^{2m}_{2(n-m)}\, X^{2(n-m)}\, Y^{2m} \\ h(X) = \displaystyle\sum_{n=0}^{\infty} A_{2n}\, X^{2n} \end{array}\right\} \qquad (2.49)\ (2.50)\ (2.51)$$

$$= \sum_{n=0}^{\infty}\sum_{m=0}^{n} A^{2m}_{2(n-m)}\, X^{2(n-m)}\, Y^{2m} \tag{2.54}$$

$$h(X) = \frac{f(X)}{D_r(X)} \quad \left\{\begin{array}{l} f(X) = \displaystyle\sum_{n=2}^{\infty} D_{2n}\, X^{2n} \\ D_r^{-1}(X) = R_0\left[1 + \displaystyle\sum_{n=2}^{\infty} R_{2n}\, X^{2n}\right] \end{array}\right\} \qquad (2.50)\ (2.46)$$

TABLE 2.1. TABULATION OF IMPORTANT SERIES RELATIONSHIPS.

$$E^{(i)}(g_k;r) = -2k_i^2(ik_ir)^2 e^{ik_ir}\,\Phi^{(1)} \quad (\text{Note that } \Phi^{(0)} \equiv 0)$$

$$E_1^{(i)}(g_k) = 2(ik_ir)\frac{\Phi^{(2)}}{\Phi^{(1)}} \quad ; \quad E_2(g_k) = 8(ik_ir)^2\frac{\Phi^{(3)}}{\Phi^{(1)}}$$

$$E_3^{(i)}(g_k) = 48(ik_ir)^3\frac{\Phi^{(4)}}{\Phi^{(1)}} \qquad \begin{pmatrix}2.14\\2.55\\2.58\end{pmatrix}$$

$$\Phi^{(n)} = \sum_{m=0}^{n}\frac{(2m)!\left[2(n-m)\right]!}{2^n\,m!\,(n-m)!}A^{2m}_{2(n-m)} \quad ; \quad A^{2m}_{2(n-m)} = \sum_{\ell=0}^{n-m}A_{2\ell}\,B^{2m}_{2(n-m+\ell)} \qquad \begin{pmatrix}2.56\\2.53\end{pmatrix}$$

$$A_{2\ell} = D_{2\ell} + \left[\sum_{k=1}^{\ell-1}D_{2k}\,R_{2(\ell-k)}\right]_{\ell>1} \qquad (2.54)$$

$$\left.\begin{aligned}
&B^0_0 = \frac{1}{2}c \\
&B^0_2 = \frac{1}{8}c^3 \qquad B^2_0 = \frac{1}{16}c^3 \\
&B^0_4 = \frac{3}{64}c^5 \qquad B^2_2 = \frac{3}{64}c^5 \qquad B^4_0 = \frac{3}{256}c^5 \\
&B^0_6 = \frac{5}{256}c^7 \qquad B^2_2 = \frac{15}{512}c^7 \qquad B^4_2 = \frac{15}{1024}c^7 \qquad B^6_0 = \frac{5}{2048}c^7
\end{aligned}\right\} \qquad (2.42)$$

TABLE 2.2. TABULATION OF IMPORTANT SERIES COEFFICIENTS AND THEIR RELATIONSHIPS.

$$Q_0 = \prod_{j=1}^{4} e^{d_j m_{ji}}$$

$$Q_2 = \frac{1}{2} \sum_{j=1}^{4} d_j n_{ji}^2 m_{ji}^{-1}$$

$$Q_4 = -\frac{1}{8} \sum_{j=1}^{4} d_j n_{ji}^2 m_{ji}^{-3} + \frac{1}{8} \left[\sum_{j=1}^{4} d_j n_{ji}^2 m_{ji}^{-1} \right]^2$$ From (2.34)

$$Q_6 = \frac{1}{16} \sum_{j=1}^{4} d_j n_{ji}^4 m_{ji}^{-5} - \frac{1}{16} \left[\sum_{j=1}^{4} d_j n_{ji}^2 m_{ji}^{-1} \right] \left[\sum_{j=1}^{4} d_j n_{ji}^2 m_j^{-3} \right] + \frac{1}{48} \left[\sum_{j=1}^{4} d_j n_{ji}^2 m_{ji}^{-1} \right]^3$$

$$\frac{D_4}{c^2 D_2} = \left(C_2 - \frac{1}{2} \right) = \left(Q_2 + P_2 - \frac{1}{2} \right)$$

$$\frac{D_6}{c^2 D_2} = \left(C_4 - \frac{1}{2} C_2 \right) = \left(Q_4 + Q_2 P_2 + P_4 - \frac{1}{2} Q_2 - \frac{1}{2} P_2 \right)$$ From (2.36, 2.38)

$$\frac{D_8}{c^2 D_2} = \left(C_6 - \frac{1}{2} C_4 \right) = \left(Q_6 + Q_4 P_2 + Q_2 P_4 + P_6 - \frac{1}{2} Q_4 - \frac{1}{2} Q_2 P_2 - \frac{1}{2} P_4 \right)$$

TABLE 2.3. ADDITIONAL COEFFICIENT TABULATIONS.

2.3 Subtraction of First Order Poles

As previously mentioned, the radius of convergence of the asymptotic expansion is limited by the most proximate singularity, i.e., a pole or other branch point. In typical problems, at least one pole pair can be expected to interfere with the expansion process.

2.3.1 Additional Symbols

D_r^o = rationalized denominator with zero, κ_o, removed, and evaluated with $\kappa = \kappa_o$.

erf(z) = error function of argument z.

erfc(z) = error function complement = 1 - erf(z)

H_k = expansion coefficient for $K_p^{(i)}$

$h^o(X)$ = h(X) with pole, κ_o, or X_o, removed.

$n_o = n_{oi} = \dfrac{k_i}{\kappa_o}$

Θ (X, Y) = Φ(X, Y) with pole associated with $\pm X_o$ removed.

ξ_o = ξ evaluated at $\kappa = \kappa_o$

Ψ (X, Y) = new representation of Φ (X, Y) analytic beyond the pole at X_o.

2.3.2 Series Expansion

It is desired to obtain an asymptotic expansion from which the pole has been subtracted, and its contribution added in more suitable form. Thus

$$K^{(i)} = (K^{(i)} - K_p^{(i)}) + K_p^{(i)} \tag{2.62}$$

or

$$K_s^{(i)} = K^{(i)} - K_p^{(i)} \tag{2.63}$$

We now introduce the function

$$\Psi(X, Y) = \Phi(X, Y) + \frac{1}{2k_i^2} \frac{\Theta(X_o, Y)}{X^2 - X_o^2} \tag{2.64}$$

where $\Psi(X, Y)$ yields a new series expansion not limited by the singularity at X_o and

$$\Theta(X, Y) = (X^2 - X_o^2)\,\Phi(X, Y) \tag{2.65}$$

To determine the contribution to the pole, the operation

$$-2k_i^2 \, e^{ik_i r} \frac{2}{\pi} \int_0^\infty \int_0^\infty \Big[\qquad \Big] e^{-\frac{1}{2}(X^2 + Y^2)} \, dX dY \tag{2.66}$$

is performed on equation (2.64) by inserting each term into the brackets giving expressions corresponding to terms in equation (2.63).

Since the last term requires expansion, we introduce

$$\Theta(X_o, Y) = g(X_o, Y)\, h^o(X\ ) \tag{2.67}$$

from which

$$K_p^{(i)} = - e^{ik_i r} \frac{4}{\pi} h^o(X_o) \int_0^\infty \frac{e^{-\frac{1}{2}X^2}}{X^2 - X_o^2} dX \tag{2.68}$$

$$\cdot \int_0^\infty g(X_o, Y)\, e^{-\frac{1}{2}Y^2} \, dY$$

Where
$$\int_0^\infty g\,(X_o,\,Y)\,e^{-\frac{1}{2}Y^2}\,dY = \frac{\pi}{4}\,e^{-i\kappa_o r}\,H_0^1(\kappa_o r) \quad (2.69)$$

$$h^o(X_o) = \frac{1}{D_r^o}\,\sinh\left[-g_i\,\gamma_i(\kappa_o)\right]\prod_{j=1}^{N}\exp\left[-g_j\,\gamma_j(\kappa_o)\right] \quad (2.70)$$

and

$$\int_0^\infty \frac{e^{-\frac{1}{2}X^2}}{X^2 - X_o^2}\,dX = \frac{\pi i}{2}\,e^{-\frac{1}{2}X_o^2}\left[1 - \mathrm{erf} - \frac{iX_o}{\sqrt{2}}\right] \quad (2.71)$$

Next, the functions $H_0^1\,(\kappa_o r)$ and $\exp\,(-\frac{1}{2}X_o^2)$ $\cdot\mathrm{erfc}\left(-\frac{iX_o}{\sqrt{2}}\right)$ are expanded in asymptotic series:

$$H_0^1\,(\kappa_o r)\,e^{-i\kappa_o r} = \left(\frac{2\,n_o}{\pi}\right)^{\frac{1}{2}}\,c\left[1 + \frac{n_o}{8}c^2 + \frac{9n_o^2}{128}c^4 + \frac{75n_o^3}{1024}c^6 + ----\right] \quad (2.72)$$

$$\exp\left[-\tfrac{1}{2}X_o^2\right]\mathrm{erfc}\left(-\frac{iX_o}{\sqrt{2}}\right) = i\left(\frac{n_o}{\pi(n_o-1)}\right)^{\frac{1}{2}}\,c\left[1 + \frac{n_o}{2(n_o-1)}c^2 + \frac{3n_o^2}{4(n_o-1)^2}c^4 + \frac{15\,n_o^3}{8(n_o-1)^3}c^6 + ----\right] \quad (2.73)$$

Combining the above expressions gives a closed form expression

$$\chi_p^{(i)} = -\frac{\pi i}{D_r^o}\,\sinh\left[-g_i\,\gamma_i(\kappa_o)\right]\prod_{j=1}^{N}\exp\left[-g_j\,\gamma_j(\kappa_o)\right] \quad (2.74)$$
$$\cdot H_0^1\,(\kappa_o r)\,\mathrm{erfc}\left(-\frac{iX_o}{\sqrt{2}}\right)$$

Using the asymptotic expansions from equations (2.72) and (2.73) we obtain the following series

$$K_p^{(i)} = \frac{H^{(i)}(g_k;\ r)}{(ik_i r)} \left[1 + \sum_{k=0}^{\infty} \frac{H_k}{(ik_i r)^{k+1}} \right] \tag{2.75}$$

with

$$\left.\begin{aligned}
H^{(i)}(g_k;\ r) &= \frac{n_o}{2D_r^o} \left(\frac{2}{n_o - 1} \right)^{\frac{1}{2}} e^{ik_i r} \\
&\quad \times \sinh\left[-g_i\, \gamma_i(\kappa_o)\right] \prod_{j=1}^{N} \exp\left[-g_j\, \gamma_j(\kappa_o)\right] \\
H_0 &= \frac{n_o\,(n_o + 3)}{8\,(n_o - 1)} \\
H_1 &= \frac{n_o^2(9\,n_o^2 - 10n_o + 95)}{64\,(n_o - 1)^2} \\
H_2 &= \frac{3n_o^3\,(25n_o^3 - 63n_o^2 + 83\,n_o - 595)}{128\,(n_o - 1)^3}
\end{aligned}\right\} \tag{2.76}$$

The series expansion for $K_s^{(i)}$ is obtained by termwise addition of equation (2.75) to equation (2.58). The new series is no longer limited in its radius of convergence by the first order pole at κ_o.

Further, it should be noted that the above expansion contains the residue effect attributable to the enclosed pole, $\pm\,\kappa_o$.*

---

* Reference 1, pp 73-75 and pp 149-152.

Also, the above process is repeated as often as is necessary to remove a pole.

Note that evaluation of $K_s^{(i)}$ is best performed after the specific form of the differential operations, $,_k$ and $,_o$, are performed, because the troublesome $\sinh\left[-g_i\,\gamma_i(\kappa_o)\right]$ term will usually revert to an exponential.

2.3.3 Pole Residues

In those cases where a pole does not interfere with the series expansion, and it is an actual first order pole in the upper half of the first Riemann surface, its effect can be computed by using the method of residues.

Hence, if $+\kappa_o$ satisfies these conditions, then

$$K_r(g_k;\, r) = 2\pi i \oint_{\kappa_o} \frac{\prod_{k=1}^{N} e^{-\gamma_k g_k}\, H_0^1(\kappa r)}{(\kappa^2-\kappa_o^2)\, D_r^o(\kappa^2)}\, \kappa\, d\kappa \qquad (2.77)$$

$$= \frac{\pi i}{D_r^o} \prod_{k=1}^{N} \exp\left[-g_k\, \gamma_k(\kappa_o)\right]\, H_0^1\,(\kappa_o r)$$

It is interesting to drop the erfc function in equation (2.74) and compare results.

2.4 The Scattering Matrix, $\mathbf{M}$

Up to this point, the theoretical analysis has concerned itself with an integral formalism that is capable of treating all classes of wave propagation problems involving two homogeneous media separated by an infinite plane, N-different phase velocities, and a point source of the waves.

The incorporation of the physics into the hitherto purely mathematical treatment of the various integral representations requires: a) specification of N and of complex values for the N propagation constants, k_k; and b) specification of the elements of $\mathbf{M}$ an NxN array which are derived from the boundary conditions.

In the electromagnetic case, knowledge of the k_k is sufficient to allow computation of the matrix elements of $\mathbf{M}$, but the acoustic case requires additional knowledge of the complex impedances of the N propagation modes, or at least their ratios.

Alternatively, since the form given by Equation (2.7) is ultimately desired, an equivalent amount of information must be contained in the zero pairs, $\pm \kappa_k$, and the appropriate linear combinations of operations shown in equations (2.8) and (2.9).

2.4.1 Types of Materials

The most general acoustic medium to be documented at this time is a linear micropolar medium, i.e., one characterized by a randomly inhomogeneous granular structure where the granule dimensions are statistically defined.

Parfitt and Eringen* have shown that such a medium is characterized by four distinct phase velocities, two of which correspond to classical elastic propagation modes, and two new waves involving microrotation of the granular domain.

* Reference 22.

It is further demonstrated that a certain critical frequency, corresponding to the condition that wavelength and granular dimension are comparable, must be exceeded before the latter modes begin to propagate.

Also quite difficult is a rigorous treatment of a porous solid. Biot* has conducted extensive investigations into this problem with results indicating that this is not unlike the micropolar medium above.

However, for frequencies far below the critical frequency, a porous solid can be treated as simple but lossy fluid with only one phase velocity. This limit applies to typical ground covers and will be employed for developing the theoretical model.

Another medium of general interest is the elastic solid or viscous fluid with shearing. Each such medium supports waves traveling at two distinct phase velocities corresponding to compressional and shear(ing) modes.**

In the discussion that follows, we consider the problem of two such media as the most general case, solve for M_{11}, and then develop M_{11} for other types of media and boundary conditions by appropriate limits on the general scattering element.

---

* References 3,4,5,6.

**Reference 8 pp 107 to 111.

2.4.2 Additional Symbols

$\mathbf{A}$ = vector representation of the wave amplitudes, A_k.

A_k = wave amplitude of the incident wave, k^{th} mode.

$\mathbf{B}$ = vector representation of the wave amplitudes, B_k.

B_k = wave amplitude, transmitted or reflected wave, k^{th} mode.

k' = real constant describing porous media.

n_s = n_{34}.

u, v = constants defined in equation (2.82).

U, V, W, Z = real constants describing porous media.

$\alpha, \beta, \delta, \epsilon, \phi$ = constants defined in equation (2.82).

$\alpha', \delta', \phi', \phi''$ = constants defined in equation (2.84) and in Table 2.4 .

Δ = slope change at break-point.

$\psi^{(k)}$ = general velocity potential associated with the k^{th} wave mode.

$\psi_{inc}^{(k)}$ = incident velocity potential, k^{th} wave mode.

$\psi_{ref}^{(k)}$ = reflected velocity potential, k^{th} wave mode.

$\omega_a, \omega_b, \omega_c$ = break-point frequencies in radians per second.

2.4.3 Boundary Conditions

In developing boundary conditions we will be dealing with N $\left\{ \begin{matrix} \text{plane} \\ \text{cylindrical} \end{matrix} \right\}$ modes where the k^{th} wave will have a velocity potential given by

$$\psi^{(k)} \sim e^{\pm \gamma_k z} \left\{ \begin{matrix} \cos \kappa r \\ J_0 (\kappa r) \end{matrix} \right\} \qquad (2.78)$$

where time variation has been suppressed.

We have previously stated that the largest value of N to be considered here will be N = 4, corresponding to two elastic media. Using these constraints, it is convenient to designate the wave modes associated with k as follows:

k = 1; Compressional wave, medium 1

k = 2; Compressional wave, medium 2

k = 3; Shear wave, medium 1

k = 4; Shear wave, medium 2

The ray geometry for four incident and four reflected waves sharing a common κ* is shown in Figure 2.4.

---

* This condition is nothing more than a statement of Snell's Law.

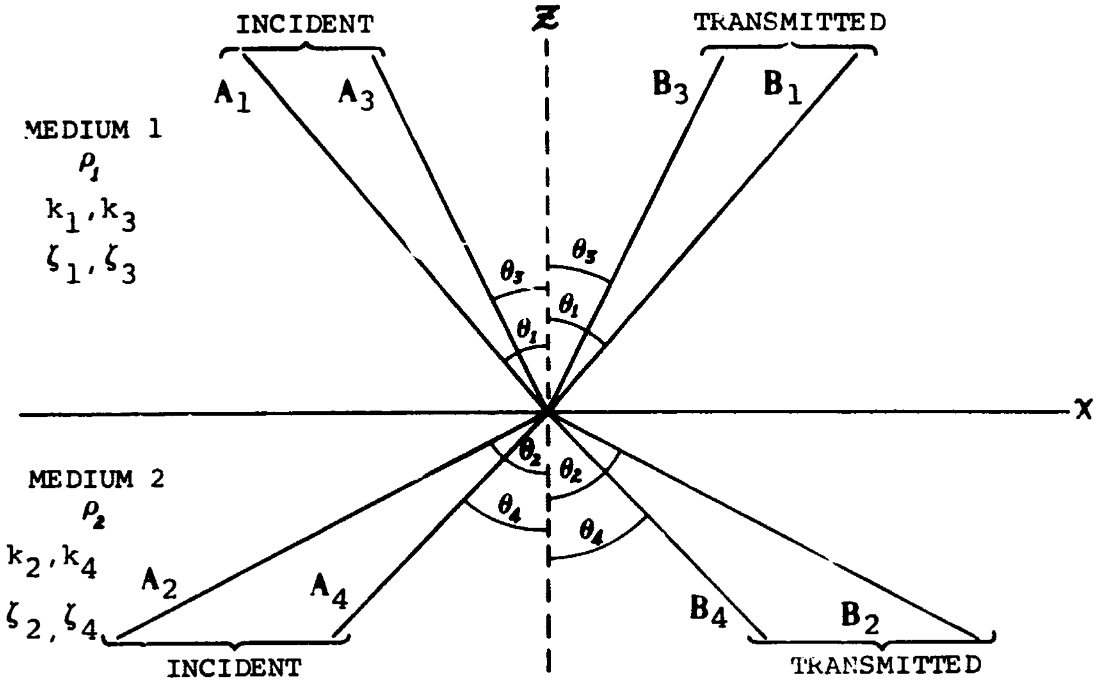

FIGURE 2.4 PLANE WAVE SCATTERING BY A PLANE BOUNDARY BETWEEN TWO BONDED ELASTIC, ISOTROPIC MEDIA.

Since primary interest is concerned with mode 1 -- mode 1 conversion in medium 1, we stipulate the form of these waves as

$$\psi^{(1)}_{inc} = A_1 \quad e^{\gamma_1 z} \left\{ \begin{matrix} \cos \kappa r \\ J_o(\kappa r) \end{matrix} \right\}$$

$$\psi^{(1)}_{ref} = B_1 \quad e^{-\gamma_1 z} \left\{ \begin{matrix} \cos \kappa r \\ J_o(\kappa r) \end{matrix} \right\} \tag{2.79}$$

with

$$B_1 = M_{11} A_1 \tag{2.80a}$$

More generally, it is possible to solve

$$\mathbf{B} = \mathbf{MA} \tag{2.80b}$$

by considering the following four boundary conditions

I) Continuity of the normal velocity component.

II) Continuity of the tangential velocity component.

III) Continuity of the compressional stress.

IV) Continuity of tangential stress.

as described in Appendix A. Application of boundary conditions gives $A(\kappa^2)$ and $B(\kappa^2)$, defined in equation (2.4):

$$\begin{aligned} A(\kappa^2) &= \alpha\gamma_3 + \epsilon\gamma_2\gamma_3\gamma_4 + \phi\gamma_4 \\ B(\kappa^2) &= \beta + \delta\gamma_2\gamma_4 + \phi\gamma_2\gamma_3 \end{aligned} \tag{2.81}$$

where

$$\begin{aligned} \alpha &= -(\kappa^2 - u)^2 \\ \beta &= (\kappa^2 + v - u)^2 \kappa^2 \\ \delta &= -(\kappa^2 + v)^2 \\ \epsilon &= \kappa^2 \\ \phi &= -uv \\ u &= \frac{1}{2}\left[1 - \nu n_s{}^2\right]^{-1} k_4{}^2 \\ v &= \frac{1}{2}\left[1 - \nu n_s{}^2\right]^{-1} \nu k_4{}^2 \end{aligned} \tag{2.82}$$

Of considerable importance to this problem is the location of the first order poles associated with $D(\kappa^2)$. For this purpose it is necessary to obtain $D_r(\kappa^2)$, the rationalized form of $D(\kappa^2)$, which in this case is a most laborious process.

This analysis is simplified considerably by considering the limit of $\nu = 0$. Then, $D(\kappa^2)$ decouples into two expressions, each of which is dependent on properties of just one medium

$$D(\kappa^2) = \left[\alpha' + \kappa^2 \gamma_2 \gamma_4 \right] \left[\kappa^2 - \gamma_1 \gamma_3 \right] \tag{2.83}$$

where

$$\alpha' = -[\kappa^2 - \tfrac{1}{2} k_4^2]^2 \tag{2.84}$$

In solving for the zeros, the first bracket gives rise to a cubic in κ^2 and the second yields a first order equation in κ^2. A brief discussion of these four pole pairs is contained in Appendix A-2.

Letting $|\nu|$ assume a small value, the denominator $D(\kappa^2)$ recouples, and clusters of four new roots appear around the original eight. These zeros are actual only on two of the Riemann surfaces so that some care must be exercised when computing residues and pole contributions.

A further computational complication arises from the fact that the poles tend to cluster. If $D_r(\kappa^2)$ is used in most polynomial root-finding programs, good convergence will not usually occur because of the proximity of so many roots.

Thus, the best root finding procedure appears to be:

1) Determine zeros of equation (2.83) and use these for initial values.

2) Let ν assume its physically correct value in small increments if necessary.

3) Iterate on the above zeros using new values of ν .

4) Caution -- program must contain Riemann surface identifiers and must be capable of "following" a root onto a neighboring Riemann surface.

5) Repeat for all Riemann surfaces.

This algorithm should locate the 16 zero pairs of $D_r(\kappa^2)$ or of $D_r(\kappa^2)$ on all 16 Riemann surfaces.

Finally, for completeness, we outline this and seven other related acoustical problems in Table 2.4. The case of greatest interest is 6, where medium 1 is a simple fluid (air) and medium 2 is a porous solid (ground cover).

2.4.4 Discussion of Porous Media

It was previously mentioned that, for the frequencies of interest in this study, coupling to medium 2 wave modes other than compressional is negligible. Effects of viscous shearing appear in the form of an imaginary part of k_2 only.

Following Beranek*, k_2 can now be written in the form

$$k_2 = k'Z^{-\frac{1}{2}} \sqrt{\frac{V + U^2\omega^2 - jWU\omega}{1 + U^2\omega^2}} \tag{2.85}$$

---

* Reference 2 p 840.

LEGEND

C:	Continuous	O:	Zero Value
E:	Elastic	P:	Porous Medium
F:	Fluid	R:	Rigid
N:	Vacuum	V:	Viscous
		X:	Not Applicable

	Medium 1	Medium 2	Boundary Conditions: Normal Velocity	Tangential Velocity	Compressional Stress	Tangential Stress	Example & Comments	N	M	$A(\kappa^2)$	$B(\kappa^2)$
1	E/V	E/V	C	C	C	C	Two Bonded Elastic Solids	4	16	$\alpha\gamma_3+\epsilon\gamma_2\gamma_3\gamma_4+\phi\gamma_4$ See text for α, ϵ, ϕ.	$\beta+\delta\gamma_2\gamma_4+\phi\gamma_2\gamma_3$ See text for β, δ, ϕ.
2	F/P	E/V	C	C	C	X	Elastic Solid & Fluid $\lim_{k_3\to\infty}$ of #1	3	8	$\alpha'+\kappa^2\gamma_2\gamma_4$ where $\alpha'=-(\kappa^2-\frac{1}{2}k_4^2)^2$	$\phi'\gamma_2$ where $\phi'=-\frac{1}{4}\nu\ k_4^4$
3	E/V	F/P	C	C	C	X	Same as 2 except $\lim_{k_4\to\infty}$ of #1	3	8	$\kappa^2\gamma_2\gamma_3+\phi''$ $\phi''=-\frac{1}{4}\nu^{-1}k_3^4$	δ' where $\delta'=-(\kappa^2-\frac{1}{2}\delta_3^2)^2$
4	E/V	N	X	X	O	O	Free Boundary of Elastic Solid $\lim_{k_2\to\infty}$ & $\lim_{k_4\to\infty}$ of #1	2	3	$\kappa^2\gamma_3$	δ' where δ' is same as in #3.
5	E/V	R	O	O	X	X	Rigid Boundary of Elastic Solid	2	1	γ_3	κ^2
6	F/P	F/P	C	X	C	X	Two Fluids $\lim_{k_3\to\infty}$ & $\lim_{k_4\to\infty}$ of #1	2	1	1	$\nu\gamma^2$
7	E/V	E/V	C	X	C	O	Two Elastic Solids with Transverse Slip*	4	16	$\alpha'+\kappa^2\gamma_2\gamma_4+\nu n_s^4\kappa^2\gamma_2\gamma_3$ where α' is same as in #2	$\nu n_s^4\delta'$ where δ' is same as in #3.
8	E/V	R	O	X	X	O	Rigid Boundary of Viscous Fluid. Transverse Slip	2	1	γ_3	$-(\kappa^2-\frac{1}{2}k_3^2)$

*Reference 16.

TABLE 2.4 M_{11} COMPONENTS, $A(\kappa^2)$ AND $B(\kappa^2)$, AS DEFINED BY EQUATION (2.4), FOR A WIDE VARIETY OF BOUNDARY CONDITIONS ENCOUNTERED IN ACOUSTICS.

The specific acoustic impedance of medium 2 relative to air is given by

$$\zeta_2 = Z \frac{1}{k'} k_2 = \frac{1}{\nu n} \tag{2.86}$$

Relationships of derived constants to constants used by Beranek are given in Table 2.5.

TABLE 2.5

<u>RELATIONSHIP OF CONSTANTS IN EQUATION (2.85) TO BERANEK CONSTANTS</u>

$$\left.\begin{aligned} k_1 &= \frac{\omega k}{c_o} \\ Z &= \frac{kK}{\rho_o c_o^2 Y} \\ U &= \frac{\rho_m}{R_1} \\ V &= Y + \frac{\rho_m}{\rho_o k} \\ W &= \frac{\rho_m}{\rho_o k} \end{aligned}\right\} \text{ where }$$

- k = structure factor, > 1.
- K = value coefficient of elasticity of air in the interstices ($dynes/cm^2$) is < adiabatic compressibility of air, $-\rho_o c_o^2$.
- ω = frequency (radians/sec)
- R = dynamic specific flow resistance (Rayls/cm)
- ρ_o = density of air (gms/cm^3)
- ρ_m = density of porous material (gms/cm^3)
- Y = porosity < 1.

Applying break-point analysis to the impedance as found from equations (2.85) and (2.86), it is seen that

$$\begin{aligned} \lim_{\omega \to 0} \zeta_2 &= Z^{\frac{1}{2}} \quad V^{\frac{1}{2}} \\ \lim_{\omega \to \infty} \zeta_2 &= Z^{\frac{1}{2}} \end{aligned} \tag{2.87}$$

or since $V > 1$

$$\lim_{\omega \to 0} \zeta_2 > \lim_{\omega \to \infty} \zeta_2 \tag{2.88}$$

Next, we observe the break point frequencies along with their slope charge values, Δ.

$$\left.\begin{aligned} \omega_a &= \frac{1}{U} \; ; \; \Delta = -1 \\ \omega_b &= \frac{1}{U} \sqrt{\tfrac{1}{2}(2V + W^2) - \tfrac{1}{2} W \, (4V + W^2)^{\frac{1}{2}}} \; ; \; \Delta = +\tfrac{1}{2} \\ \omega_c &= \frac{1}{U} \sqrt{\tfrac{1}{2}(2V + W^2) + \tfrac{1}{2} W \, (4V + W^2)^{\frac{1}{2}}} \; ; \; \Delta = +\tfrac{1}{2} \end{aligned}\right\} \tag{2.89}$$

Note that, for typical porous media

$$\omega_a \sim \omega_b < \omega_c \tag{2.90}$$

and for the case of a dense skeleton,

$$\begin{aligned} \omega_a &\to 0 \\ \omega_b &\to 0 \\ \omega_c &\sim \frac{W}{U} \end{aligned} \tag{2.91}$$

in agreement with Beranek*.

---

* Loc. cit. equation (19.4).

2.4.5 Zeros for Two Fluids Model

Referring to Table 2.4, the characteristic denominator of the two fluids model (#6) is given by

$$\begin{aligned} n(\kappa^2) &= \gamma_1 A(\kappa^2) + B(\kappa^2) \\ &= \gamma_1 + \nu\gamma_2 \end{aligned} \tag{2.92}$$

Rationalizing consists of multiplicative combinations over all different Riemann surface representations, i.e.

$$D_r(\kappa^2) = (\gamma_1 + \nu\gamma_2)(\gamma_1 - \nu\gamma_2) \tag{2.93}$$

Setting $D_r(\kappa^2)$ equal to zero gives a single pair of first order poles

$$\kappa_o = \pm k_1 \left(\frac{1 - \nu^2 n^2}{1 - \nu^2} \right)^{\frac{1}{2}} \tag{2.94}$$

For the case where $|\nu| \ll 1$ and $|n| < 1$ and both are approximately real, the poles lie very near to $\pm k_1$ and we have

$$2\theta_z - \pi < 2 \operatorname{Arg}\left\{ \gamma_k \right\} < 2\theta_1 \tag{2.95}$$

$$\text{for } k = 1, 2$$

and

$$\gamma_1(\kappa_o) = \left\{ \begin{array}{ll} \nu k_1 \kappa_o & \text{on surfaces 1 and 3} \\ -\nu k_1 \kappa_o & \text{on surfaces 2 and 4} \end{array} \right\} \tag{2.96}$$

$$\gamma_2(\kappa_o) = \left\{ \begin{array}{ll} k_1 \kappa_o & \text{on surfaces 1 and 2} \\ k_1 \kappa_o & \text{on surfaces 3 and 4} \end{array} \right\} \tag{2.97}$$

Finally

$$D(\kappa_o^2) = \begin{Bmatrix} 0 \text{ on surfaces 2 and 3} \\ +2\ \nu\, k_1\kappa_o \text{ on surface 1} \\ -2\ \nu\, k_1\kappa_o \text{ on surface 4} \end{Bmatrix} \tag{2.98}$$

In the case of a porous medium, $|\nu| < 1$, $|n| \gtrsim 1$, and

$$\operatorname{Arg}(\nu) = -2 \operatorname{Arg}(n) \tag{2.99}$$

The pole remains in the neighborhood of k_1, but its position is shifted $\pi/2$ radians relative to the branch cut. It now becomes a real pole on surfaces 1 and 4, i.e.

$$D(\kappa_o^2) = \begin{Bmatrix} 0 \text{ on surfaces 1 and 4} \\ -2\,\nu\, k_1\kappa_o \text{ on surface 2} \\ +2\,\nu\, k_1\kappa_o \text{ on surface 3} \end{Bmatrix} \tag{2.100}$$

2.5 Theoretical Solution

Before outlining the theoretical expansions, it is interesting to consider some of the historical aspects to the problem of acoustic radiation of a point source when a ground plane is present.

On the basis of ray theory, we would expect that the velocity potential might be given by

$$\psi(r, z; 0, h) = \frac{Q}{4\pi}\left[\frac{e^{ik_1R}}{R} + \frac{\gamma_1 - \nu\gamma_2}{\gamma_1 + \nu\gamma_2}\ \frac{e^{ik_1R'}}{R'}\right] \tag{2.101}$$

where now

$$\begin{aligned} \gamma_1 &= ik_1 \cos\theta_1 \\ \gamma_2 &= ik_1\left[n^2 - \sin^2\theta_1\right]^{\frac{1}{2}} = \frac{ik_1}{\nu}\ \zeta^{-1} \end{aligned} \tag{2.102}$$

with ζ being the surface impedance. In the simple ray theory, this is a function of θ_1, i.e.,

$$\frac{\gamma_1 - \nu\gamma_2}{\gamma_1 + \nu\gamma_2} = \left[\frac{\cos\theta_1 - \zeta^{-1}}{\cos\theta_1 + \zeta^{-1}}\right] \tag{2.103}$$

Unfortunately, the ray theory representation does not take into account important surface effects, and its validity is restricted to the region that g_1 is greater than a wavelength*. For sufficiently large r and small g_1, we have the approximation

$$\psi(r,\ z;\ 0,\ h) \sim \frac{Q}{4\pi}\left[\frac{e^{ik_1 R}}{R} - \frac{e^{ik_1 R'}}{R'}\right] \tag{2.104}$$

which are the leading terms of equations (2.1) and (2.5) combined. Further analysis along the same lines gives

$$\psi(r,\ z;\ 0,\ h) \quad \frac{Q}{4\pi} \quad \frac{e^{ik_1 r}}{r} \left[\frac{(ik_1 z)(ik_1 h)}{(ik_1 r)} + O\,(ik_1 r)^{-2}\right] \tag{2.105}$$

so that at least the leading terms of the representation allow attenuation rates twice that of 6 db/double distance associated with a simple source.

However, these terms vanish on the surface which is quite at variance with the generalized boundary conditions. Hence, the inclusion of important surface effects for small g_1 requires detailed analysis of the term, $V(g_1;r)$.

*Reference 19, p. 371

2.5.1 Final Manipulations

The desired solution is found when the functions $A(\kappa^2)$ and $B(\kappa^2)$, are inserted in equation (2.6). For the two fluids model, these are found in Table 2.4, whereupon

$$V(g_i;\ r) = -\frac{K_{,1}(g_1,\ g_2;\ r)\ -\ \nu\ K_{,2}(g_1,\ g_2;\ r)}{(1\ -\ \nu^2)} \tag{2.106}$$

with similar relationships obtaining for $V^{(i)}(g_i;\ r)$, $V_p^{(i)}(g_i;\ r)$, $V_s^{(i)}(g_i,\ r)$ etc.

This particular problem has only one pole (M=1) so that

$$\left.\begin{aligned} D_r(\kappa^2) &= \kappa^2 - \kappa_o^{\,2} \\ D_r^o(\kappa^2) &= 1 \end{aligned}\right\} \tag{2.107}$$

Also, the pole, κ_o, will typically lie very near the branch point, k_1, so that the treatment of paragraph 2.3.2 is required.

While $V(g_i;\ r)$ can, in principle, be evaluated for all g_i and r, to obtain ψ, i.e.

$$\psi\,(r,\ z;\ 0,\ h) = \frac{Q}{4\,\pi}\left[\frac{e^{ik_1R}}{R} - \frac{e^{ik_1R}}{R} + V(g_i;\ r)\right] \tag{2.108}$$

we have seen that the more accurate representation in the neighborhood of the interface is,

$$V(g_i;\ r) = V_s^{(1)} + V_p^{(1)} + V^{(2)} \tag{2.109}$$

where the form has been adjusted to the problem under discussion.

Noting that the asymptotic series can be differentiated term by term, we can also obtain series representations for the three expressions on the left hand side of equation (2.108).

These will have the form

$$\left.\begin{aligned} V^{(2)}(g_1, g_2; r) &= \frac{F^{(2)}(g_1; r)}{(ik_2 r)^2}\left[F_0^{(2)}(g_2)\right. \\ &\left. + \sum_{k=1}^{N'} \frac{F_k^{(2)}(g_1, g_2)}{(ik_2 r)^k}\right] \end{aligned}\right\} \quad (2.110)$$

$$\left.\begin{aligned} V_p^{(1)}(g_1, g_2; r) &= -\frac{i\pi k_2 \quad \nu(1-n^2)^{\frac{1}{2}}}{[1-\nu^2]^{\frac{3}{2}}} \\ &\times e^{-g_1\gamma_1(\kappa_0)} e^{-g_2\gamma_2(\kappa_0)} \\ &\times H_0^1(\kappa_0 r)\ \mathrm{erfc}\left(-\frac{iX_0}{\sqrt{2}}\right) \end{aligned}\right\} \quad (2.111)$$

$$V_s^{(1)}(g_1, g_2; r) = \frac{G^{(1)}(g_1, g_2, r)}{(ik_1 r)}\left[1 + \sum_{k=1}^{N'} \frac{G_k(g_1, g_2)}{(ik_1 r)^k}\right] \quad (2.112)$$

Expansion of the various functions, F and G, are carried out in Table 2.6 for $N' = 2$ and $g_2 = 0$. These results are in complete agreement with those obtained by Paul*, and will give an asymptotic representation of the velocity potential provided

$$r > \frac{1}{|k_1|} \text{ and } r > (z+h) \quad (2.113)$$

It should be obvious that economical evaluation of these expressions for numerous combinations of k_1 (or frequency), n, ν, g_1 (=z+h), and r requires the aid of a computer.

---

* Reference 23

Contribution from k_2 - Branch Cut	$F^{(2)}(g_1;r) = \frac{2in^2k_2}{m} \; e^{ik_2 r} \; e^{ik_1 g_1 m}$ $F_0^{(2)}(0) = -\frac{\nu}{m}$ $\quad$ $F_0^{(2)}(g_2) = n^{-1}d_2 - \frac{\nu}{m}$ $F_1^{(2)}(g_1,0) = -\frac{\nu}{m^3}\left[-2(1+2n^2) + 3n^2md_1 + 6\nu^2n^2\right]$ $F_2^{(2)}(g_1,0) = -\frac{n^2\nu}{m^5}\Big\{24(3+2n^2) - 3(12+13n^2)md_1 + 15n^2m^2d_1^2 - \nu^2\Big[24(3+7n^2) - 6\nu n^2md_1\Big] + 120\nu^4n^2\Big\}$
Contribution from k_1 - Branch Cut and Pole, κ_o	$G^{(1)}(g_1g_2;r) = \frac{2ik_1}{\sqrt{2}(1-\nu^2)} \; \frac{\tau\nu}{\sigma^{\frac{1}{2}}\lambda} \; e^{ik_1 r} \; e^{k_1 g_1 \tau} \; e^{-k_1 g_2 \tau}$ $G_1^{(1)}(g_1,0) = \frac{1}{2}d_1^2 + \nu\left[\frac{1}{2}im^{-1}d_1 + \frac{1}{3}imd_1^3\right] + \nu^2\left[-\frac{9}{128}m^2 + \frac{1}{16}(7+n^2)d_1^2 - \frac{1}{8}m^2d_1^4\right] + O(\nu^3)$ $G_2^{(1)}(g_1,0) = -d_1^2 + \frac{1}{4}d_1^4 + \nu\left[\frac{1}{4}im^{-3}(1-4n^2)d_1 - \frac{1}{6}im^{-1}(1-4n^2)d_1^3 + \frac{1}{5}imd_1^5\right] + O(\nu^2)$
Contribution from k_1 - Branch Cut - 1st Term.	$F^{(1)}(g_2;r) = \frac{2ik_1}{\nu^2m^2} \; e^{ik_1 r} \; e^{-k_1 g_2 m}$ $F_0^{(1)}(g_1) = 1 - i\nu m g_1$
Auxilliary Information	$g_1 = z + h;\; g_2 = 0$ $d_k = ik_k g_k$ $m = (1-n^2)^{\frac{1}{2}}$ $\sigma = \left(\frac{1-\nu^2n^2}{1-\nu^2}\right)^{\frac{1}{2}}$ $\tau = \left(\frac{1-n^2}{1-\nu^2}\right)^{\frac{1}{2}}$ $\lambda = (\sigma - 1)^{\frac{1}{2}}$ Note that $\kappa_o = k_1\sigma$ $X_o = i(2ik_1 r)^{\frac{1}{2}}\lambda$

TABLE 2.6 TABULATION OF COEFFICIENTS FOR VELOCITY POTENTIAL SERIES.

2.5.2 Interpretation of Theory

Because of the complexity of the formulae, a generalized interpretation is not easily carried out. For $g_1 = 0$, some interesting comments can be made about the radial behavior of the velocity potential.

Four basic regions can be described:

1) Quasi-static $\quad r < \frac{1}{k_1}$ and $< \frac{1}{k_2}$

2) Intermediate I $\quad \frac{1}{k_1} < r < r_b$

3) Intermediate II $\quad r_b < r < \frac{1}{|k_1 - \kappa_o|}$

4) Far field $\quad \frac{1}{|k_1 - \kappa_o|} < r$

where r_b is a frequency dependent radius, and where

regions 1 and 2 $\longrightarrow \psi \sim r^{-1}$ (6dB/double distance)

region 3 $\longrightarrow \psi \sim r^{-3}$ (up to 18dB/double distance)

region 4 $\longrightarrow \psi \sim r^{-2}$ (12dB/double distance)

For fixed r, ψ in regions 1 and 2 is generally insensitive to frequency variations if phase effects between the various terms are ignored by averaging. For region 3 radii, both bounds of the region and the amplitude decreases monotonically with frequency in a manner which is not easily predicted from the formulae. Finally, in region 4, at fixed r, there is a monotonically decreasing ψ which varies as k_1^{-1} for constant n and ν.

If phase cancellation effects are included, however, we obtain an interaction between the leading terms of $V_s^{(1)}$ and

$V_p^{(1)}$. It is felt that this term will produce the pronounced dip in frequency response in the 100 - 1000 Hz range, and that this effect will be primarily exhibited in regions 3.

2.5.3 Theoretical Data

Available funds did not allow complete programming, debugging and running of a computer program to compute field pressure data from equations (2.110), (2.111), and (2.112).

In lieu of these computations, equation (2.101) was evaluated to obtain a first order indication of the field data. This data is presented in tabular form in Appendix C.

Some order of magnitude calculations show that, for the frequencies of interest, attenuation in air plays a negligible part in accounting for the observed attenuation rates.*

---

* References 9, 10.

3. Experimental Effort

The purpose of the experimental effort is twofold; namely, a) further verification and reinforcement of the data obtained in stationary tests using the Saturn V booster, and b) a critical test of the theoretical derivations contained in section 2 of this report.

Since theoretical evaluation of boundary value problems is ultimately dependent on determining the appropriate Green's function, the starting phase of the experimental effort consisted of designing and fabricating a good practical simulation of an acoustic point source radiator.

3.1 Spherical Generator System (SGS)

Since simple point sources are not practical the best approximation is one which generates a spherically symmetric wave. In fact, it will be seen in section 3.2 that there are definite limits on the minimum source dimensions if radiator efficiency is desired.

In this case, an SGS capable of exceeding (e.g., 10-15 dB) ambients of 60 dB-SPL* at 1000 feet while radiating broadband random noise (100-1000 Hz) was to have been designed. Considering a typical loudspeaker in this frequency range, we can expect an EIA sensitivity of 50 dB** and distance attenuation (including ground

* dB-SPL is referred to .0002 μ bar.

** Sound pressure in dB-SPL at 30 feet for 1 mwatt electrical input.

cover effects) of 50 dB from 30 feet to 1000 feet. Thus, the speakers used must be able to handle in excess of 1000 electrical watts.

Consistent with these requirements and limitations it was decided that positioning one speaker in each face of a regular polyhedron would accomplish these objectives. Further, it was determined that a dodecahedral geometry with 15" loudspeakers would optimize the conflicting criteria of efficiency, small dimensions, and low cost.

3.1.1 SGS Construction

Having determined the required dimensional parameters, materials were procured for the SGS and construction commenced.

The SGS enclosure consists of twelve individually cut pentagonal plywood panels 1-1/2 inches thick. This thickness was obtained by gluing together two 3/4 inch sheets of plywood. A circular baffle hole of the appropriate dimension was cut in each panel to accommodate an Altec Lansing 421-A loudspeaker, whose specifications are given in Table 3.1.

After the loudspeakers were mounted, the cabinet interior was lined with six-inch thick Fiberglas, the back of the speakers covered with burlap to further attenuate the backwave, and protective metal covers placed over the front of speakers.

Figures 3.1-3.4 show the SGS in various stages of construction. Figure 3.5 shows the SGS suspended from the support

TABLE 3.1

MANUFACTURER'S LOUDSPEAKER DATA

Manufacturer	Altec Lansing
Model Number	421-A
Physical	
Diameter	15 inches
Bolt Hole Diameter	14-9/16
Baffle Hole Diameter	13.5 inches
Weight	21 lbs.
Voice Coil Data	
Impedance (nominal)	8 ohms
Maximum Power, RMS	100 watts
Diameter	3 inches
Voice Coil	Edgewound Copper ribbon
Magnet	
Magnet Assembly Weight	17.5 lbs.
Magnet Material	Ceramic-Ferrimag type V
Flux Density	13,000 Gauss
Total Flux	(Note 2)
Acoustical/Mechanical	
Free Air Resonance	44 Hz
Enclosure Volume/Unit	$\geq$ 3.5 Feet^3
Maximum Peak-To-Peak Excursion	.8 inch
EIA Sensitivity (Note 1)	51 dB
Frequency Range, Upper Limit	2 kHz
Price Per Unit	$52.50 (Note 3)

Notes:

1. Sound pressure level in dB ref. .0002 microbar at 30 feet for 1 milliwatt electrical input.
2. Specification not given.
3. Factory discount price for 12 units or more.

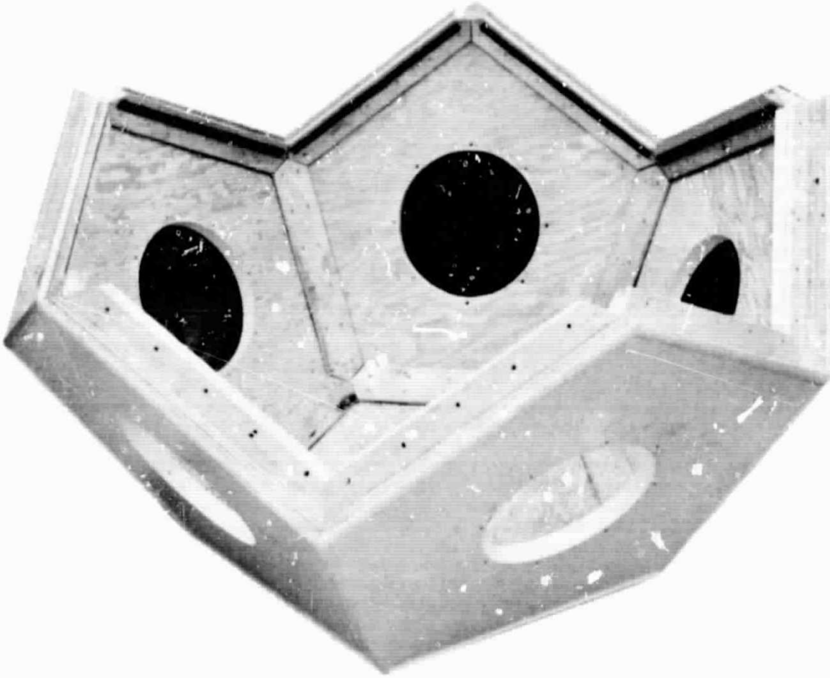

FIGURE 3.1 ONE-HALF OF DODECAHEDRON SPEAKER ENCLOSURE.

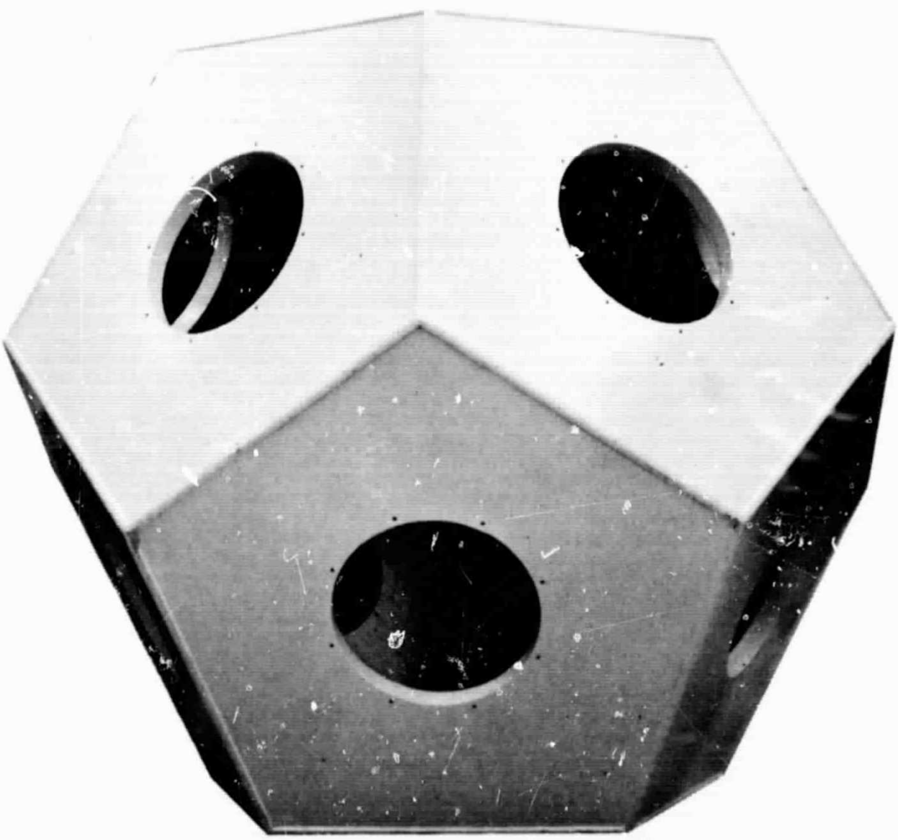

FIGURE 3.2 ASSEMBLED DODECAHEDRON ENCLOSURE.

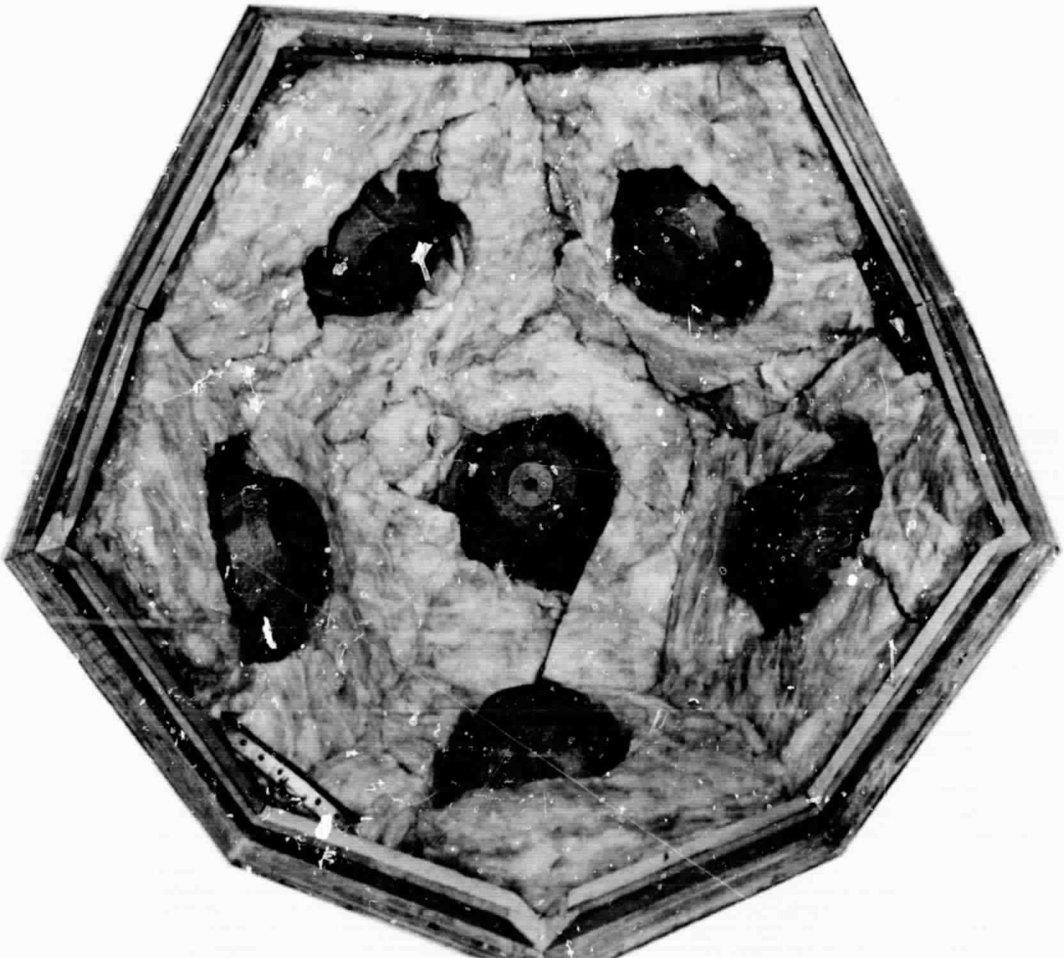

FIGURE 3.3 INTERIOR VIEW SHOWING FIBERGLASS AND BURLAP COVER.

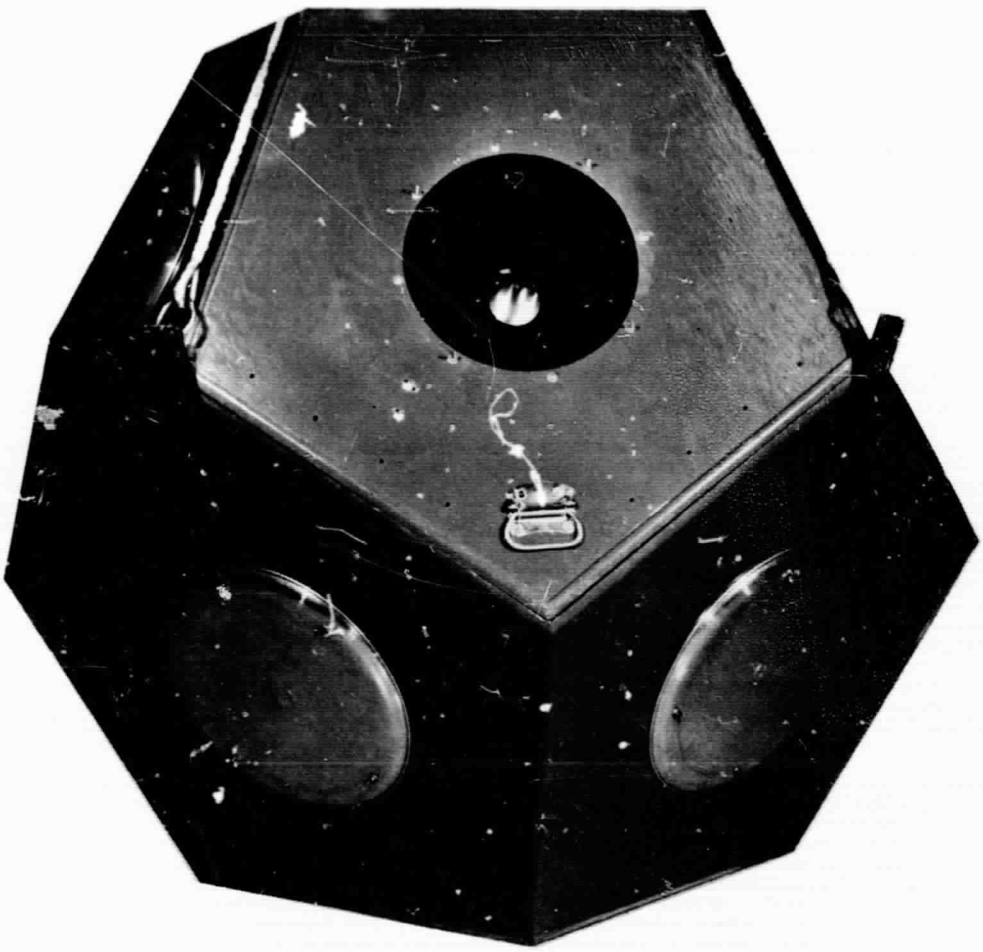

FIGURE 3.4 ASSEMBLED SGS.

FIGURE 3.5 SGS AND SUPPORT TRIPOD.

tripod as it was used in performing the experimental tests in this program.

Completed weight of the SGS is 625 lbs. All speaker terminal pairs are available on the outside so that the SGS can be matched to a variety of impedances.

3.1.2 Calibration of the SGS

After construction was completed, the SGS was transported in two halves to the NSL anechoic test facility for evaluation and calibration. These tests were primarily concerned with measurement of the EIA sensitivity and verification of spherical symmetry. Also of interest was the maximum power handling capacity of the SGS.

Inside the anechoic chamber, the SGS halves were joined and the assembled unit was positioned on a turntable. Electrical connections shown in Figure 3.6 then were completed. Equipment used for testing, in addition to the anechoic facility and its turntable, is listed in Table 3.2.

The frequency response was measured for several SGS and microphone positions and the results were averaged and extrapolated to 30' radius to obtain the EIA sensitivity curve plotted in Figure 3.7. The resultant curve generally lies in the neighborhood of 51 dB, the rated EIA sensitivity of the transducers used. Note the periodically spaced dips which are attributed to internal spherical resonances of the enclosed air. A pronounced peak at 55 Hz corresponds to the speaker resonance.

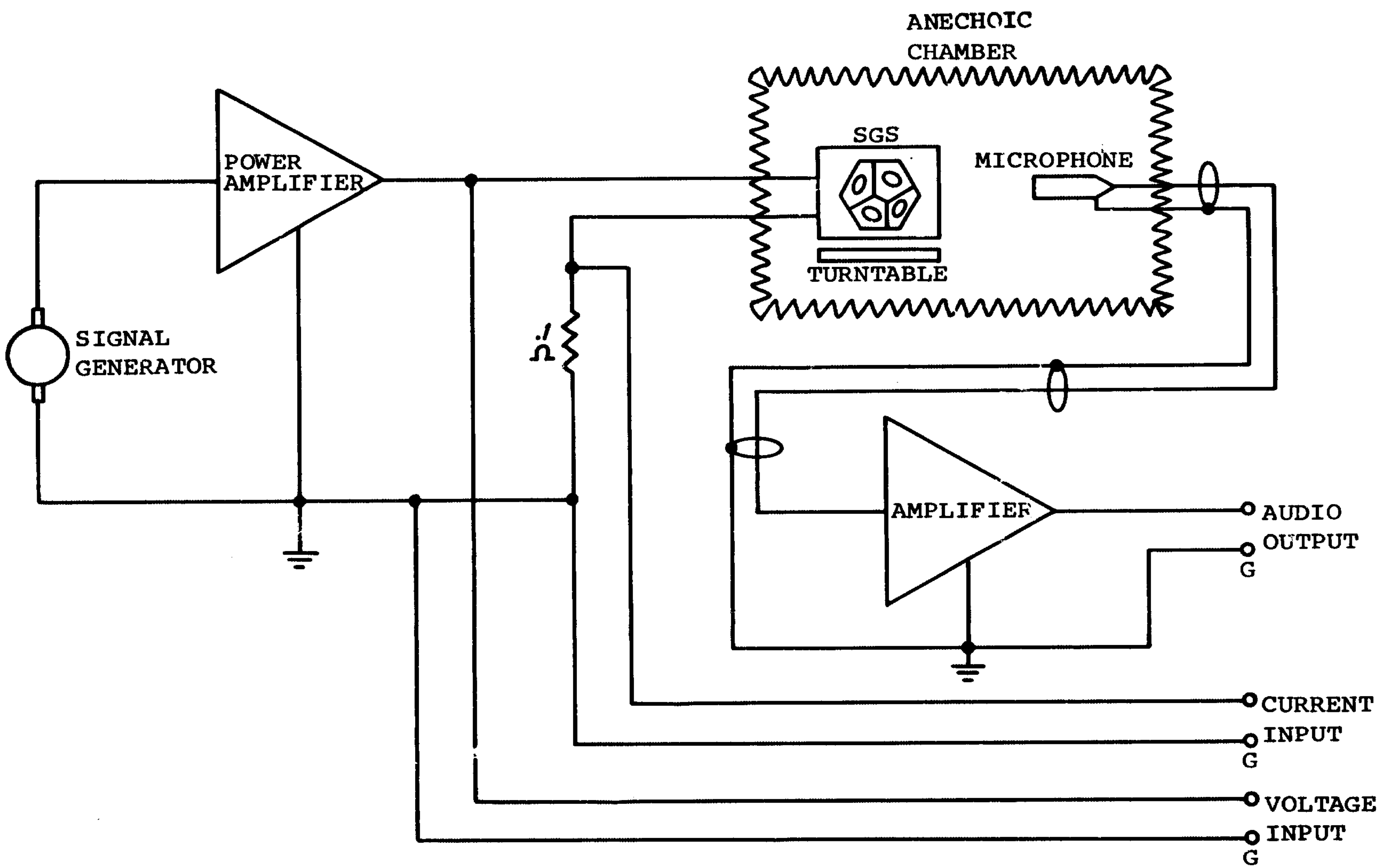

FIGURE 3.6 TEST SETUP -- ELECTRICAL DETAILS.

TABLE 3.2

TEST EQUIPMENT COMPLEMENT.

TEST	SIGNAL GENERATOR	POWER AMPLIFIER	MICROPHONE & AMPLIFIER	OUTPUT MONITOR
EIA Sensitivity Response	Tracking Oscillator of G.R. Spectrum Analyzer,1900-A	Acrosound Ultra-Linear II @ 1mw	B&K - 1" Condenser Microphone	General Radio Spectrum Analyzer & Chart Recorder (1521B)
Spherical Symmetry Test	Sine Wave Oscillator	Acrosound Ultra-Linear II @ 2w	B&K - 1" Condenser Microphone	General Radio Spectrum Analyzer & Chart Recorder
Power Handling Capability	Sine Wave Oscillator @ 22 Hz	3 Acrosound Ultra-Linear II's @ 150w	B&K - 1" Condenser Microphone	General Radio Spectrum Analyzer (used as filter - voltmeter

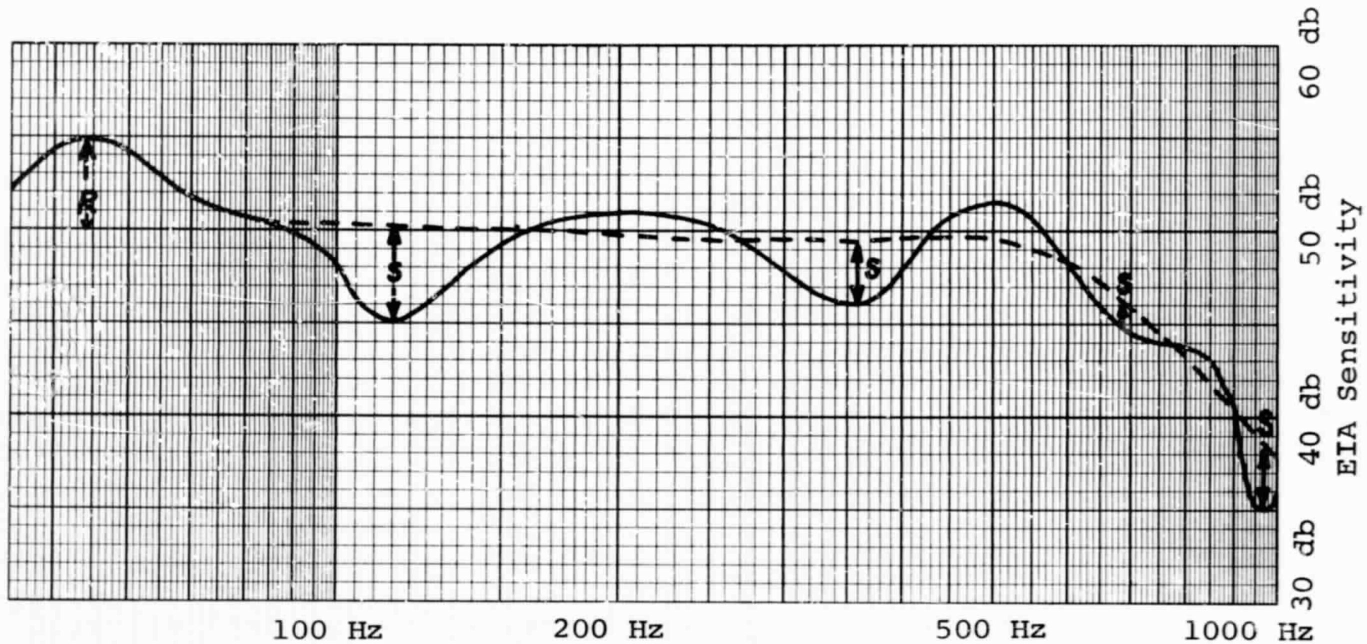

AVERAGE SENSITIVITY INCLUDING NORMAL MODES
APPROXIMATE SENSITIVITY, NORMAL MODES REMOVED
R = LOUD SPEAKER RESONANCE
S = EFFECT OF INTERNAL MODES OF VIBRATION

FIGURE 3.7 EIA SENSITIVITY AS A FUNCTION OF FREQUENCY.

To measure the azimuthal radiation patterns, the turntable rotated the SGS about an axis passing through the center of two opposite faces. In free space conditions, we would expect that any asymmetry at the azimuth would be a tenfold one.

This is, however, not the case, as the graphs of Figure 3.8a show a definite fivefold repetition per 360° rotation of the SGS for single frequencies greater than 250 Hz. The explanation for this lies in the fact that the bottom speaker faced the turntable so that free space conditions of symmetry do not actually prevail.

One-third octave random noise tests illustrated in Figure 3.8b indicate that the asymmetry still exists above 250 Hz, but the nulls are not as pronounced for this test mode.

Finally, referring back to Figure 3.8a, it is seen that the pattern is essentially spherical ($\pm$.5 dB) at 250 Hz. Tests at frequencies below 250 Hz gave rise to even flatter characteristics.

Next, the SGS was fed a 22 Hz signal at 150 watts before substantial harmonic distortion became evident. At this power level, peak to peak excursions of 1/2" could be observed. While this is close to the limit of excursion for the particular speaker used, it is safe to assume a fivefold increase in power can be tolerated at a frequency five times as great, i.e., $\sim$ 100 Hz.

Full power tests (1200 watts) could not be performed under this program since amplifier power was not available.

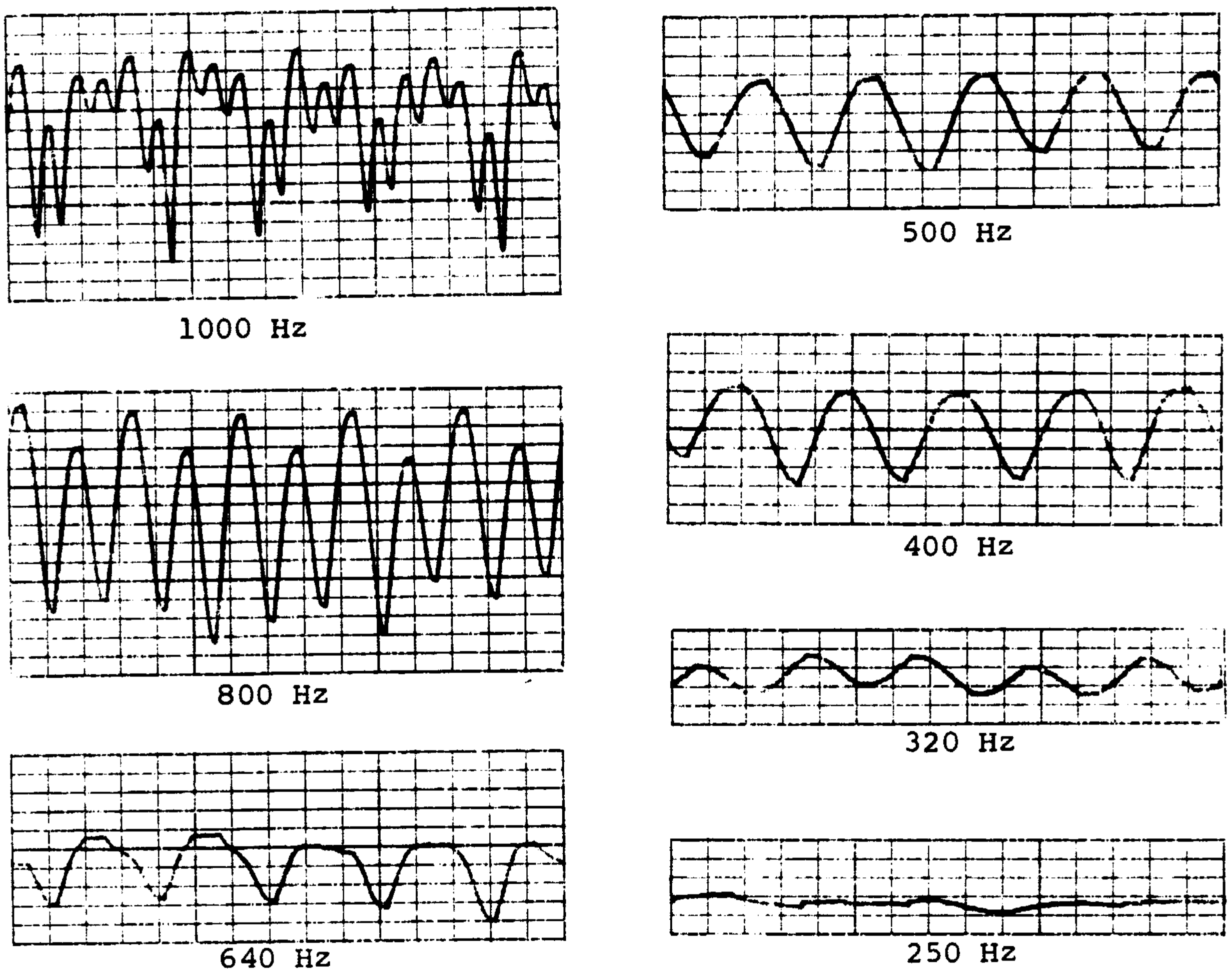

a) Sine Wave tests, 6 frequencies

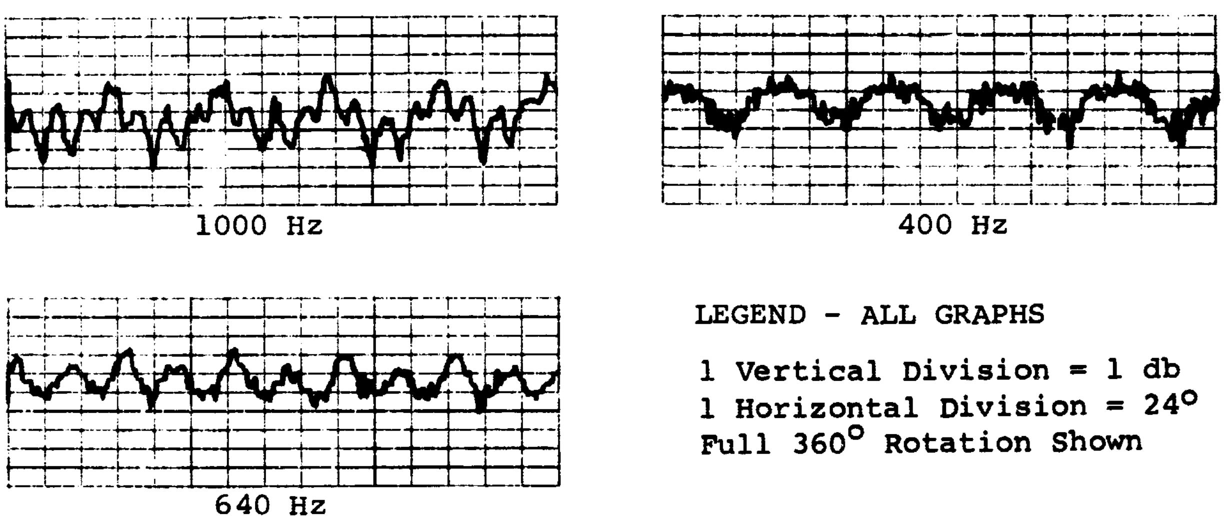

b) 1/3 Octave Random Noise Tests, 3 center frequencies.

FIGURE 3.8 ANECHOIC CHAMBER TESTS FOR AZIMUTHAL SYMMETRY OF SGS RADIATION PATTERN @ TEN FEET.

However, the arrival of a Crown DC 300 amplifier did allow outdoor and on-site testing at 300 watts, 6 dB below full power. Addition of an identical DC-300 would easily triple the input because of an improved impedance match between amplifiers and the SGS load.

3.1.3 Capabilities and Limitations

Based on the data and information in the preceding paragraphs, the SGS designed under this program appears to be capable of handling 1000 watts of electrical power in the form of broadband random noise (100 Hz-1000 Hz).

Sine wave tests indicate that the radiation pattern below 250 Hz is extremely uniform, being spherical to within $\pm \frac{1}{2}$ dB at the worst case frequency. At higher frequencies, this uniform pattern breaks up. The outdoor tests with broadband random noise revealed that this pattern was audible when the SGS was rotated, even at great distances.

In all other regards, the SGS performed at its design values.

3.2 Source Theory

To aid in SGS evaluation and recommendations regarding future areas of investigation, some aspects of source theory are presented in this section.

3.2.1 Table of Symbols

In addition to symbols listed in paragraph 2.1 the following also apply to section 3.2.

A_{mn} = expansion coefficients for spherical harmonics.

c = velocity of sound.

$h_m(z)$ = half integer Hankel function of argument z.

$P_n^m(\cos\theta)$ = Legender's associated function of the first kind.

$p(r)$ = pressure as a function of r only.

$p(r, \theta, \phi)$ = pressure as a function of r, θ, ϕ.

$Q_{x....z}$ = multipole moment.

r = radius from source, i.e., radius in spherical coordinates with source at origin.

$V(r)$ = radial velocity as a function of r.

$Y_{mn}(\theta, \phi) = Y_{mn}$ = spherical harmonic.

ζ = source impedance ratio referred to specific impedance of medium.

θ = z-axis angle in spherical coordinates.

ϕ = azimuthal angle in spherical coordinates.

$\psi(r)$ = velocity potential as a function of r.

$\psi(\mathbf{x})$ = velocity potential as a function of position vector, $\mathbf{x}$.

3.2.2 Analysis

In analyzing sources, we consider first the case where the source has finite dimensions and is indeed spherically symmetric, i.e., the pulsating sphere. In a free space environment, such a source, if located at the origin, will have the: velocity potential;

$$\psi(r) = \frac{Q}{4\pi} \frac{e^{ikr}}{r} \tag{3.1}$$

radial velocity;

$$v(r) = \frac{Q}{4\pi} \frac{e^{ikr}}{r^2} (1 - ikr) \tag{3.2}$$

and pressure field;

$$p(r) = -i\rho\omega\psi(r) \tag{3.3}$$

Next we consider the impedance ratio ζ, of a sphere of radius a.

This will be given by

$$\zeta = \frac{-ika}{(1 - ika)} \tag{3.4}$$

Note that if the sphere is sufficiently large ($ka \gg 1$), its impedance approaches that of the medium. Referred to this ideal condition, the power radiation efficiency of the source will be reduced by 3 dB when

$$a \cong \frac{\lambda}{2\pi} = \frac{c}{2\pi f} \tag{3.5}$$

Hence, if better than 50% of the attainable efficiency is to be realized at frequencies over 80 Hz, then the source radius must be at least two feet.

A second factor dictating source dimensions, is concerned with the physical characteristics of the transducer. High efficiency 15" loudspeakers generally require 3.5 to 4 feet^3 of baffle volume if the lower frequency resonance is not to be increased. Further, the possibility of damage to the speaker cone and its suspension is greatly increased when baffle volumes are inadequate and the speaker is worked near its excursion limits. Coincidentally, this criterion also dictates a radius near 2½ feet.

It has already been seen that the current SGS design is limited by asymmetries in the radiation pattern above 250 Hz. With the view that the effect of these anomalies should be analyzed, some of the applicable techniques are outlined below.

The velocity potential from an arbitrary spherical source located at the origin can be written

$$p(r, \theta, \phi) = \sum_{m=o}^{\infty} \sum_{n=-m}^{m} A_{mn} h_m(kr) Y_{mn}(\theta, \phi) \tag{3.6}$$

where

$$Y_{mn}(\theta, \phi) = \sqrt{\frac{2m+1}{4\pi}} \frac{(m-n)!}{(m+n)!} P_m^n(\cos\theta) e^{in\psi} \tag{3.7}$$

On the azimuth, $\cos\theta = 0$ and

$$P_m^n(0) = \frac{(m+n-1)!\ \cos\left[(m-n)\frac{\pi}{2}\right]}{2^{m-1}\left[\frac{1}{2}(m-n)\right]!\left[\frac{1}{2}(m+n)-1\right]!} \tag{3.8}$$

Hence, if the azimuthal amplitude and phase pattern is known, a simple Fourier analysis would yield a partial set of the complex A_{mn} corresponding to even values of m+n.

This is not a serious limitation since we can rotate around more than one axis and use the addition theorem of spherical harmonics. In particular, the following three rotation axes possess obvious symmetry which tends to ease computations:

a) Axis through the center of two opposing faces $\rightarrow$ tenfold symmetry.

b) Axis through two opposing vertices $\rightarrow$ sixfold symmetry.

c) Axis through the midpoints of two opposing edges $\rightarrow$ twofold symmetry.

3.2.3 Incorporation into Theory

The incorporation of the evaluations discussed in the previous paragraph can be carried over into the theory by either of two techniques:

a) Each of the A_{mn} corresponds to a linear combination of Cartesian point multipoles. These latter, according to their order, correspond to successive gradient operations on the point source Green's function, $\frac{e^{ikr}}{r}$. Hence, the complex Cartesian octupole moment, Q_{xyz}, would prescribe the velocity potential given by

$$\psi(x) = Q_{xyz} \frac{\partial}{\partial x} \frac{\partial}{\partial y} \frac{\partial}{\partial z} \left(\frac{e^{ikr}}{r} \right) \tag{3.9}$$

Relating to the moments in other coordinate systems is accomplished through knowledge of the transformation metrics and of the Christoffel symbol representation for the various differential operations.*

b) A second technique calls for re-evaluation of the ground plane problem in bi-spherical coordinates. This would be a very risky operation since the relevant separated functions are virtually unexplored.

In any event, the coordinates of the spherical surface would be only slightly perturbed from those in spherical coordinates. Hence, the A_{mn} obtained by techniques of paragraph 3.2.2 could be applied directly.

3.2.4 <u>Modification of SGS</u>

Since incorporation of SGS imperfections into the theory appears to heap laborious manipulations on what is already a difficult process, it is felt that some form of SGS modification to make it more spherical, or the introduction of a second smaller

* Reference 18.

SGS for frequencies in the range of 250 - 1000 Hz merits attention.

The frequency range in question comprises, roughly, a four-to-one ratio between upper and lower limits. Since the existing SGS experiences no difficulties in covering a similar range (80 - 250 Hz), a scaled down version with dimensions 1/4 to 1/5 those of the large unit would accomplish this objective.

Another benefit of this approach is the reduced power requirement of the midrange SGS since typical EIA sensitivities for speakers in this frequency range increases to 56 dB, and ambients are lower over this range.

Alternatively, 5 inch or 6 inch midrange speakers could be incorporated at the vertices of the existing SGS. Because of the high back pressures associated with low frequency operation of the SGS, these units would require separate baffling. Also their level and possibly their amplitude and phase response would require adjustment to minimize the asymetries.

As another possibility, the exterior of the SGS could be built up so that each speaker looks out into free space through a horn. As a result of this gradual matching to free space, diffraction effects are greatly reduced and the range of the source is extended. The obvious difficulty is that this technique greatly increases the bulk and handling problems associated with the SGS.

While both of the modification methods would yield improvement, they would probably extend the range of spherical symmetry no higher than 500 Hz.

3.3 Impedance and Propagation Constant Measurements

As mentioned previously, complete knowledge of acoustic wave propagation requires specification of the complex quantities, ζ, n, and ν. By virtue of various constitutive relationships, this reduces to the specification of at least three of the six real numbers at each frequency.*

The discussion that follows outlines two *in situ* test techniques for evaluating these constants locally. Unfortunately, this type of testing is not well documented. Attempts to apply mathematically tractable boundary conditions to the first met with only partial success. The second constitutes a new technique requiring additional hardware, but makes use of a special case of existing theory developed in section 2.

3.3.1 List of Symbols

In addition to symbols listed in paragraph 2.1, the following apply to section 3.3.

B = total velocity flux

f(x,y) = Velocity potential or velocity profile.

L_a, L_b = Distance from surface under test to first null, normal and angle incidence measurement respectively.

---

*Reference 2, p 840. Also note that on the basis of this reference and paragraph 2.4.4, that five real numbers will completely define propagation in porous media at all frequencies.

M_a, M_b = Standing wave ratios, normal incidence and angle incidence, respectively.

v = Normal velocity

v_o = Normal velocity amplitude

α, β = Impedance Parameter, see eqn's 3.10 and 3.11

ζ_a, ζ_b = Termination impedances as determined from normal incidence and angle incidence measurements respectively.

ζ_r = Correction for "rigid" termination expressed in terms of the impedance ratio.

Λ_a, Λ_b = Displacement of null from position of rigid null for normal and angle incidence measurements respectively.

σ_a, σ_b = Real part of ζ_a and ζ_b.

τ_a, τ_b = Imaginary part of ζ_a and ζ_b.

ψ = Velocity potential

ψ_o = Velocity potential amplitude

3.3.2 Theory - Impedance Tube

The standard impedance tube utilizes an acoustic transmission line as the basis for evaluating the impedance of a boundary. A small probe tube is used to monitor the interior acoustic field without appreciably altering it.

A diagram illustrating the use of a impedance tube is shown in Figure 3.9. As a result of a linear interaction of the incident and reflected wave, a standing wave pattern develops. In the normal incidence case, (a), it is possible to evaluate the specific acoustic impedance ratio by measuring the two quantities, M_a (in dB) and L_a (in wavelengths) from which

$$\alpha = \coth^{-1}\left[10^{M_a/20}\right] \tag{3.10}$$

$$\left.\begin{aligned} \beta &= 2\,\pi\,\Lambda_a \\ \Lambda_a &= \frac{L_a}{\lambda} - .25 \end{aligned}\right\} \tag{3.11}$$

and

$$\zeta_a = \sigma_a + i\tau_a = \coth\,(\alpha + i\beta) \tag{3.12}$$

For angular incidence, (b), the wave interacts twice with the impedance under test, and once with a "rigid" termination. For this case the formulism prescribes

$$\zeta = \left[\frac{1}{\zeta_r}\coth\,(\alpha + i\beta)\right]^{\frac{1}{2}} \tag{3.13}$$

with α and β being given in terms of M_b and Λ_b by relationships similar to those of equations (3.10) and (3.11).

If we are willing to ignore diffraction effects, then ζ can be computed from equation (2.102), i.e.,

$$\zeta = \frac{1}{\nu}\left[n^2 - \sin^2\theta\right]^{-\frac{1}{2}} \tag{3.14}$$

Using this relationship, normal incidence data from the three test sites was processed and is shown in Figure 3.10.

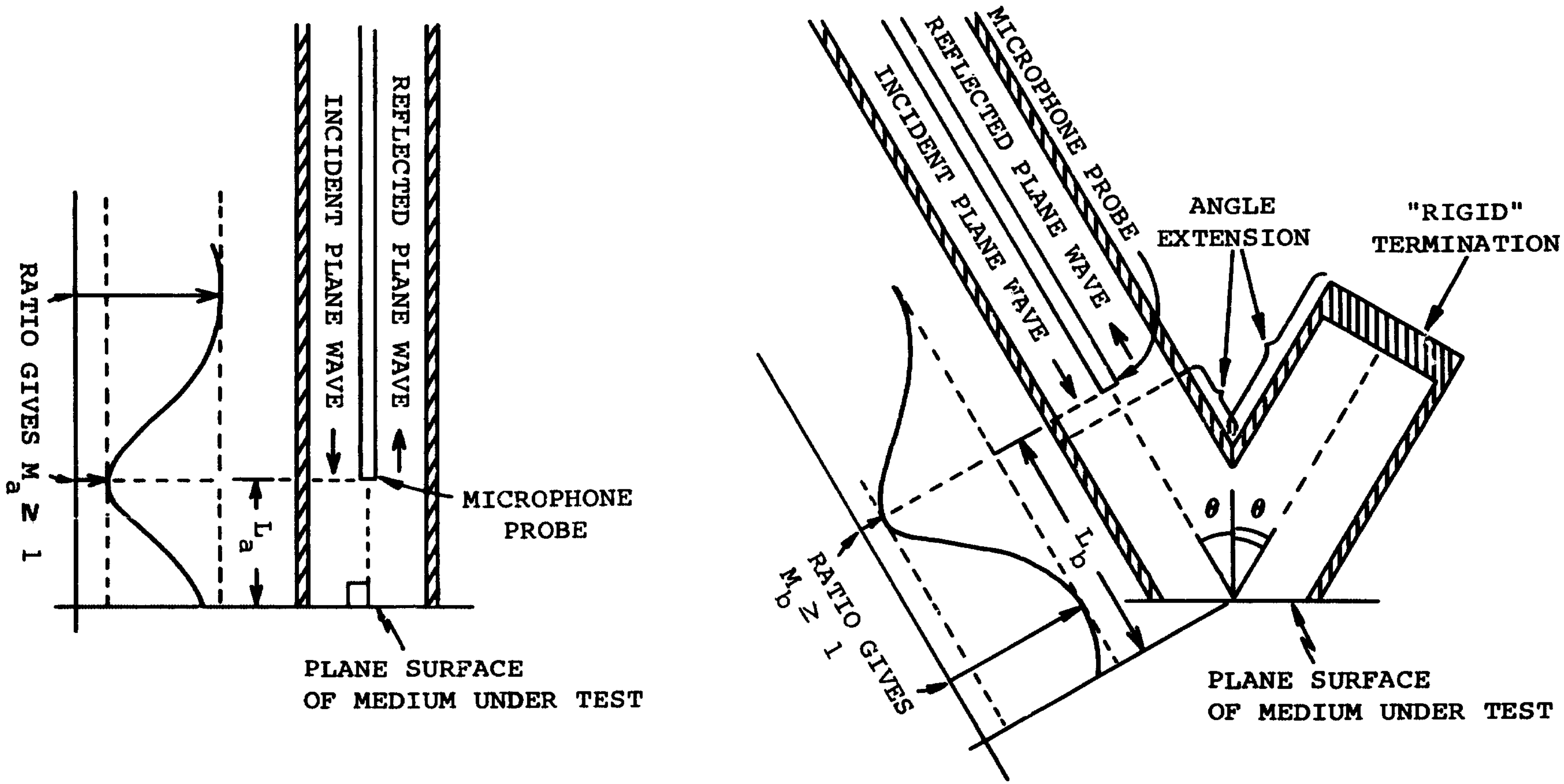

a) NORMAL INCIDENCE

b) ANGLE θ - INCIDENCE

FIGURE 3.9 IMPEDANCE TUBE METHODS FOR OBTAINING <u>IN SITU</u> INFORMATION ON THE GROUND IMPEDANCE.

Comparison of the amplitude data with the theory developed in section 2.4.4 shows general agreement in the location of break points. However, slopes are twice that predicted by theory indicating that diffraction effects are indeed involved, and that a relationship like

$$\zeta \propto \left[\coth(\alpha + i\beta) \right]^{\frac{1}{2}} \tag{3.15}$$

may actually result from the diffraction effects. Also, a phase maximum of 45° is exceeded by almost a factor of 2.

Actually, this result is quite plausible when we consider that, for $|\zeta| >> 1$, diffraction effects should approach the usual impedance tube limits, and as ζ becomes much less, the reduction of impedance, because of diffraction, should be proportional to the non-corrected impedance.

On the other hand, the phase data of Figure 3.10 is much more difficult to explain, and, in order to better interpret this and the amplitude data, an attempt to solve boundary value problem of <u>in situ</u> impedances was begun.

For the general case of angular incidence at an angle, θ, we have

$$\left.\begin{array}{l} \left.\begin{array}{l} \psi = \psi_o \; f(x,y) \, e^{ikx \sin\theta} \\ \quad \text{or} \\ v = v_o \; f(x,y) \, e^{ikx \sin\theta} \end{array}\right\} \left\{ \begin{array}{l} |x| < \\ \qquad \frac{1}{\cos\theta} (a^2 - y^2)^{\frac{1}{2}} \end{array}\right. \\ \psi \cong 0 \qquad \text{for} \qquad |x| > \frac{1}{\cos\theta} (a^2 - y^2)^{\frac{1}{2}} \end{array}\right\} \tag{3.16}$$

for which the geometry of Figure 3.11 applies.

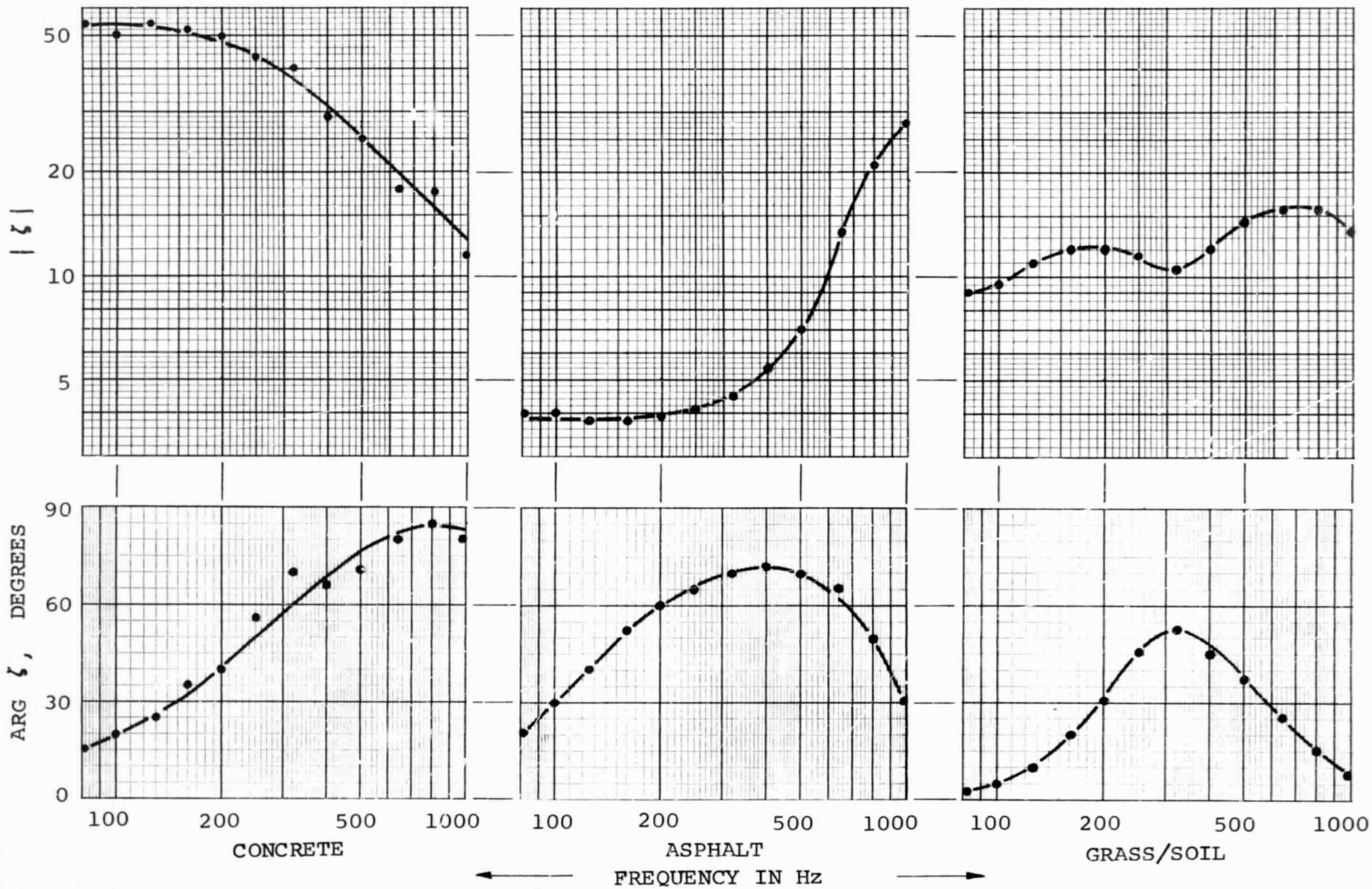

FIGURE 3.10 COMPLEX IMPEDANCE RATIO AS A FUNCTION OF FREQUENCY FOR THE THREE GROUND COVERS INVESTIGATED.

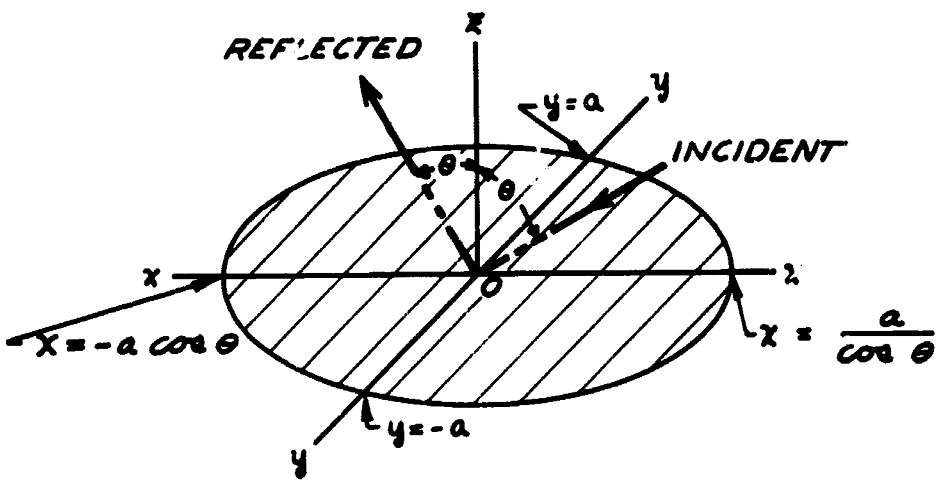

FIGURE 3.11 GEOMETRY OF BOUNDARY CONDITIONS.

Note that we are free to choose either Dirichlet or Neumann boundary conditions inside, as in equation (3.15), or the ratio of ψ to v. The condition of $\psi = 0$ outside is based on the absence of an audible signal in all tests conducted to date and corresponds to imposing a force-free boundary.

In the only case worked so far, the normal incidence boundary conditions ($\theta = 0$) were used in order to develop a feeling for the calculations involved. The velocity potential profile, f(x,y) of Figure 3.12a was assumed. The resultant integral for velocity flux was

$$B \propto \int_0^{\infty} \frac{J_1^{\,2}(\xi)}{\xi} \quad (\xi^2 - \xi_o^{\,2})^{\frac{1}{2}}\, d\xi \qquad (3.17)$$

which is a form of Sonine's integral*. Evaluated for the real part from 0 to ξ_o, the integral will give a value, but the imaginary part, from ξ_o to ∞, diverges.

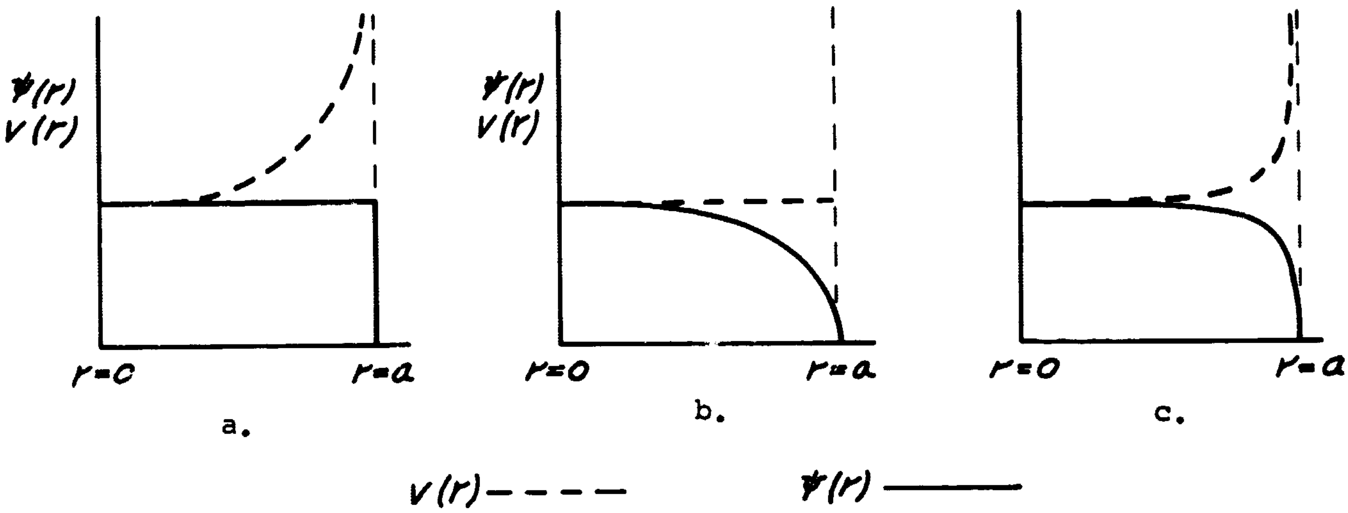

FIGURE 3.12 VELOCITY AND VELOCITY POTENTIAL PROFILES AT BOUNDARY INSIDE OF A NORMALLY INCIDENT IMPEDANCE TUBE.

A second boundary condition, shown in Figure 3.12(b), is mixed, i.e., v is specified inside and ψ outside. It represents the opposite extreme of the conditions already discussed and is solved by assuming a uniform velocity dipole layer over the termination. The average pressure over this area is ultimately desired.

* Reference 30, p 417.

It is expected that the actual boundary condition lies somewhere between the two cases, i.e., that shown in Figure 3.12(c).

3.3.3 Point Source Technique

A second *in situ* technique would utilize a point velocity source applied to the surface under test, and velocity sensitive pickups at fixed distances from the source.

This new source would be a dipole along the z-axis, so that an operation, $\frac{\partial}{\partial z}$ would be performed on the $V(g_1, g_2; r)$ already derived in section 2. Further, we are interested in the z-component of the velocity, which is obtained through the operation, $-\frac{\partial}{\partial z}$. After performing these differentiations, g_1 can be set equal to zero; so that the resultant three-term asymptotic expressions would be much simpler than those derived in section 2.

3.4 Site Testing

Site testing was concerned with performing experimental measurements of the local acoustic propagation parameters for the lower or ground medium, and of the large-scale sound pressure field radiated from a spherically symmetrical source as a function of source height, receiver height, source to receiver distance, and frequency.

The former data is to be converted into a form suitable for evaluation of the various functions, $K(g_1, 0; r)$, as listed in paragraph 2.5.1. In the large scale test, broadband random noise, as previously described, was radiated and recorded on Data from the experiment was obtained by 1/3 octave band analysis of loop tapes covering frequencies from 80-1000 Hz.

A brief description of the test sites is outlined in Table 3.3. Note that all of these sites exhibit lower ambients than the 60 db expected level (paragraph 3.2). This is fortunate in view of the reduced operating level of the SGS.

Additional features of these sites are their flatness and dimensions which proved to be ideal in all cases. They also gave rise to an excellent spread in impedance data, as already seen in Figure 3.10.

3.4.1 Propagation Measurements of Medium 2

Impedance tube measurements were conducted at each test site for both normal incidence, which gave values of impedance, and at two angles, i.e., $\theta = 30^{\circ}$ and 60°, to obtain information concerning a real constant, A, such that

$$A = Z \frac{k_2}{k'} \tag{3.18}$$

and

$$\zeta_2 = An \tag{3.19}$$

where quantities other than A are defined and discussed in paragraphs 2.4.1 and 2.4.4, respectively.

TABLE 3.3

TEST SITE DATA

LOCATION & GROUND COVER	AMBIENT NOISE LEVEL, dB, SPL	WIND	TEMPERATURE & REL. HUMIDITY	DIMENSIONS OF GROUND COVER UNDER TEST	A (CONSTANT DEFINED IN EQ. 3.18)
Rosecroft Gravel over Asphalt	< 55 dB during tests	2 - 4 knots Perpendicular	89^{o} F 79%	300 ft W 1400 ft L	10
Dulles Int. Arpt. Concrete	< 50 dB during tests	Undetectable (< 2 knots)	69^{o} F 49%	75 ft W * >>1000 ft L	65
Dulles Int. Arpt. Grass	< 52 dB during tests	2.5 knots Max. Parallel toward SGS	78^{o} F 48%	200 ft W >>1000 ft L	16

* Site consisted of a concrete run-up strip, 75 ft wide with asphalt shoulders 25 ft wide on either side, and flat grass extending indefinitely beyond.

Additional tests, aimed at evaluating A, included: a hammer tap test in which the time of arrival for the fastest wave was recorded; and break point analysis as discussed in the aforementioned paragraph. All three techniques gave A's within 10% of one another. Once in possession of this constant and the impedance ζ, all other physical features relevant to propagation can be determined. Values of this constant for the three surfaces investigated are given in Table 3.3. Graphs showing the location of the first order pole as computed by equation 2.94 are shown in Figure 3.13.

Photographs showing the impedance tube extensions and their application to angular incidence measurements, are shown in Figures 3.14 - 3.16. The series of photographs in Figure 3.16 also illustrates the use of caulking compound in effecting a good air seal which is imperative if meaningful measurements are to be obtained.

3.4.2 Large Scale Test

As previously mentioned, the large scale test is concerned with measuring four parameters associated with the radiated sound pressure field. Specifically, variation of pressure with respect to the following ranges of variables in all combinations is desired:

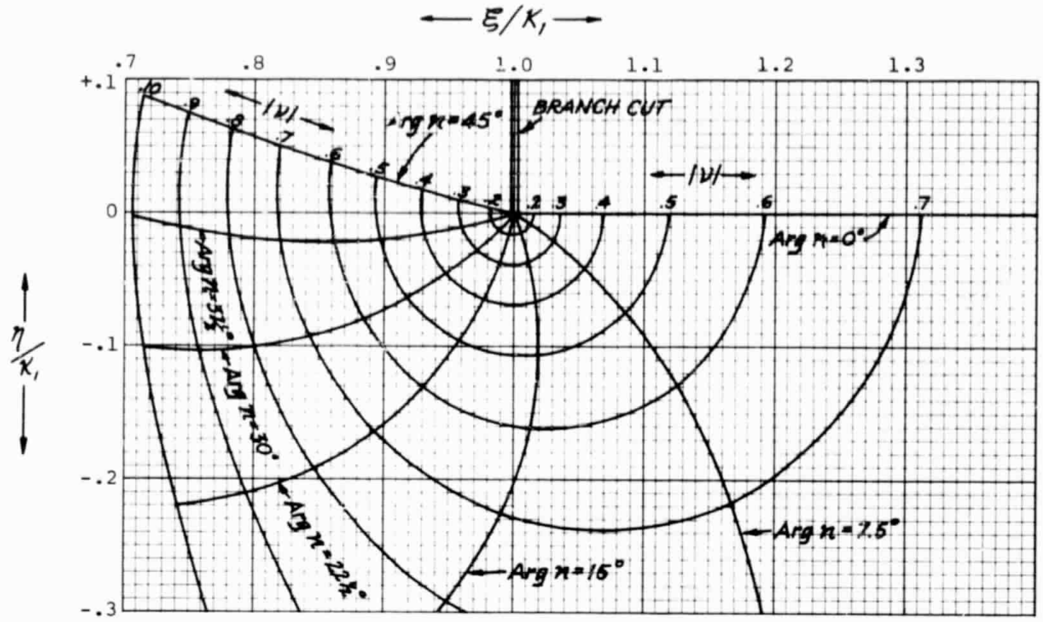

a) POLE LOCATION IS $\frac{K}{K_1}$ PLANE AS A FUNCTION OF $|\nu|$ AND Arg n, $|n| = .5$

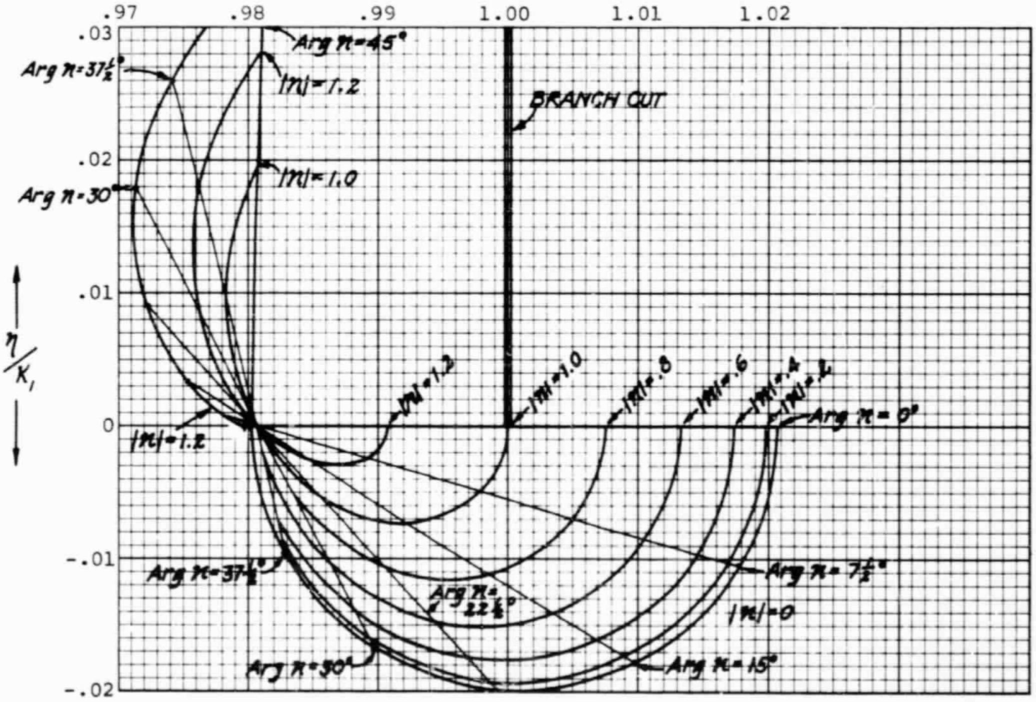

b) POLE LOCATION IS $\frac{K}{K_1}$ PLANE AS A FUNCTIC" OF $|n|$ AND Arg n, $|\nu| = .2$

FIGURE 3.13. POLE POSITION RELATIVE TO k_1.

FIGURE 3.14 ANGLE OF INCIDENCE EXTENSIONS FOR THE ACOUSTIC IMPEDANCE TUBE.

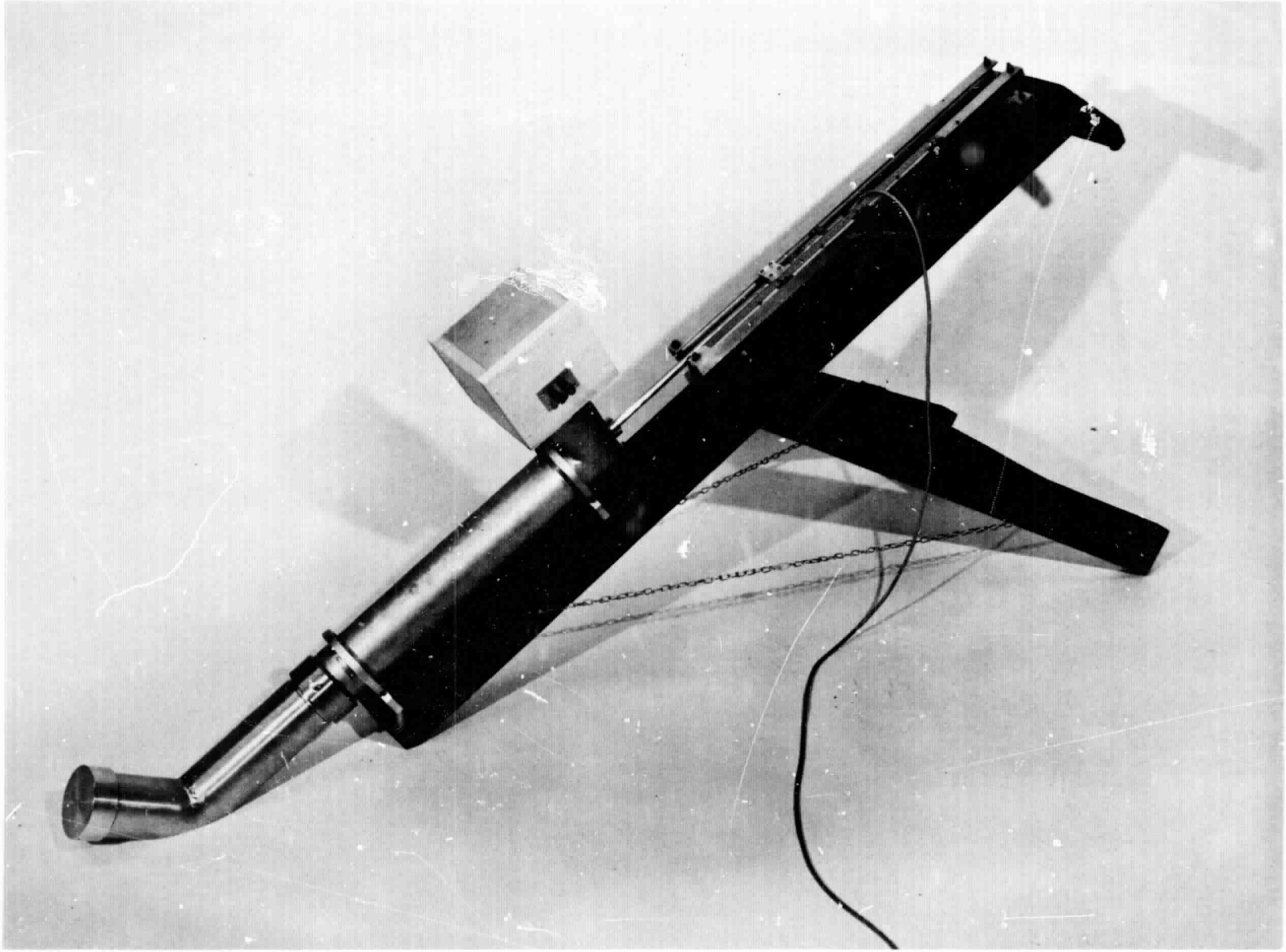

FIGURE 3.15 IMPEDANCE TUBE SET-UP FOR 60° ANGLE-OF-INCIDENCE MEASUREMENTS

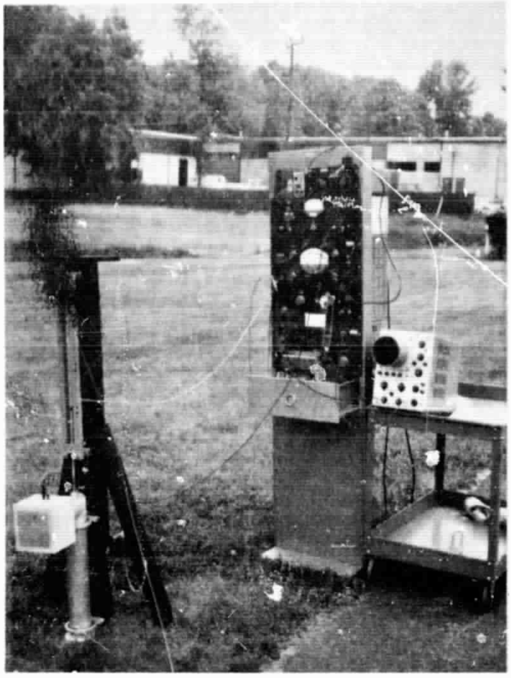

a) Normal Incidence

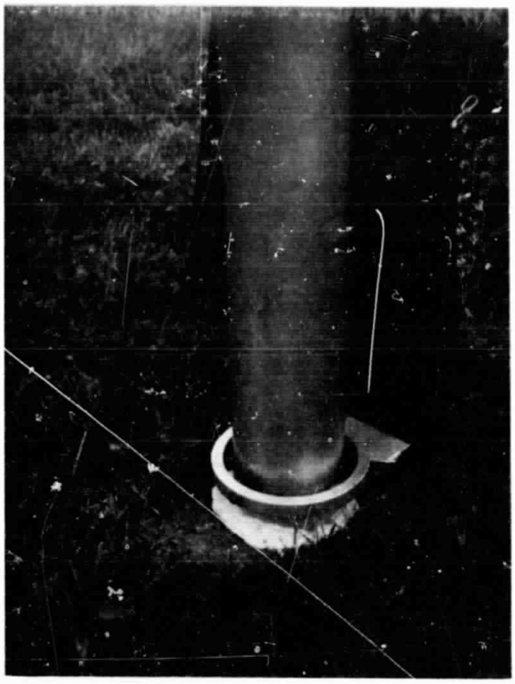

b) Normal Incidence - Close up

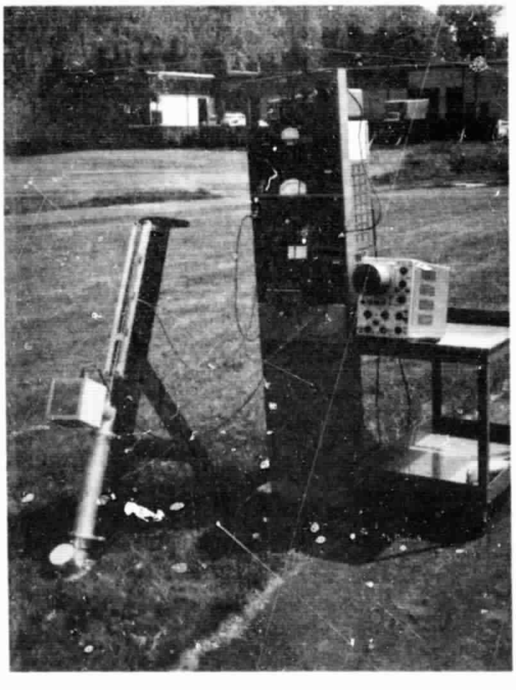

c) 30° Incidence

d) 30° Incidence - Close up

FIGURE 3.16. EARTH TESTS USING ACOUSTIC IMPEDANCE TUBE AND ITS MODIFICATIONS

a) Source height, h: $\left[5 \leq h \leq 30 \right]$ ft.

b) Microphone height, z: $\left[5 \leq z \leq 30 \right]$ ft.

c) Source-Microphone distance, r : $\left[30 \leqslant r \leqslant 1000 \right]$ ft.

d) Frequency, f: $\left[80 \leqslant f \leqslant 1000 \right]$ Hz.

e) Ground cover acoustic propagation characteristics - 3 different covers were tested.*

Because of the great size of the SGS and the attendant costs of hoisting it safely to heights of 30 feet, variation of the parameter, h, was not carried out in these tests. This does not represent a great loss to the experimental program since the well established principle of reciprocity can be used.

Further, the functions that are under critical analysis here, i.e., $K^{(2)}$, $K_p^{(1)}$ and $K_s^{(1)}$, are all functions of $g_1 = h + z$. Hence, as far as these kernels are concerned, $h = 30$ and $z = 30$ is equivalent to $h = 5$ and $z = 55$.

Since the interfering effects of wind are to be avoided, it is desirable to gather as much data as is possible on a simultaneous basis. Hence, the reason for using random noise covering the frequency range above is established. Further, the correlation of random noise transmitted through an arbitrary transfer function gives the impulse response corresponding to that transfer function.

---

* Because of the onset of continuously unsettled weather at the end of June, a fourth test site was dropped from the program.

In addition, it would be desirable to position an array of microphones at many discrete combinations of z and r and to record their output for later analysis. Since NSL does not presently own a large number of microphones, microphone preamplifiers, and the multi-channel (e.g. 14) tape recorder necessary for this elaborate test, its cost would exceed current availability of funds.

Accordingly, a compromise test program was adopted using two microphones and a two-channel tape recorder. The microphones were positioned according to the following plan:

Microphone No. 1 (control) at $r = 250$ ft. and

$z = 5$ ft. at all times. *

Microphone No. 2 (moved)

$r = 31.25$ ft., $z = 5$ ft.	$r = 31.25$ ft., $z = 10$ ft.
$r = 62.5$ ft., $z = 5$ ft.	$r = 31.25$ ft., $z = 20$ ft.
$r = 125$ ft., $z = 5$ ft.	$r = 31.25$ ft., $z = 30$ ft.
$r = 250$ ft., $z = 5$ ft.	$r = 125$ ft., $z = 10$ ft.
$r = 500$ ft., $z = 5$ ft.	$r = 125$ ft., $z = 20$ ft.
$r = 1000$ ft., $z = 5$ ft.	$r = 125$ ft., $z = 30$ ft.

In order to obtain readings at greater than $z = 5$ ft., the microphone stand shown in Figures 3.17 and 3.18 was devised.

Instrumentation for these tests included:

---

* If atmospheric stability warranted, this microphone also was moved to speed up the testing procedure.

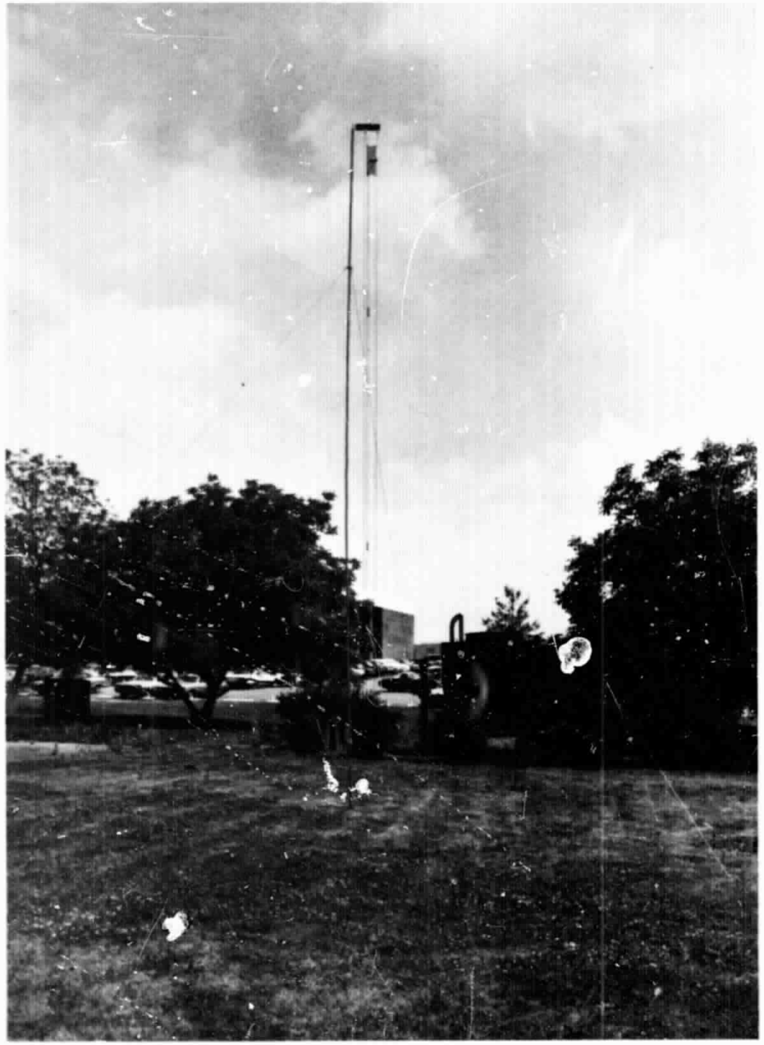

FIGURE 3.17 MICROPHONE STAND FOR THIRTY FOOT MEASUREMENTS.

FIGURE 3.18 CLOSE-UP VIEW OF MICROPHONE SUPPORT.

General Radio	Random Noise Generator
Crown DC-300	Power Amplifier
Bruel & Kjaer	1/2" Condenser Microphone
Bruel & Kjaer	Amplifier Complement
General Radio	2-Channel Tape Recorder

Other instrumentation included voltage amplifiers, VTVMS, and high/low-pass filters.

Recorded tapes were returned to the laboratory facilities where they were spliced into small continuous loops corresponding to the test configurations above, and analyzed into 1/3-octave bands.

3.4.3 Pressure Field Data

The data, consisting of rms voltage measurements of the above loops was analyzed and is presented in graphical form in Appendix D.

4. Conclusions

4.1 Summary of Findings

In investigating the linear theory of point source propagation in the presence of a porous medium, some heuristic reasoning was applied to a three term asymptotic series in order to determine some of the far field effects. This theoretical model does predict a frequency dependent field that ultimately attenuates at the rate of 12 dB/double distance in the neighborhood of the interface -- more than twice the rate of a simple point source in free space.

While computation using this formulation would have been highly desirable, available funds did not allow for completion, debugging, and execution of a computer program that was this elaborate. Hand computation for one frequency, radius, and summed height required in excess of two man-days, and gave dubious results.

Since some theoretical formulation predicting excess attenuation of velocity potential* is better than none at all, equation (2.101) was programmed for computer evaluation at heights, radial separations, frequencies and ground cover impedances encountered in the experimental effort. As mentioned

---

* Excess attenuation is that above and beyond the 6 dB/double distance predicted for the same point source operating in free space conditions. Excess attenuation for pressure field velocity potential will be equal.

in paragraph 2.5, validity of equation (2.101) as an approximation is restricted to frequencies sufficiently great that $(h + z) > $ wavelength, i.e., 100 Hz for $h = z = 5$ ft.

Explanatory notes, the computer program described above, and the data print-out are presented in Appendix C. This excess attenuation data was compared with the corresponding experimental data graphically presented in Appendix D. While agreement is not exact, a result of comparing discrete frequency and random noise situations, a distinct correlation exists with regard to such major features as frequency and distance effects.

Both sets of data predict excess attenuation rates that become substantial at intermediate frequencies exhibiting a pronounced dip in the 100-1000 Hz range.

It should be noted that the theoretical approach cited above applies to discrete frequencies and ignores the possible influence of one of the ground waves.

4.2 Recommendations for Future Study -- A Five-Point Program

Consistent with the findings and experiences of this effort, the following five-point effort is recommended to refine both the theoretical and experimental aspects of point source radiation in the presence of a reflecting and refracting plane.

4.2.1 Extension of the Theory for Random Effects

Two features of the experimental program merit consideration for the possibility of introducing random fluctuations in the theoretical model. These consist of random inhomogeneities in the ground cover and wind induced fluctuations.

For a given experimental setup, ground cover inhomogeneities are fixed and are not expected to pose great problems in introducing temporal fluctuations. These appear to be adequately handled by averaging many impedance and propagation measurements, and a form of rms addition carried out between the e^{ik_1r} components and the e^{ik_2r} components found in section 2.5.*

Wind effects are more problematic. Ingard** has already described how corrections can be incorporated into real air-propagated modes, i.e., modes that can be represented by a ray. Application of these techniques to the case where propagation cannot be so represented may require further study.

Finally, the questions raised about treatment of experimental random noise data require answers.

4.2.2 Extension of the Theory for the Entire Upper Half-Space

The theory derived throughout section 2 of this report is limited in that the expansions are valid only near the interface. A ray theory formulation, valid for heights greater than ½ wavelength, is also presented but it is not so accurate as the asymptotic series that it is to complement.

---

* References 3-6, 11.
** References 12-14. Also note Reference 24.

Baños does extend the technique of saddle point integration to the case of expansions valid near the vertical axis, and a more cumbersome expansion valid over an entire hemisphere.*

The former case is worked out by Paul for acoustic waves in the two fluids model.**

It is felt that the unification of the theory is most accurately accomplished by means of direct numerical evaluation of the $K^{(i)}$ while they are in the form

$$\int_0^\infty\int_0^\infty \Phi(X, Y)\, e^{-\frac{1}{2}(X^2 + Y^2)}\, dXdY \tag{4.1}$$

for values of

$$\tan^{-1}\left|\frac{g_1}{r}\right| < \frac{\pi}{2} \tag{4.2}$$

and that a similar representation of K be evaluated when

$$\tan^{-1}\left|\frac{g_1}{r}\right| > \frac{\pi}{2} \tag{4.3}$$

where the above symbols are listed in paragraph 2.1.

As before, in those cases where the path of integration passes near a pole, especially near a terminus of the path, the techniques of paragraph 2.3.2 apply.

---

* Reference 1, pp 159-172 and pp 173-194, respectively.

** Reference 23.

4.2.3 Expanded Test Plan

It was mentioned in paragraph 3.4.2 that simultaneity of measurements constituted a highly desirable aspect of the experimental program. For this reason, broadband random noise was used in the original test program.

The concept of simultaneity is greatly enhanced by incorporation of many microphones and a fourteen channel instrumentation tape recorder in the test setup as shown in Figure 4.1. Other improvements shown include:

a) Use of a warble signal in place of random noise. Such a signal might consist of a square wave sweeping rapidly from a low frequency of, say, 80 Hz, to a frequency twice as great in about one second. The obvious advantage is that we are now working with a predictable signal and ambient effects can be removed.

b) A microphone to monitor the geometric center of the SGS. This position represents the optimal acoustic monitoring point since it is isolated from externally reflected waves.

c) Use of correlation to obtain impulse responses when random noise is used.

Values of the distances cited in Figure 4.1 are given in Table 4.1.

4.2.4 Impedance and Propagation Constant Measurements

The weak point of the experimental effort appears to

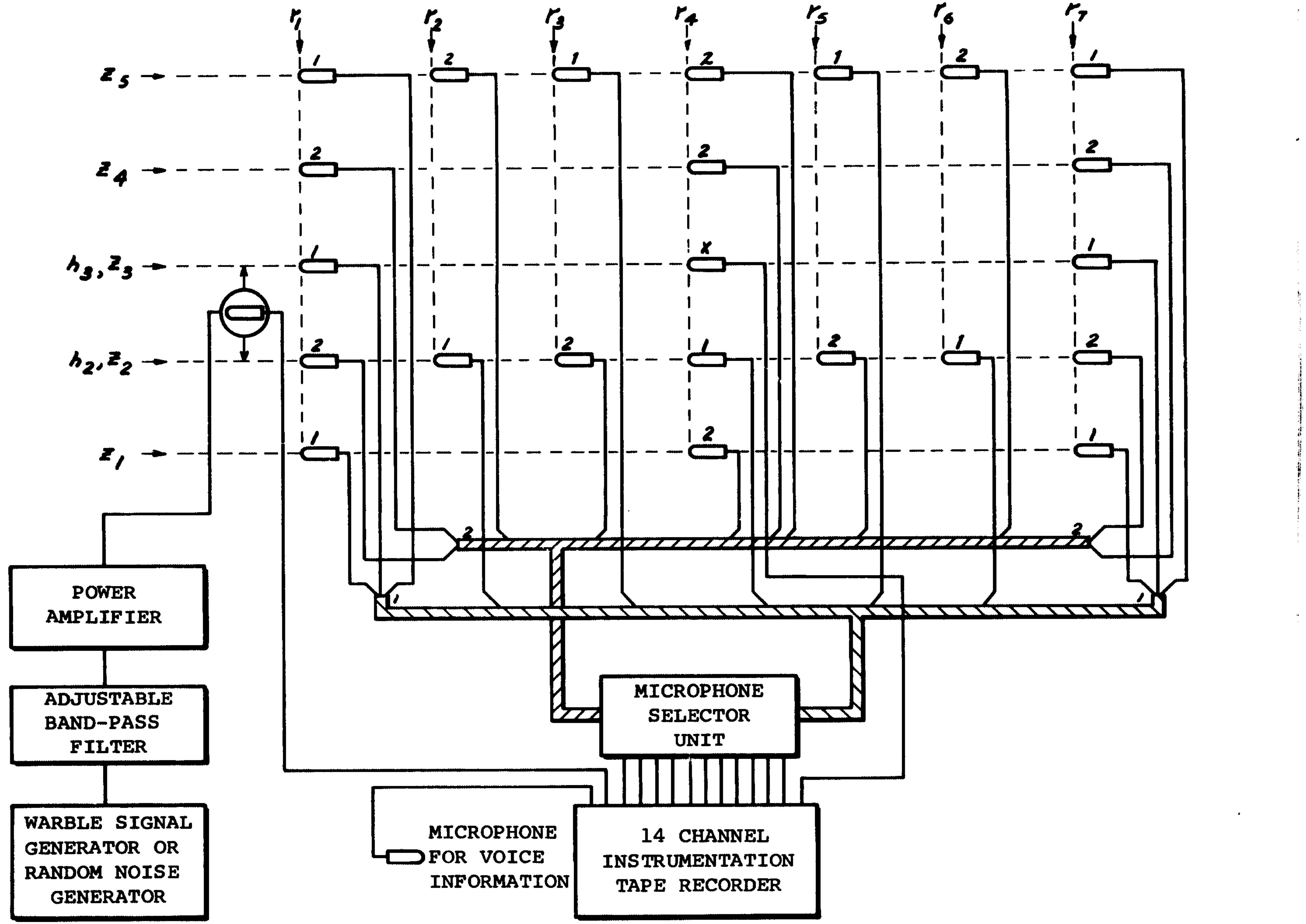

FIGURE 4.1. DIAGRAM OF TEST SETUP

TABLE 4.1

TEST PLAN DIMENSIONS

Symbol	Dimension	Symbol	Dimension
z_1	2 ½ ft.	r_1	16 ft.
z_2	5 ft.	r_2	31 ft.
z_3	10 ft.	r_3	62 ft.
z_4	20 ft.	r_4	125 ft.
z_5	40 ft.	r_5	250 ft.
h_2	5 ft.	r_6	500 ft.
h_3	10 ft.	r_7	1000 ft.

concern <u>in situ</u> techniques of measuring the impedance and propagation constant of the ground (lower) medium. Specifically, we must know real and imaginary parts of the impedance at all frequencies and a real constant from which the complex propagation constant can be evaluated through the constitutive relationships.

Alternatively, if it is known that the medium is porous, the five constants, U, V, W, Z, and k' of paragraph 2.4.4 can be determined independently, or from break-point analysis.

In section 3.3 two methods are discussed for more accurate interpretation of acoustic wave guide techniques. One attempt to solve a set of assumed boundary conditions was unsuccessful. However, as is later pointed out, this results from the assumption of an unrealistic pressure distribution.

Accordingly, it is recommended that this phase of investigation be concerned with the following activity:

a) Determine the pressure field distribution at the termination of the impedance tube by using small probe techniques.

b) Use a small vibration pick-up to determine the normal velocity field of the lower medium. This may not be an important piece of data in the case of very porous media where the velocity measured would tend to be that of the skeleton.

c) Determine if the pressure field is affected seriously by slight variations in the method of seal.

d) Ascertain the validity of other techniques, e.g., air volume flow, for measuring porosity, structure constant, specific flow resistance, etc.

In addition to the impedance tube technique above, investigation of the point source technique discussed in paragraph 3.3.2 also is encouraged.

4.2.5 Treatment of SGS Radiation Pattern

As mentioned in section 3.2.3 and 3.2.4, several methods avail themselves for the purposes of correcting the spherical asymmetry encountered in the SGS at frequencies above 250 Hz.

A first step would evaluate the relative costs, advantages and disadvantages of each method or combination of methods as it affects the type of signal and subsequent analysis. In particular, radiated wideband random noise analyzed in 1/3-octave intervals is not seriously impaired, whereas analysis of narrower bandwidths, discrete frequencies, or transient waveforms would be adversely affected.

Recapitulating, these methods include: a) Incorporation of the SGS asymmetry into the theory by evaluating the point source problem in bispherical coordinates and using spherical harmonics; b) theoretical treatment using Cartesian multipoles converted to cylindrical coordinates; c) a separate, smaller SGS to cover the frequency range from 250 Hz to 1000 Hz or more; d) addition of high frequency radiators at the vertices of the existing SGS; e) building up SGS exterior so that each speaker matches to free space conditions through a horn.

Some aspects of the relative merits of each of these methods are all discussed in 2.3. Prior to embarking on a solution, it is recommended that these considerations be further studied. Intuitively, it appears that method (c), because of its certitude, represents the optimal course.

BIBLIOGRAPHY

1. A. Baños, Jr., "Dipole Radiation in the Presence of a Conducting Half-Space" Pergamon Press, New York, 1966.

2. L. L. Beranek, "Acoustic Measurements", John Wiley & Sons, New York, 1949.

3. M. A. Biot, "Theory of Propagation of Elastic Waves in A Fluid Saturated Porous Solid. I. Low Frequency Range", J. Acoust. Soc. Am. 28, p. 168 (1956).

4. M. A. Biot, "Theory of Propagation of Elastic Waves in A Fluid Saturated Porous Solid. II. Higher Frequency Range", J. Acoust. Soc. Am. 28, p. 179 (1956).

5. M. A. Biot, "Generalized Theory of Acoustic Propagation in Porous Dissipative Media" J. Acoust. Soc. Am. 34, p.1254 (1962).

6. M. A. Biot, "Generalized Boundary Condition for Multiple Scatter in Acoustic Reflection", J. Acoust. Soc. Am. 44, p. 1616, (1968).

7. L. M. Brekhovskikh, "Waves in Layered Media", Academic Press, New York, 1960.

8. W. M. Ewing, W. S. Jardetsky and F. Press, "Elastic Waves in Layered Media" McGraw Hill Book Co., New York, 1957.

9. C. M. Harris, "Absorption of Sound in Air in the Audio Frequency Range", J. Acoust. Soc. Am. 35, p. 11, (196).

10. C. M. Harris, "Absorption of Sound in Air Versus Humidity and Temperature", J. Acoust. Soc. Am. 40, p. 148, (1966).

11. C. M. Harris, and L. Kirvida, "Observation Concerning the Attenuation of Elastic Waves in the Ground", J. Acoust. Soc. Am. 31, p. 1037, (1959).

12. U. Ingard, "Influence of Fluid Motion Past a Plane Boundary on Sound Reflection, Absorption and Transmission", J. Acoust. Soc. Am. 31, p. 1035, (1959).

13. U. Ingard, and G. C. Maling, Jr., "On the Effect of Atmospheric Turbulence on Sound Propagated Over the Ground", J. Acoust. Soc. Am. 35, p. 1056, (1963).

14. U. Ingard, "A Review of the Influence of Meterological Conditions on Sound Propagation", J. Acoust. Soc. Am. 25 p. 405, (1953).

15. U. Ingard, "On the Reflection of a Spherical Sound Wave from an Infinite Plane", J. Acoust. Soc. Am. 23, p. 329, (1951).

16. G. J. Kuhn, and A. Lutsch, "Elastic Wave Mode Conversion with Transverse Slip", J. Acoust. Soc. Am. 33, p. 949, (1961).

17. P. M. Morse, "Vibration and Sound", McGraw Hill Book Co., New York, 1948.

18. P. M. Morse, and H. Feshback, "Methods of Theoretical Physics", McGraw Hill Book Co., New York, 1953.

19. P. M. Morse, and U. Ingard, "Theoretical Acoustics", McGraw-Hill Book Co., New York, 1968.

20. H. L. Oestreicher, "Field of a Spatially Extended Moving Sound Source", J. Acoust. Soc. Am. 29, p. 1223, (1957).

21. H. L. Oestreicher, "Representation of the Field of an Acoustic Source as A Series of Multipole Fields", J. Acoust. Soc. Am. 29, p. 1219, (1957).

22. V. R. Parfitt, and A. C. Eringen, "Reflection of Plane Waves from the Flat Boundary of a Micropolar Half-Space", J. Acoust. Soc. Am 45, p. 1258, (1969).

23. D. I. Paul, "Acoustic Radiation from A Point Source in the Presence of Two Media", J. Acoust. Soc. Am. 29, p. 1102, (1957).

24. D. C. Pridmore-Brown, "Sound Propagation in a Temperature and Wind Stratified Medium", J. Acoust. Soc. Am. 34, p. 785, (1962).

25. E. A. G. Shaw, "Acoustic Wave Guide. I. An Apparatus for the Measurement of Acoustic Impedance Using Plane Waves and Higher Order Mode Waves in Tubes", J. Acoust. Soc. Am. 25, p. 224, (1953).

26. E. A. G. Shaw, "Acoustic Wave Guide. II. Some Specific Normal Impedance Measurements of Typical Porous Surfaces with Respect to Normally and Obliquely Incident Waves", J. Acoust. Soc. Am. 25, p. 231, (1953).

27. R. N. Tedrick, "Acoustical Measurements of Static Tests of Clustered and Single-Nozzled Rocket Engines", J. Acoust. Soc. Am. 11, p. 2027, (1964).

28. D. H. Towne, "Pulse Shape of Totally Reflected Plane Waves as a Limiting Case of the Cagniard Solution for Spherical Waves", J. Acoust. Soc. Am. 44, p. 77, (1968).

29. D. H. Towne, "Pulse Shapes of Spherical Waves Reflected and Refracted at a Plane Interface Separating Two Homogeneous Fluids", J. Acoust. Soc. Am. 44, p. 65, (1968).

30. G. N. Watson, "A Treatise on the Theory of Bessel Functions", Cambridge University Press, London, 1966.

31. F. M. Wiener, and D. N. Keast, "Experimental Study of the Propagation of Sound Over Ground", J. Acoust. Soc. Am. 31, p. 724, (1959).

32. F. M. Wiener, K. W. Goff, and D. N. Keast, "Instrumentation for the Study of Propagation of Sound Over Ground", J. Acoust. Soc. Am. 30, p. 860, (1958).

33. G. A. Wilhold, "Acoustic Environments of Rocket Exhausts", Aero-Astrodynamics Laboratory, Marshall Space Flight Center, Huntsville, Alabama.

APPENDIX A: COMPUTATION OF M_{11} FOR THE CASE OF TWO ELASTIC OR VISCOUS MEDIA.

In its original conception, it was felt that the problem of acoustic propagation would require the two bonded elastic media model for a complete description of point source-ground plane propagation. In this model there are four propagation constants corresponding to the four modes, i.e.

k_1 - compressional wave in air

k_2 - compressional wave in ground medium

k_3 - shearing wave in air

k_4 - shear wave is ground medium

Since the details of this model were worked out during the course of the theoretical program, and since the results are applicable to the general problem of two elastic media, they are presented in this and the following appendix.

A.1 <u>List of Symbols</u>

A_i = Complex incident wave amplitude for the i^{th} wave, $i = 1,2,3,4$.

$\mathbf{A_e}$ = Vector representation of the even components, A_i, i.e., A_2 and A_4.

$\mathbf{A_o}$ = Vector representation of the odd components, A_i, i.e., A_1 and A_3.

a_i = $\frac{\gamma_i}{\kappa}$, γ_i and κ defined in paragraph 2.1.

B_i = Complex transmitted wave amplitude for the i^{th} wave, $i = 1, 2, 3, 4$

$\mathbf{B_e}$ = Vector representation of the even components, B_i, i.e., B_2 and B_4.

$\mathbf{B_o}$ = Vector representation of the odd components, B_i, i.e., B_1 and B_3.

b_i = $\dfrac{2a_i}{(1 + a_m^2)}$

g = Matrix inversion metric.

$\mathbf{I}$ = Identity matrix.

i = Positive integer subscript.

i = $\sqrt{-1}$

j = Positive integer subscript.

k = Propagation constant general case.

k_i = Propagation constant for the i^{th} wave, $i = 1,2,3,4$.

$\mathbf{M}$ = Complete scattering matrix.

M_{ij} = Matrix elements of $\mathbf{M}$, $i, j = 1,2,3,4$.

$\mathbf{M}_{ij}$ = Partitioned matrix components of $\mathbf{M}$, $i, j = 1,2$.

m = Positive integer = $\begin{cases} 3 \text{ when } i \text{ or } n \text{ is odd.} \\ 4 \text{ when } i \text{ or } n \text{ is even.} \end{cases}$

n = Positive integer = $\begin{cases} 1 \text{ when } i \text{ or } m \text{ is odd.} \\ 2 \text{ when } i \text{ or } m \text{ is even.} \end{cases}$

q_1 = $\nu \dfrac{(1 + a_3^2)}{(1 + a_4^2)}$, ν defined in paragraph 2.1.

q_2 = Constant defined in text.

$\mathbf{S}, \mathbf{T}$ = Unreduced mixed mode scattering matrices

$\mathbf{S}_{ij}, \mathbf{T}_{ij}$ = Partitioned matrix components of $\mathbf{S}$ and $\mathbf{T}$, $i,j = 1,2$.

A.2 Boundary Conditions

In terms of the waves of Figure 2.4 and the elastic boundary conditions cited in paragraph 2.4.3, the following relationships obtain

$$(A_1 + B_1) - a_3(A_3 - B_3) = (A_2 + B_2) + a_4(A_4 - B_4) \,,$$

$$- a_1(A_1 - B_1) + (A_3 + B_3) = a_2(A_2 - B_2) + (A_4 + B_4) \,,$$

$$q_1\left[(A_1 + B_1) - \frac{2a_3}{1 + a_3^2}(A_3 - B_3)\right] = \left[(A_2 + B_2) + \frac{2a_4}{1 + a_4^2}(A_4 - B_4)\right], \tag{A.1}$$

$$q_1\left[\frac{2a_1}{1 + a_3^2}(A_1 - B_1) + (A_3 + B_3)\right] = \left[\frac{2a_2}{1 + a_4^2}(A_2 - B_2) + (A_4 + B_4)\right].$$

These can be condensed into the matrix equation

$$\begin{vmatrix} 1 & -a_3 & 1 & a_3 \\ -a_1 & 1 & a_1 & 1 \\ q_1 & q_1 b_3 & q_1 & q_1 b_3 \\ -q_1 b_1 & q_1 & q_1 b_1 & q_1 \end{vmatrix} \begin{vmatrix} A_1 \\ A_3 \\ B_1 \\ B_3 \end{vmatrix} = \begin{vmatrix} 1 & a_4 & 1 & -a_4 \\ a_2 & 1 & -a_2 & 1 \\ 1 & b_4 & 1 & -a_4 \\ b_2 & 1 & -a_2 & 1 \end{vmatrix} \begin{vmatrix} A_2 \\ A_4 \\ B_2 \\ B_4 \end{vmatrix} \tag{A.2}$$

which in condensed form becomes

$$\mathbf{S} \begin{vmatrix} \mathbf{A_o} \\ \mathbf{B_o} \end{vmatrix} = \mathbf{T} \begin{vmatrix} \mathbf{A_e} \\ \mathbf{B_e} \end{vmatrix}$$

or using quantities defined in the list of symbols,

$$\begin{vmatrix} \mathbf{S}_{11} & \mathbf{S}_{12} \\ q_1 \mathbf{S}_{21} & q_1 \mathbf{S}_{22} \end{vmatrix} \begin{vmatrix} \mathbf{A}_o \\ \mathbf{B}_o \end{vmatrix} = \begin{vmatrix} \mathbf{T}_{11} & \mathbf{T}_{12} \\ \mathbf{T}_{21} & \mathbf{T}_{22} \end{vmatrix} \begin{vmatrix} \mathbf{A}_e \\ \mathbf{B}_e \end{vmatrix} \tag{A.3}$$

for which, it is desired to find

$$\begin{vmatrix} \mathbf{B}_o \\ \mathbf{B}_e \end{vmatrix} = \begin{vmatrix} \mathbf{M}_{11} & \mathbf{M}_{12} \\ \mathbf{M}_{21} & \mathbf{M}_{22} \end{vmatrix} \begin{vmatrix} \mathbf{B}_o \\ \mathbf{B}_e \end{vmatrix} = \mathbf{M} \begin{vmatrix} \mathbf{A}_o \\ \mathbf{A}_e \end{vmatrix} \tag{A.4}$$

Equation A.4 will give the transmitted wave amplitude in terms of any combination of the four incident wave amplitudes.

Note that

$$\begin{aligned} \mathbf{S}_{11} &= \begin{vmatrix} 1 & -a_3 \\ -a_1 & 1 \end{vmatrix} , \\ \mathbf{S}_{12} &= \begin{vmatrix} 1 & a_3 \\ a_1 & 1 \end{vmatrix} , \\ \mathbf{S}_{21} &= \begin{vmatrix} 1 & -b_3 \\ -b_1 & 1 \end{vmatrix} , \\ \mathbf{S}_{22} &= \begin{vmatrix} 1 & b_3 \\ b_1 & 1 \end{vmatrix} , \end{aligned} \tag{A.5}$$

and that similar relationships exist for $\mathbf{T}_{ij}$. In terms of M_{ij}, the $\mathbf{M}_{ij}$ are given by

$$\mathbf{M}_{11} = \begin{vmatrix} M_{11} & M_{13} \\ M_{31} & M_{33} \end{vmatrix}$$

$$\mathbf{M}_{12} = \begin{vmatrix} M_{12} & M_{14} \\ M_{32} & M_{34} \end{vmatrix}$$

$$\mathbf{M}_{21} = \begin{vmatrix} M_{21} & M_{23} \\ M_{41} & M_{43} \end{vmatrix} \qquad \text{(A.6)}$$

$$\mathbf{M}_{22} = \begin{vmatrix} M_{22} & M_{24} \\ M_{42} & M_{44} \end{vmatrix}$$

The only element of $\mathbf{M}$ of interest is M_{11} and since

$$B_i = \sum_{j=1}^{4} M_{ij} A_j \qquad \text{(A.7)}$$

it follows that

$$B_1 = M_{11} A_1 \qquad \text{(A.8)}$$

A.3 Mechanics of Inversion

The inversion is accomplished by treating equation (A.4) as two linear simultaneous equations in two unknowns, $\mathbf{B_o}$ and $\mathbf{B_e}$. The only precaution is that $\mathbf{S}_{ij}$ and $\mathbf{T}_{ij}$ are matrix quantities that are not commutative under multiplication.

As a result it is found that

$$\mathbf{M}_{11} = -\left[\mathbf{T}_{12}^{-1}\mathbf{S}_{12} - q_1\mathbf{T}_{22}^{-1}\mathbf{S}_{22}\right]^{-1}\left[\mathbf{T}_{12}^{-1}\mathbf{S}_{11} - q_1\mathbf{T}_{22}^{-1}\mathbf{S}_{21}\right] \quad (A.9)$$

Similar formulae can be found for $\mathbf{M}_{12}$, $\mathbf{M}_{21}$ and $\mathbf{M}_{22}$, but since M_{11} is the only quantity of interest, only $\mathbf{M}_{11}$ is required.

The principal problem at this point is the inversion of

$$\left[\mathbf{T}_{12}^{-1}\mathbf{S}_{12} - q_1\mathbf{T}_{22}^{-1}\mathbf{S}_{22}\right] \quad (A.10)$$

It can be shown that there exists a q_2 such that

$$\left[\mathbf{T}_{12}^{-1}\mathbf{S}_{12} - q_1\mathbf{T}_{22}^{-1}\mathbf{S}_{22}\right]\left[\mathbf{S}_{12}^{-1}\mathbf{T}_{12} - q_2\mathbf{S}_{22}^{-1}\mathbf{T}_{22}\right] = g \quad (A.11)$$

with

$$q_2 = q_1 \frac{(1 - a_2a_4)\ (1 - b_1b_3)}{(1 - b_2b_4)\ (1 - a_1a_3)} \quad (A.12)$$

and

$$g = \left[\left(\frac{1 + a_1a_4}{1 - a_2a_4} - q_1\frac{1 + b_1b_4}{1 - b_2b_4}\right)\left(\frac{1 + a_2a_3}{1 - a_1a_3} - q_2\frac{1 + b_2b_3}{1 - b_1b_3}\right) - \left(\frac{a_3 + a_4}{1 - a_2a_4} - q_1\frac{b_3 + b_4}{1 - b_2b_4}\right)\left(\frac{a_1 + a_2}{1 - a_1a_3} - q_2\frac{b_1 + b_2}{1 - b_1b_3}\right)\right] \quad (A.13)$$

Hence,

$$\mathbf{M}_{11} = -\frac{1}{g}\left[\mathbf{S}_{12}^{-1}\mathbf{T}_{12} - q_2\mathbf{S}_{22}^{-1}\mathbf{T}_{22}\right]\left[\mathbf{T}_{12}^{-1}\mathbf{S}_{11} - q_1\mathbf{T}_{22}^{-1}\mathbf{S}_{21}\right] \quad (A.14)$$

For future reference, it is helpful to note that

$$\left(\frac{a_3 + a_4}{1 - a_2a_4} - q_1\,\frac{b_3 + b_4}{1 - b_2b_4}\right)\left(\frac{a_1 + a_2}{1 - a_1a_3} - q_2\,\frac{b_1 + b_2}{1 - b_1b_3}\right)$$
$$= \left(\frac{a_3 + a_4}{1 - a_1a_3} - q_2\,\frac{b_3 + b_4}{1 - b_1b_3}\right)\left(\frac{a_1 + a_2}{1 - a_2a_4} - q_1\,\frac{b_1 + b_2}{1 - b_2b_4}\right) \qquad \text{(A.15)}$$

Using all of the relationships developed thus far, M_{11} reduces to the following result:

$$M_{11} = -\frac{\left[\begin{aligned}&\left(\frac{1 + a_2a_3}{1 - a_1a_3} - q_2\,\frac{1 + b_2b_3}{1 - b_1b_3}\right)\times\left(\frac{1 - a_1a_4}{1 - a_2a_4} - q_1\,\frac{1 - b_1b_4}{1 - b_2b_4}\right)\\ &+\left(\frac{a_3 + a_4}{1 - a_1a_3} - q_2\,\frac{b_3 + b_4}{1 - b_1b_3}\right)\times\left(\frac{a_1 - a_2}{1 - a_2a_4} - q_1\,\frac{b_1 - b_2}{1 - b_2b_4}\right)\end{aligned}\right]}{\left[\begin{aligned}&\left(\frac{1 + a_2a_3}{1 - a_1a_3} - q_2\,\frac{1 + b_2b_3}{1 - b_1b_3}\right)\times\left(\frac{1 + a_1a_4}{1 - a_2a_4} - q_1\,\frac{1 + b_1b_4}{1 - b_2b_4}\right)\\ &-\left(\frac{a_3 + a_4}{1 - a_1a_3} - q_2\,\frac{b_3 + b_4}{1 - b_1b_3}\right)\times\left(\frac{a_1 + a_2}{1 - a_2a_4} - q_1\,\frac{b_1 + b_2}{1 - b_2b_4}\right)\end{aligned}\right]} \qquad \text{(A.16)}$$

It is a simple process of algebraic manipulation from this point to solve for $A(\kappa^2)$ and $B(\kappa^2)$ in example 1 of Table 2.4.

APPENDIX B: STARTING ROOTS AND APPLICABLE RIEMANN SURFACE FOR TWO BONDED ELASTIC MEDIA

B.1 List of Symbols

In addition to symbols listed in paragraph 2.1, the following characters were used in this appendix.

C_o, C_+, C_-	=	constants related to ν_i -- see text.
d	=	$\left(\frac{k_2}{k_4}\right)^2$
i, j	=	integer subscripts
S(d)	=	cubic polynomial in d -- see text.
T(d)	=	cubic polynomial in d -- see text.
u_i	=	coefficients in series expansion of ν_3 and ν_4.
v_i	=	coefficients in series expansion of ν_2.
α'	=	$-\left(\kappa^2 - \frac{1}{2} k_4^{\ 2}\right)^2$
θ_i	=	Arg (k_i)
κ_i	=	Root of decoupled denominator and starting point for the i^{th} root cluster.
κ_{ij}	=	j^{th} root in the i^{th} cluster, i, j = 1, 2, 3, 4.
σ_i	=	Re (k_i)
τ_i	=	Im(k_i)
ν	=	$\frac{\kappa}{k_4}^2$

$\nu_i \quad = \left(\frac{\kappa_i}{k_4}\right)^2$

$\nu_a, \nu_b \quad$ = constants related to ν_i -- see text.

$\phi_i \quad = \text{Arg}\ (\kappa_i)$

$\psi_i \quad$ = angular arguments in series expansion for ν_3 and ν_4.

B.2 Decoupled Denominator

In paragraph 2.4.3 , we decoupled the characteristic denominator for this problem into two terms from which starting values for the zeros could be determined. These were given by

$$(\kappa^2 - \gamma_1 \gamma_3) = 0 \tag{B.1a}$$

and

$$(\alpha' + \kappa^2 \gamma_2 \gamma_4) = 0 \tag{B.1b}$$

Thus, it is quite evident that the characteristic denominator decouples into two terms that are individually dependent on the properties of each medium. An additional feature of interest concerns equation (B.1a) only. This term resembles, in many respects, the Sommerfeld denominator encountered in electromagnetic theory.* In fact, the roots are identical, namely

$$\kappa_1 = \pm \left(1 - n_{13}{}^2\right)^{-\frac{1}{2}} \tag{B.2}$$

---

* Reference 1, pp. 59-61.

Three additional pole pairs are given by an expansion of equation (B.1b), yielding the cubic

$$(1 - d)\nu^3 - \left(\frac{3}{2} - d\right)\nu^2 + \frac{1}{2}\nu - \frac{1}{16} = 0 \tag{B.3}$$

where

$$\nu = \left(\frac{\kappa}{k_4}\right)^2$$

$$d = \left(\frac{k_2}{k_4}\right)^2 \tag{B.4}$$

Unfortunately, these roots are not representable in a simple closed form such as equation (B.2). The following generalization is possible for real values of d as indicated

$$\begin{aligned}
&1.10 < \nu_1 < 1.23 \text{ for } .04 < d < .4 \\
&.209 < \mathrm{Re}(\nu_2) = \mathrm{Re}(\nu_3) < .27969 \text{ for } .04 < d < .32150 \\
&.123 > \mathrm{Im}(\nu_2) = -\mathrm{Im}(\nu_3) > 0 \text{ for } .04 < d < .32150 \\
&.27969 < \mathrm{Re}(\nu_2) \text{ for } .32150 < d < .4 \\
&\mathrm{Im}(\nu_2) = \mathrm{Im}(\nu_3) = 0 \text{ for } .32150 < d < .4
\end{aligned} \tag{B.5}$$

which is sufficiently adequate to cover most isotropic elastic media. Graphical representations of the roots as a function of d are shown in Figure B.1.

Having found roots in each of the three examples presented so far, it is now desirable to develop decision criteria for specifying the applicable Riemann surface.

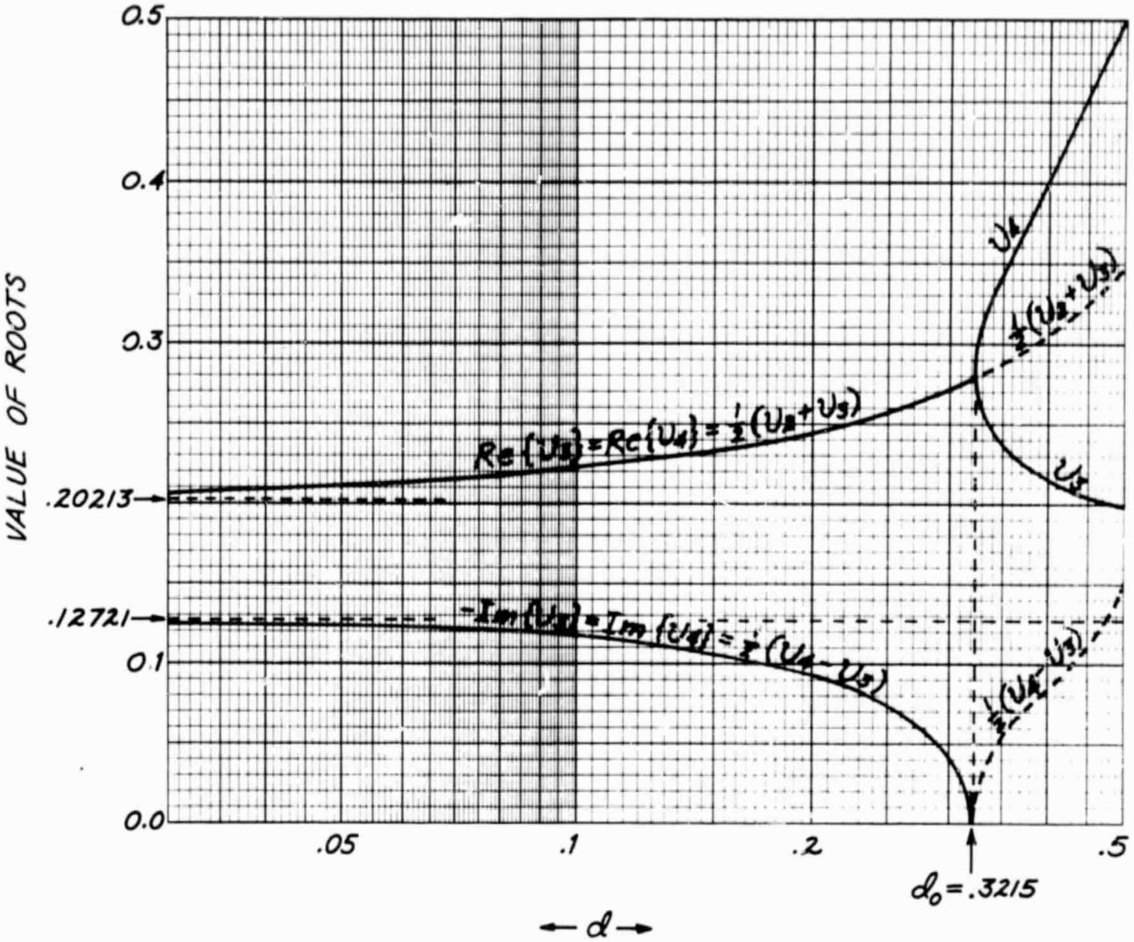

FIGURE B.1. VALUES OF THE ROOTS AS A FUNCTION OF d.

Note that each limiting case considered involves only two quantities, γ_i, so that the four Riemann surfaces in each case represents a suitably chosen subset of the overall sixteen surfaces illustrated in Figure 2.3.

At this point, it is of interest to consider the zeros of each of the three denominator limits, and their applicable Riemann surfaces.

B.2.1 Part containing γ_1 and γ_3

In order to determine the applicable Riemann Surface, it is necessary to consider the proper sign and phase of

$$\gamma_1(\kappa_1) = \pm i\, n_{13} \kappa_1$$

and

$$\gamma_3(\kappa_1) = \pm i\, n_{13}^{-1} \kappa_1 \tag{B.6}$$

In particular, we wish to compute the phases of γ_1 and γ_3 in order to determine on which surfaces $D(\kappa_1^2)$ vanishes.

Consider first the cuts originally used by Summerfeld, i.e.

$$\begin{aligned} \xi\eta &= \sigma_1 \tau_1 \qquad |\eta| > |\tau_1| \\ \xi\eta &= \sigma_3 \tau_3 \qquad |\eta| > |\tau_3| \end{aligned} \tag{B.7}$$

and recall that

θ_1 and θ_3 are small positive angles. (B.8)

Next note that $|n_{31}| < 1$ so that, to first order

$$\begin{aligned} |\kappa_1| &\cong |k_1| \left(1 + \tfrac{1}{2} |n_{31}|^2\right) \\ \phi_1 &\cong \theta_1 \end{aligned} \tag{B.9}$$

where

$$\mathrm{Arg}\ (n_{31}) = \theta_1 - \theta_3$$

$$\mathrm{Arg}\left[\gamma_1(\kappa_1)\right] = \pm\frac{\pi}{2} + \mathrm{Arg}\ (n_{31}) + \phi_1 \tag{B.10}$$

$$= \left\{\begin{array}{l} \frac{\pi}{2} + 2\,\theta_1 - \theta_3 + \frac{1}{2}\ n_{31}{}^{2} \\ \text{...on surfaces XXX0} \end{array}\right\} \tag{B.11}$$

$$= \left\{\begin{array}{l} \frac{\pi}{2} + 2\,\theta_1 - \theta_3 + \frac{1}{2}\ n_{31}{}^{2} \\ \text{...on surfaces XXX1} \end{array}\right\} \tag{B.11*}$$

where the condition, $[\mathrm{Re}\ \gamma_i(\kappa)] > 0$ on $X = 0$ surfaces has been invoked.

Taking note of the sign correspondence between $\pm\ i$ and $\pm\ \pi/2$, it follows that

$$\gamma_1(\kappa_1) = \left\{\begin{array}{ll} +\ i\ n_{31}\,\kappa_1 & \text{on surfaces XXX0} \\ -\ i\ n_{31}\,\kappa_1 & \text{on surfaces XXX1} \end{array}\right\} \tag{B.12}$$

Using identical reasoning, it is found that

$$\mathrm{Arg}\ [\gamma_3(\kappa_1)] = \pm\frac{\pi}{2} - \mathrm{Arg}\ (n_{31}) + \phi_1$$

---

* As an artifice to keep track of Riemann surfaces, the four-digit designator containing symbols 0, 1, and X has been devised where X is free to take on either value, i.e., 0 or 1. If the symbols are now denoted by X_4, X_3, X_2, and X_1 (to correspond to γ_4, γ_3, etc.), then the applicable surface number is given by $X_4 \cdot 2^3 + X_3 \cdot 2^2 + X_2 \cdot 2 + X_1 + 1$.

$$
= \left\{ \begin{array}{l} \frac{\pi}{2} + \theta_3 + \tfrac{1}{2} |n_{31}|^2 \\ \text{... on surfaces X1XX} \end{array} \right.
$$

$$
= \left\{ \begin{array}{l} -\frac{\pi}{2} + \theta_3 + \tfrac{1}{2} |n_{31}|^2 \\ \text{... on surfaces X0XX} \end{array} \right. \tag{B.13}
$$

or

$$
\gamma_3(\kappa_1) = \left\{ \begin{array}{l} - i \frac{1}{n_{31}} \kappa_1 \text{ on surfaces X0XX} \\ \\ + i \frac{1}{n_{31}} \kappa_1 \text{ on surfaces X1XX} \end{array} \right\} \tag{B.14}
$$

combining the results of equations (B.12) and (B.14) it is found that

$$
\kappa^2 - \gamma_1 \gamma_3 \Big|_{\kappa = \kappa_1} = \left\{ \begin{array}{l} 0 \text{ on surfaces X0X0 and X1X1} \\ 2 \kappa_1^2 \text{ on surfaces X0X1 and X1X0} \end{array} \right\} \tag{B.15}
$$

It is easily seen from equation (B.9) that the root, κ_1, in the first quadrant lies above and right of k_1. If the branch cut associated with k_1 is allowed to sweep smoothly from the Sommerfeld to the Baños branch cut, it will not cut across the pole as long as θ_1 and θ_3 are small.

If, however, this medium is a viscous fluid so that $\theta_3 = \frac{\pi}{4}$, then the pole position is shifted $\frac{\pi}{2}$ radians with respect to k_1, and will lie above and to the left of this branch point. Under these conditions, if the Baños branch cuts are used, we will have

$$\kappa^2 - \gamma_1 \gamma_3 \Big|_{\kappa = \kappa_1} = \left\{ \begin{array}{l} 0 \text{ on surfaces X0X1 and X1X0} \\ 2\,\kappa_1^{\,2} \text{ on surfaces X0X0 and X1X1} \end{array} \right\} \qquad (B.16)$$

B.2.2 Part containing γ_2 and γ_4

Closed form expressions for the three roots of the cubic equation, (B.3), are given by

$$\nu_2 = \left(\frac{\kappa_2}{k_4}\right)^2 = C_o + C_+ + C_-$$

$$\nu_3 = \left(\frac{\kappa_3}{k_4}\right)^2 = C_o - \tfrac{1}{2}(C_+ + C_-) + i\frac{\sqrt{3}}{2}(C_+ - C_-) \qquad (B.17)$$

$$\nu_4 = \left(\frac{\kappa_4}{k_4}\right)^2 = C_o - \tfrac{1}{2}(C_+ + C_-) - i\frac{\sqrt{3}}{2}(C_+ - C_-)$$

where $$C_o = \frac{1}{2}\,\frac{1 - \frac{2}{3}d}{1 - d} \qquad (B.18)$$

$$C_{\pm} = \frac{1}{4(1-d)} \left\{ 2\ T(d) \pm \frac{2\sqrt{33}}{9}(1-d)\ [S(d)]^{\frac{1}{2}} \right\}^{\frac{1}{3}}$$

$$S(d) = 1 - \frac{10}{3}d + \frac{11}{3}d^2 - \frac{32}{11}d^3$$

$$T(d) = 1 - \frac{62}{11}d + \frac{107}{11}d^2 - \frac{64}{11}d^3 \qquad (B.19)$$

After performing a Taylor Series expansion around $d = 0$, we have

$$C_o = \frac{1}{2} + \frac{1}{6} d + \frac{1}{6} d^2 + \frac{1}{6} d^3 + \text{-----}, \quad |d| < 1 \tag{B.20}$$

$$C_+ = .37131840 - .06463824\, d$$
$$- .12052608\, d^2 - .20301071\, d^3 \text{-----}, \quad |d| < .3215$$

$$C_- = .22442554 + .03906747\, d$$
$$+ .15445547\, d^2 + .3188522\, d^3 + \text{-----}, \quad |d| < .3215 \tag{B.20}$$

Finally, combining these gives

$$\nu_2 = 1.09574394 + .14109590\, d$$
$$+ .20059606\, d^2 + .27554118\, d^3 + \text{-----} \tag{B.21}$$

$$\nu_a = .20212803 + .17945205\, d$$
$$+ .14970197\, d^2 + .11222941\, d^3 + \text{-----}$$

$$\nu_b = .12721294 - .08901178\, d \tag{B.21}$$
$$- .23814101\, d^2 - .44591296\, d^3 - \text{-----}$$

with $|d| < .3215$ in all cases, and

$$\nu_3 = \nu_a + i\, \nu_b$$
$$\nu_4 = \nu_a - i\, \nu_b \tag{B.22}$$

Of considerable importance in this analysis is an expansion of the roots in powers of

$$|d| \quad \exp \quad [i \text{ Arg } (d)] \tag{B.23}$$

where

$$\text{Arg } (d) = 2(\theta_2 - \theta_4) \tag{B.24}$$

with

$$0 < \theta_2 \leq \theta_4 \ll \frac{\pi}{4} \tag{B.25}$$

i.e., shear waves are assumed to be more lossy than dilational waves. Hence

$$-\frac{\pi}{2} \ll \operatorname{Arg}\{d\} < 0 \tag{B.26}$$

and

$$\begin{aligned}\upsilon_2 &= v_0 + v_1 |d| e^{i\operatorname{Arg}(d)} + v_2 |d|^2 e^{i2\operatorname{Arg}(d)} \\ &\quad + v_3 |d|^3 e^{i3\operatorname{Arg}(d)} + ----- \\ \begin{Bmatrix}\upsilon_3 \\ \upsilon_4\end{Bmatrix} &= u_0 e^{\pm i\psi_0} + u_1 |d| e^{i[\operatorname{Arg}(d) \pm \psi_1]} \\ &\quad + u_2 |d|^2 e^{i[2\operatorname{Arg}(d) \pm \psi_2]} \\ &\quad + u_3 |d|^3 e^{i[3\operatorname{Arg}(d) \pm \psi_3]} + -----\end{aligned} \tag{B.27}$$

where the $\begin{Bmatrix}\text{upper} \\ \text{lower}\end{Bmatrix}$ sign is associated with $\begin{Bmatrix}\upsilon_3 \\ \upsilon_4\end{Bmatrix}$ and

a) v_0, v_1, v_2, and v_3 are the numerical values transposed from the first of equation (B.21),

b) u_0, u_1, u_2, and u_3 are magnitudes of the corresponding coefficient combinations of the last two of equation (B.21), i.e.,

u_0 = .23882812

u_1 = .20067185

u_2 = .28128601

u_3 = .45981932

c) and ψ_0, ψ_1, ψ_2 and ψ_3 are corresponding angular arguments, i.e.,

$\psi_0 = 32^\circ\ 11'$

$\psi_1 = -26^\circ\ 35'$

$\psi_3 = -57^\circ\ 50'$

$\psi_4 = -79^\circ\ 52'$

By using heuristic reasoning and the vector diagrams in Figures B.2 and B.3, it can be shown that,

if $|d| \leq .2$ and $-\frac{\pi}{2} \leq \text{Arg}\ \{d\} \leq 0$, then

$$\begin{aligned}
v_0 - v_2\ |d| &< |\nu_2| < v_0 + v_1 + \text{-----} \\
d_{min} \equiv .2 &< |\nu_3| < .3215 \equiv d_{max} \\
u_0 &< |\nu_4| < .3215 \equiv d_{max} \\
v &< 2\ (\theta_4 - \phi_2) < 0 \\
\psi_0 - \frac{u}{d_{min}} &< 2\ (\theta_4 - \phi_3) < \psi_0 \\
-\psi_0 - \frac{u}{d_{min}} &< 2\ (\theta_4 - \phi_4) < \psi_0 + \frac{u}{d_{min}}
\end{aligned} \tag{B.28}$$

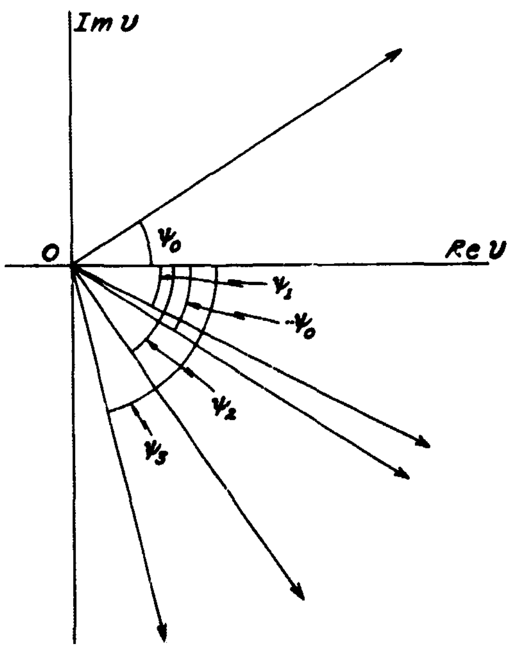

FIGURE B.2 DIRECTIONAL RELATIONSHIPS BETWEEN PHASES, ψ_i.

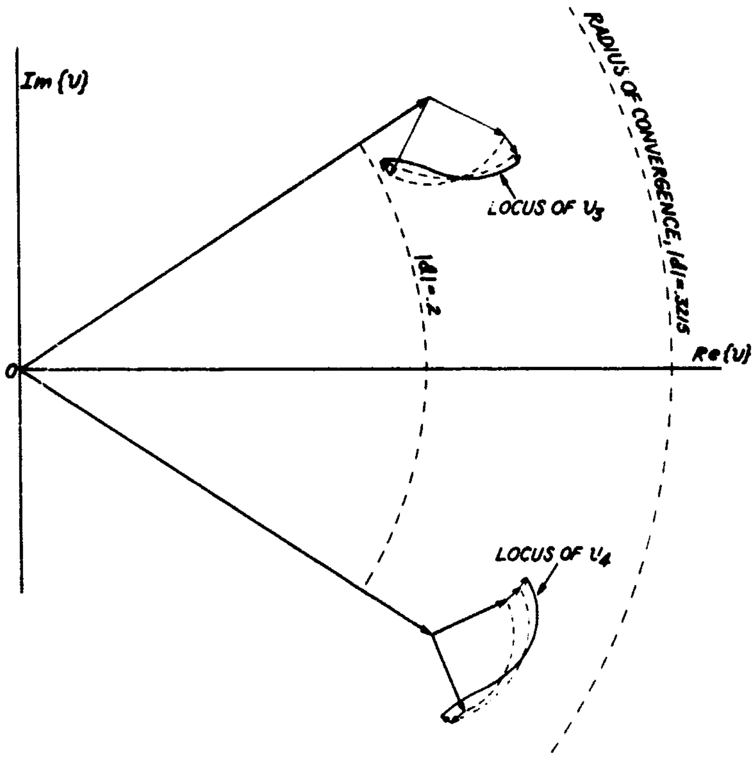

FIGURE B.3 LOCATION OF ν_3 AND ν_4 IN THE COMPLEX ν - PLANE SHOWING RELATIONSHIP TO OTHER IMPORTANT FEATURES.

Translating these results to the complex $\left(\frac{\kappa}{k_4}\right)$ plane gives the propagation constant and root loci shown in Figure B.4.

Next, it is of interest to evaluate γ_2 and γ_4 in terms of the roots κ_2, κ_3 and κ_4. To do this, it is helpful to redefine γ_2 and γ_4 so that

$$\begin{aligned} \gamma_2 &= k_4 \left[\nu - a \right]^{\frac{1}{2}} \\ \gamma_4 &= k_4 \left[\nu - 1 \right]^{\frac{1}{2}} \end{aligned} \tag{B.29}$$

This gives the limits on the phases of γ_2 and γ_4 in the κ -plane corresponding to the previously specified

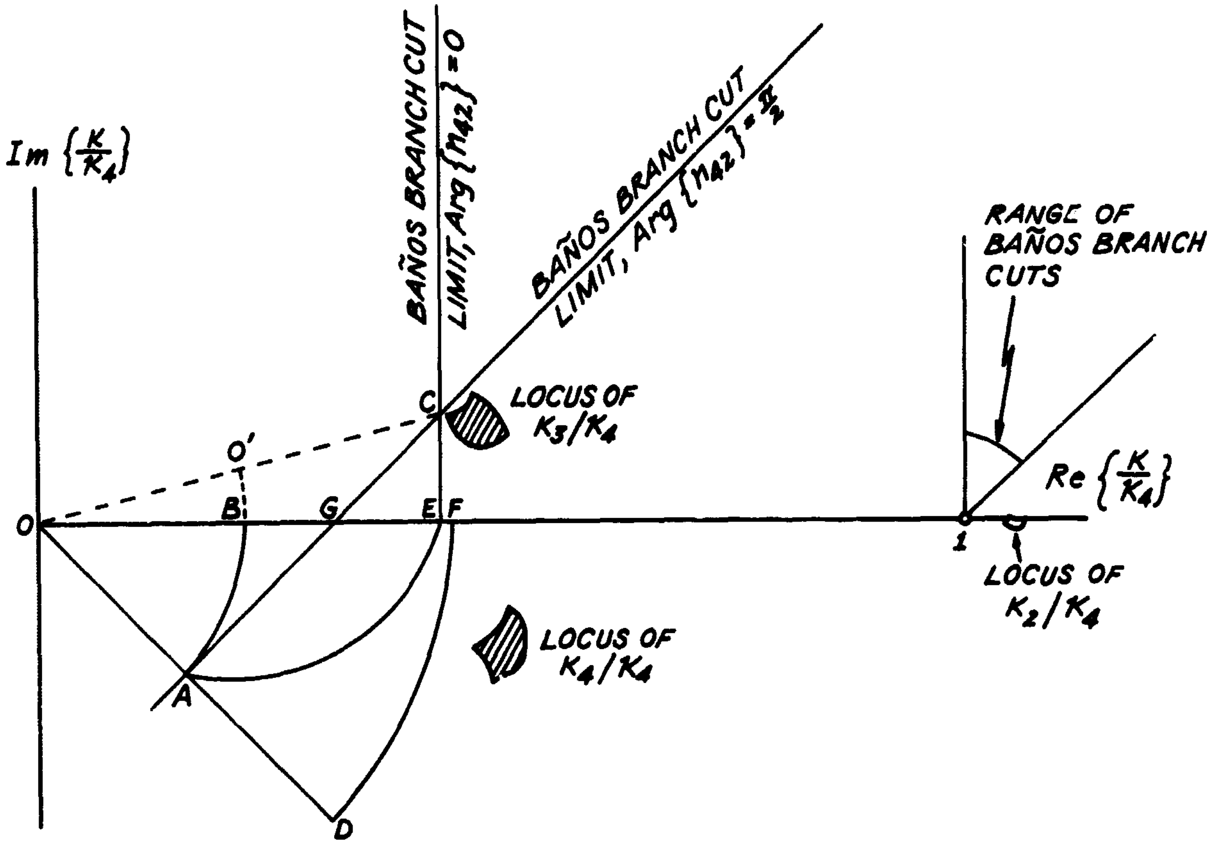

Point C: Point outside of locus of K_3/K_4 such that straight lines of slope, m, with $1 < m < \infty$, can pass completely to the left of the root locus.

Region $O\widehat{DF}$: Locus of n_{24} giving root loci illustrated, $\overline{OD} = \overline{OF} = \sqrt{2}$. Sommerfeld Branch cuts lying to the left of K_3/K_4 locus exist for all values of n_{24} in this region.

Region $O\widehat{AB}$: Locus of n_{24} inside a fixed radius giving a Baños branch cut to the left of root locus,

Region $O\widehat{AE}$: Locus of n_{24} giving Baños branch cut to the left of root locus, K_3/K_4, when K_2 is taken rigorously real.

Triangular Region OAG: Locus of n_{24} that gives Baños branch cut to the left of root locus, K_3/K_4 for arbitrary K_2 when $0 < \theta_2 < \theta_4 < \frac{\pi}{4}$

Point O': Center of AE. $\overline{OO'} = \frac{1}{2}\overline{OC}$.

FIGURE B.4. GEOMETRIC RELATIONSHIPS OF ROOT LOCI IN THE COMPLEX (κ/k_4) PLANE.

limits on $|d|$, Arg $\{d\}$ and θ_4. The following ranges apply to the first and other appropriate Riemann surfaces:

$$
\begin{aligned}
&\theta_4 - \theta_2 \le \operatorname{Arg}\left[\gamma_2(\nu_2)\right] \le \rho - \theta_2 + \tfrac{1}{2}|d| \\
&\theta_4 - \tfrac{1}{2}|d| \frac{v_1}{v_0 - v_2 |d|^2 - 1} \le \operatorname{Arg} \gamma_4(\nu_2) \le \theta_4 \\
&\tfrac{1}{2}\psi_0 + \theta_4 \le \operatorname{Arg}\left[\gamma_2(\nu_3)\right] \le \frac{\pi}{4} + \theta_4 \\
&-\frac{u_0 \psi_0}{2\,(1-u_c)} - \frac{\pi}{2} + \theta_4 \le \operatorname{Arg}\left[\gamma_4(\nu_3)\right] \le -\frac{\pi}{2} + \theta_4 \\
&-\frac{\pi}{4} + \theta_4 \le \operatorname{Arg}\left[\gamma_2(\nu_4)\right] \le \theta_4 - \psi_0 + \frac{|d|}{v_0} \\
&-\frac{\pi}{2} + \theta_4 \le \operatorname{Arg}\left[\gamma_4(\nu_4)\right] \le -\frac{\pi}{2} + \theta_4 + \tfrac{1}{2}u_0
\end{aligned}
\tag{B.30*}
$$

In addition to these ranges of arguments there is an identical set removed by π corresponding to the alternate choice of sign of γ_2 and γ_4.

Further, in this analysis, it is necessary to consider

$$2\operatorname{Arg}(\kappa_i^2 - \tfrac{1}{2}k_4^2) = 4\theta_4 + 2\operatorname{Arg}(\nu_i - 1) \tag{B.31}$$

which is to be compared with

$$
\begin{aligned}
\operatorname{Arg}[\kappa_i \gamma_1(\kappa_i)\gamma_2(\kappa_i)] = {} & 2\theta_4 + 2\operatorname{Arg}(\nu_i) \\
& + 2\operatorname{Arg}[\gamma_2(\nu_i)] + 2\operatorname{Arg}[\gamma_4(\nu_i)]
\end{aligned}
\tag{B.32}
$$

---

* The fourth limit gives uncertain results when the Sommerfeld branch cuts are used. The condition stated applies to OXXX surfaces when the Baños branch cuts are used.

Hence, the condition to be satisfied in order to obtain an actual pole on a particular surface requires that

$$2\left[\mathrm{Arg}\ (\nu_i - \tfrac{1}{2}) - \mathrm{Arg}\ (\nu_i)\right]$$
$$= \left\{ \mathrm{Arg}\left[\gamma_2\ (\nu_i)\right] - \theta_4 \quad + \quad \mathrm{Arg}\left[\gamma_4\ (\nu_i)\right] \quad - \theta_4 \right\} \tag{B.33}$$

By reasoning similar to that used to obtain equations (B.30), it is found that

$$- \ |d| \ \frac{v_1}{v_0 - v_2\ |d|^2 - \tfrac{1}{2}} \leq 2\mathrm{Arg}\ (\nu_2 - \tfrac{1}{2}) \leq 0$$
$$0 \leq 2\mathrm{Arg}\ (\nu_3 - \tfrac{1}{2}) \leq \psi_0 \tag{B.34}$$
$$-\psi_0 \leq 2\mathrm{Arg}\ (\nu_4 - \tfrac{1}{2}) \leq 0$$

Combining equations (B.28), (B.30), (B.33), and (B.34), it is possible to show that

$$\alpha' + \kappa^2\ \gamma_2\ \gamma_4\Big|_{\kappa = \kappa_2} = \begin{cases} 0 \text{ on surfaces 0X0X and 1X1X} \\ 2\ \alpha'\ (\kappa_3) \text{ on surfaces 0X1X and 1X0X} \end{cases} \tag{B.35}$$

for Baños branch cuts only. For Sommerfeld branch cuts and $I_m\{k_4\} \ll R\ \{k_4\}$, the k_4 - branch cut passes to the other side of the pole giving

$$\alpha' + \epsilon\ \gamma_2\ \gamma_4\ \Big|_{\kappa = \kappa_3} = \begin{cases} 0 \text{ on surfaces 0X1X and 1X0X} \\ 2\ \alpha'(\kappa_3) \text{ on surfaces 0X0X and 1X1X} \end{cases} \tag{B.36}$$

Finally,

$$\alpha' + \epsilon\ \gamma_2\ \gamma_4\Big|_{\kappa = \kappa_4} = \begin{cases} 0 \text{ on surfaces 0X1X and 1X0X} \\ 2\alpha'(\kappa_4) \text{ on surfaces 0X0X and 1X1X} \end{cases} \tag{B.37}$$

for either Sommerfeld or Baños branch cuts.

Thus, as the first Riemann surface, with $\upsilon \ll 0$ and for the Baños choice of branch cuts, κ_1 and κ_4 represent virtual poles and κ_2 and κ_3 represent real poles.

In terms of a closed contour integral, virtual poles will not contribute a residue. However, if one is concerned about the evaluation of bounded line integral, i.e., one whose path is not closed, and if such a path passes within the neighborhood of such a virtual pole, its effect must be included.

B.3 Summary of Roots

Based on the foregoing discussion, it has been established that the decoupled denominator, obtained by taking $\upsilon \equiv 0$, gives rise to four root pairs in the complex κ plane. Approximate location and type of root are shown in Figure B.5.

By re-introducing a non-zero value for υ, the denominator is recoupled. Each of the four root pairs will readjust to new values which are dependent on the applicable Riemann surface.

For small ν, this approach will provide clusters of four new roots near each decoupled root or all 16 Riemann Surfaces.

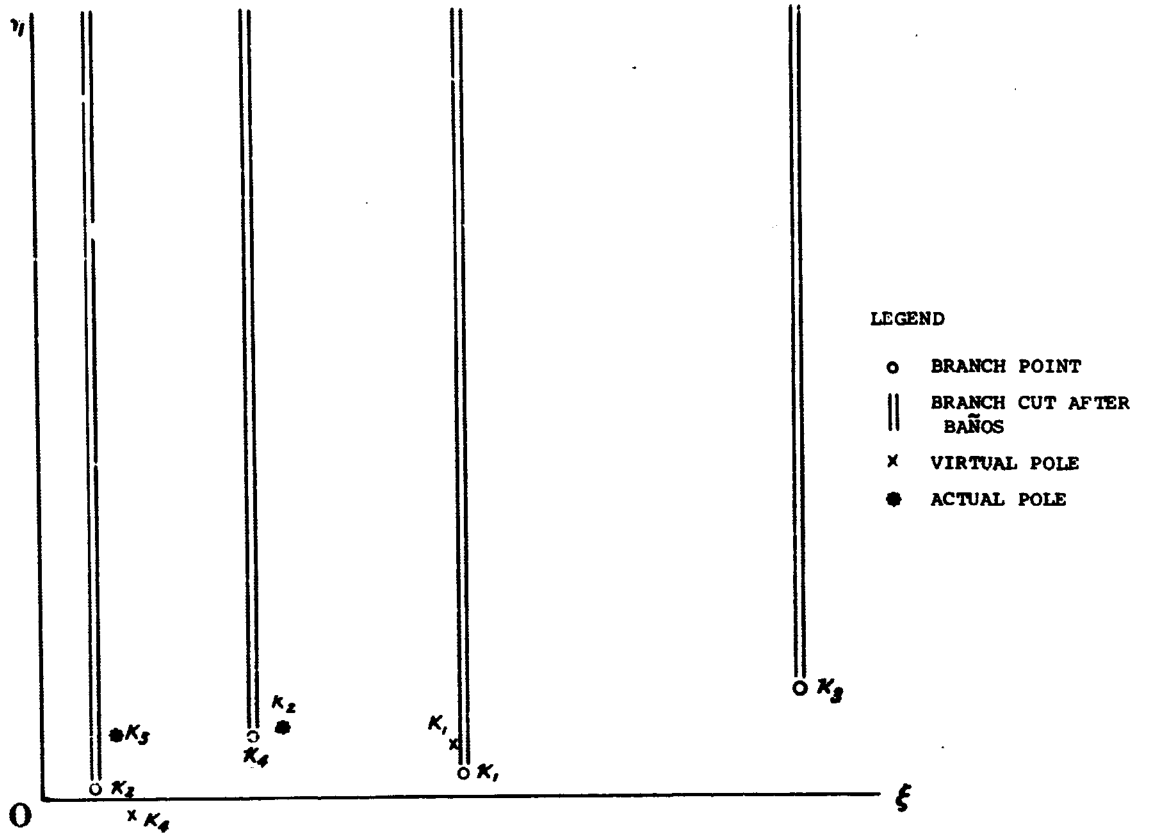

FIGURE B.5 DISPOSITION OF BRANCH POINTS, BRANCH CUTS, ACTUAL AND VIRTUAL POLES, ETC. ON THE 1ST RIEMANN SURFACE, κ PLANE.

The final value of these roots is then determined by using Newton-Raphson techniques with the decoupled root-value serving as initial guesses.

In retrospect, it is of interest to note that for the Baños choice of branch cuts, for $k_2 < k_4 < k_1 \ll k_3$, and for the case where the decoupled model holds approximately

1) The κ_1 group lies near the branch point.

2) The κ_2 group lies near the terminus of C_4.

3) The κ_3 group can be expected to lie near C_2.

4) The κ_4 group will lie nearest to C_2 and may also require inclusion in the C_2 treatment.

Location and applicability of the 16 resultant roots are listed in Table B.1.

Root	Riemann Surfaces (First Order Estimate)			
κ_{11}	0001	=	2	
	0100	=	5	
κ_{12}	0011	=	4	
	0110	=	7	
κ_{13}	1001	=	10	X0X1 and X1X0
	1100	=	13	
κ_{14}	1011	=	12	
	1011	=	15	
κ_{21}	0000	=	1	
	1010	=	11	
κ_{22}	0001	=	2	
	1011	=	12	
κ_{23}	0100	=	5	0X0X and 1X1X
	1110	=	15	
κ_{24}	0101	=	6	
	1111	=	16	
κ_{31}	0000	=	1	
	1010	=	11	
κ_{32}	0001	=	2	
	1011	=	12	0X0X and 1X1X
κ_{33}	0100	=	5	
	1110	=	15	
κ_{34}	0101	=	6	
	1111	=	16	
κ_{41}	0010	=	3	
	1000	=	9	
κ_{42}	0011	=	4	
	1001	=	10	0X1X and 1X0X
κ_{43}	0110	=	7	
	1100	=	13	
κ_{44}	0111	=	8	
	1101	=	14	

TABLE B.1. Riemann Surfaces on which the Roots, κ_{ij}, are Actual Roots

APPENDIX C: THEORETICALLY DERIVED DATA

C.1 Discussion

In Section 2 of this report, two formulations were presented describing the interaction of a spherical outgoing wave with a reflecting and refracting plane boundary.

The first formulation used a ray theory approach with an image located on the source axis and at a distance below the surface equal to the source height. Such a treatment gives rise to equation (2.101) and the associated relationships of equation (2.102).

A more rigorous treatment reduces the problem to the evaluation of an integral or kernel expression. Evaluation of this kernel is accomplished using Debye's method to obtain an asymptotic series expression for the integral. Results of this formulation are delineated in equations (2.109) through (2.112).

The primary difference in the two techniques is that the latter predicts the existence of a Love wave associated with the first order pole, κ_0. However, when the lower medium exhibits characteristics that are drastically different than those of the upper medium, a situation that typically prevails even for porous media, the effects of the Love wave attenuate to e^{-1} in approximately a wavelength from the boundary.

Both techniques account for a direct wave, a reflected wave from an equal and opposite image, and an interaction term that accounts for Rayleigh waves where applicable. Thus, equation (2.101) can be rewritten*

$$\psi(r,\ z;\ 0,\ h) = \frac{e^{ik_1 R}}{R} - \frac{e^{ik_1 R'}}{R'} + \frac{2\cos\theta}{\cos\theta + \zeta^{-1}}\ \frac{e^{ik_1 R'}}{R'} \tag{C1}$$

Since we are interested in the magnitude of excess attenuation, we will want to compute*

$$r\left|\psi(r,\ z;\ 0,\ h)\right| = \left|\frac{r}{R} - \frac{r}{R'}\ e^{ik_1\Delta} + \frac{r}{R'}\ \frac{2\cos\theta}{\cos\theta + \zeta^{-1}}\ e^{ik_1\Delta}\right| \tag{C2}$$

where

$$\Delta = R' - R$$

$$\zeta^{-1} = \eta(\theta) = \eta(0)\left[1 - \eta^2(0)A^2\sin^2\theta\right]^{\frac{1}{2}} \tag{C3}$$

ζ^{-1} = complex specific admittance for angle, θ,

This operation is performed by the computer program, written in USASI Fortran, in Section C.2 below.

---

* Symbols used here are defined in Section 2.1.

C.2 Computer Program

```
C       THIS PROGRAM COMPUTES THE COMPLEX FIELD VARIABLES REQUIRED
C       FOR THE EVALUATION OF EQUATION (C.2) OF THE TEXT. THE DATA
C       OUTPUT INCLUDES THESE FIELD VARIABLES AS THEY APPLY TO THE
C       DIRECT, REFLECTED, AND INTERACTION MODES, THE MAGNITUDE OF
C       THE ALGEBRAIC COMBINATION, AND THE EXCESS ATTENUATION IN
C       DB REFERRED TO A -6DB/DOUBLE R(LOWER CASE).
C       THE FIRST PART OF THIS PROGRAM CONTAINS FUNCTION DEF-
C       INITIONS, FORMAT SPECIFICATIONS, AND THE ARRAY DIMEN-
C       SION STATEMENTS.

300     CCHK(M,N) = ABSF(FLOATF(M)-.5*(FLOATF(N+1))-.5*FLOATF(N)

100     FORMAT(2F15.7,2I2)
110     FORMAT(5(2A6,F15.7,2(/12F6.3)))
200     FORMAT('1ADMITTANCE DATA FOR ',2A6,' A = ',F9.4/
      X ' FREQUENCY    RE ADM.    IM ADM.'/12(2X,F7.1,2X,2(4X,
      X F7.3)))
210     FORMAT('1FIELD DATA FOR ',2A6,' CP = ',F9.3/' H = ',
      X F6.1,' Z = ',F6.1//' RAD.  F(HZ)',3X,' A',6X,' B',6X,
      X ' C',6X,' D',6X,' E',6X,' F',3X,' -F(DB)',72(/2(1X,
      X F5.0),6(1X,F7.5),1X,F5.1))

310     DIMENSION A(5),R(6),F(12),X(12,5),Y(12,5),Q(2,5),FA(6,4),
      X FB(6,4),RA(6,4),SA(6,4,12),SB(6,4,12),TA(6,4,12),
      X TB(6,4,12),GA(6,4,12),GB(6,4,12)

C       DATA INPUT: ON EACH OF THE FIRST THREE CARDS, PLEASE SUPPLY
C       ME WITH THE INITIAL VALUS, THE INCREMENTING RATIO FOR THE
C       VALUE, AND THE TOTAL NUMBER OF VALUES TO BE TESTED FOR:
C       RADIAL SEPARATIONS (R-ARRAY), MICROPHONE HEIGHTS (Z-ARRAY)
C       AND FREQUENCIES (F-ARRAY) RESPECTIVELY. IF YOU INPUT A 0
C       OR A NEGATIVE NUMBER IN ANY DATA FIELD, I WILL SUPPLY AN
C       APPROPRIATE VALUE. IN THE CASE OF FREQUENCY, YOU CAN GIVE ME
C       A FOURTH DATUM CONSISTING OF AN INTEGER WHICH WILL START ME
C       AT THAT NUMBER OF 1/3 OCTAVES FROM 100 HERTZ.

330     READ(0,100)R(1),R(6),N6
        READ(0,100)Z(1),Z(4),N4
        READ(0,100)F(1),F(12),N12,N0

        EB = 0.4342944819
        PP = 6.2831853072
        IF(R(6))400,400,401
400     R(6) = 2.
401     IF(R(1))402,402,403
402     R(1) = 31.25
403     IF(Z(4))404,404,405
404     Z(4) = 2.
405     IF(Z(1))406,406,407
406     Z(1) = 5.
407     IF(F(12))408,408,409
408     F(12) = 10.**.1
409     IF(F(1))410,410,411
410     F(1) = 100. * F(12)**N0
411     IF(CCHK(N6,6))412,412,413
412     N6 = 6
```

```
413     IF(CCHK(N4,4)414,414,415
414     N4 = 4
415     IF(CCHK(N12,12)416,416,417
416     N12 = 12
417     DO 418 N = 2,N6
418     R(N) = R(6)*R(N-1)
        DO 419 N = 2,N4
419     Z(N) = Z(4)*Z(N-1)
        DO 420 N = 2,N10
420     F(N) = F(10)*F(N-1)

C       ADDITIONAL DATA INPUT: NOW I NEED TO KNOW SOME ADDITIONAL
C       INFORMATION. ON A SINGLE CARD, PLEASE TELL ME THE SOURCE
C       HEIGHT, SPEED OF SOUND IN THE UPPER MEDIUM, THE NUMBER OF
C       GROUND COVERS TO BE TESTED, AND WHETHER I SHOULD COME BACK
C       TO THIS POINT FOR FUTURE DATA INPUT. IF SO, GIVE ME A NON-0
C       INTEGER, OTHERWISE GIVE ME A 0. BE SURE TO GIVE ME A CARD
C       SUITABLY MADE OUT, FOR EVERY TIME I RETURN TO THIS SPOT.
C       THIS WILL BE THE TRICKY PART!

430     READ(0,100)H,CP,N5,N0
        DO 440 L = 1,N6
        DO 440 M = 1,N4
        UP = Z(M) - H
        CALL GENE(3,R(L),UP,U,V,TA(L,M,1))
        UP = Z(M) + H
        CALL GENE(3,R(L),UP,U,V,TB(L,M,1))
        FA(L,M) = UP/TB(L,M,1)
        RA(L,M) = R(L)/TA(L,M,1)
        FB(L,M) = R(L)/TB(L,M,1)
        TA(L,M,2) = 4.*Z(M)*H/((TA(L,M,1) + TB(L,M,1))*CP)
        DO 440 N = 1,N10
        UP = PP*AMODF(TA(L,M,2)*F(N),1.)
        SA(L,M,N) = FB(L,M)*COSF(UP)
440     SB(L,M,N) = FB(L,M)*SINF(UP)
431     IF(CCHK)(NN,5)432,432,433
432     NN = NN - 5
        N5 = 5
        GO TO 435
433     N5 = NN
        NN = 0

C       FINALLY I NEED TO KNOW THE SPECIFIC ADMITTANCE DATA. FOR
C       EACH OF THE GROUND COVERS, PLEASE GIVE ME FIVE CARDS. THE
C       FIRST SHOULD CONTAIN THE GROUND COVER NAME AND THE CONSTANT,
C       A. THE SECOND AND THIRD SHOULD LIST THE REAL AND IMAGINARY
C       PARTS OF THE ADMITTANCE, RESPECTIVELY. SINCE THIS PART IS
C       ALSO DIFFICULT, I WILL RETURN THE ADMITTANCE DATA AHEAD
C       OF THE FIELD DATA SO THAT YOU CAN CHECK ON ME.

435     READ(0,110)(Q(1,J),Q(2,J),A(J),(X(N,J),N=1,N12),(Y(N,J),
      X N=1,N12),J=1,N5)

        DO 460 J = 1,N5

        WRITE(1,200)Q(1,J),Q(2,J),A(J),(F(N),X(N,J),Y(N,J),N=1,N12)

        DO 450 N = 1,N10
        UP = X(N,J)
        VP = Y(N,J)
        CALL GENE(1,X(N,J),Y(N,J),UP,VP,RR)
```

```
      DO 450 M = 1,N4
      DO 450 L = 1,N6
      RR = (A(J) * FB(L,M))**2
      UP = 1. - UP*RR
      VP = -VP*RR
      CALL GENE(4,UP,VP,U,V,RR)
      CALL GENE(1,X(N,J),Y(N,J),U,V,RR)
      U = FA(L,M) + U
      RR = 2.*FA(L,M)
      TA(L,M,N) = SA(L,M,N)*RR
      TB(L,M,N) = SB(L,M,N)*RR
      CALL GENE(2,U,V,TA(L,M,N),TB(L,M,N),RR)
      U =  RA(L,M) - SA(L,M,N) + TA(L,M,N)
      V = -SA(L,M,N) + TA(L,M,N)
      CALL GENE(3,U,V,UP,VP,GA(L,M,N))
450   GB(L,M,N) = -20.*EB*ALOGF(GA(L,M,N))
      DO 460 M = 1,N4

C     NOW I RETURN THE LONG AWAITED DATA COMPLETE WITH PAGE
C     HEADINGS, PAGE DATA, AND COLUMN HEADINGS. THE LATTER ARE
C     MORE FULLY EXPLAINED IN PARAGRAPH (C.3) OF THIS REPORT.

460   WRITE(1,210)Q(1,J),Q(2,J),CP,H,F(M),(((R(L),F(N),RA(L,M),
     X SA(L,M,N),SB(L,M,N),TA(L,M,N),TB(L,M,N),GA(L,M,N),
      IF(NN)480,480,431
480   IF(N0)490,490,430
     X GB(L,M,N)),N=1,N12),L=1,N6)

490   STOP
      END

C     THE FOLLOWING SUBROUTINE, WHICH IS CALLED MANY TIMES DURING
C     THE COURSE OF A TYPICAL EXECUTION OF THE ABOVE PROGRAM,
C     CONSISTS OF A COMPLEX ARITHMETIC PACKAGE. OPERATIONAL
C     CONTROL IS EXERCISED BY THE INTEGER ARGUMENT WHERE 1,2,3,
C     AND 4 CALLS FOR MULTIPLICATION, DIVISION, MAGNITUDE, AND
C     SQUARE ROOT RESPECTIVELY. REAL AND IMAGINARY PARTS OF
C     COMPLEX NUMBERS AND MAGNITUDES ARE INPUT/OUTPUT ON THE FIVE
C     FLOATING POINT ARGUMENTS.

      SUBROUTINE GENE(N,X,Y,U,V,R)
      IF(N-1)810,820,830
830   R = SQRTF(X**2 + Y**2)
      A = -1.
      IF(N-3)840,810,850
820   A = 1.
840   T = U*X - A*V*Y
      V = V*X + A*U*Y
      U = T
      IF(N-1)810,810,860
860   V = V/R
      U = U/R
      GO TO 810
850   U = SQRTF(.5*ABSF(R + X))
      V = SQRTF(.5*ABSF(R - X))
810   RETURN
      END
*
```

C.3 <u>Program Output Data</u>

The program output consists of 12 pages of data, each page containing the results for a given ground cover and microphone/receiver height. The data on each page is delineated in nine columns, the first two of which list the frequency and frequency and radial separation r.

$$A \longrightarrow \frac{r}{R}$$

$$\left\{\begin{matrix} B \\ C \end{matrix}\right\} \longrightarrow \left\{\begin{matrix} \mathrm{Re} \\ \mathrm{Im} \end{matrix}\right\} \left[\frac{r}{R'} \, e^{ik\Delta} \right]$$

$$\left\{\begin{matrix} D \\ E \end{matrix}\right\} \longrightarrow \left\{\begin{matrix} \mathrm{Re} \\ \mathrm{Im} \end{matrix}\right\} \left[\frac{r}{R'} \, \frac{2 \cos \theta}{\cos \theta - \eta(\theta)} \, e^{ik\Delta} \right]$$

$$F \longrightarrow r \left| \psi (r, z; 0, h) \right|$$

$$-F(\mathrm{dB}) \longrightarrow -20 \log \left\{ r \left| \psi (r, z; 0, h) \right| \right.$$

TABLE C.1

ATTENUATION DATA FOR Z = 5 FEET FOR CONCRETE

f(Hz)	r(ft)	A	B	C	D	E	F	-F(dB)
158.	31.	1.00000	.13474	.94285	.21496	.53929	1.15314	-1.2
200.	31.	1.00000	-.21529	.92777	-.00237	.58055	1.26165	-2.0
251.	31.	1.00000	-.60902	.73226	-.28736	.50444	1.34115	-2.5
316.	31.	1.00000	-.91247	.27295	-.53676	.22120	1.37669	-2.8
398.	31.	1.00000	-.85863	-.41214	-.55749	-.16199	1.32497	-2.4
501.	31.	1.00000	-.18359	-.93456	-.19180	-.54795	1.06448	-.5
631.	31.	1.00000	.78884	-.53371	.45304	-.36303	.68578	3.3
794.	31.	1.00000	.60829	.73287	.38583	.43379	.83308	1.6
1000.	31.	1.00000	-.87374	.37908	-.50614	.28436	1.37087	-2.7
158.	62.	1.00000	.73737	.65676	.24152	.19753	.68195	3.3
200.	62.	1.00000	.60131	.78324	.20091	.23872	.80995	1.8
251.	62.	1.00000	.40044	.90260	.13991	.27888	.96739	.3
316.	62.	1.00000	.11719	.98046	.05222	.30761	1.15196	-1.2
398.	62.	1.00000	-.25094	.95502	-.06884	.30432	1.34936	-2.6
501.	62.	1.00000	-.65865	.73568	-.20091	.23872	1.54011	-3.8
631.	62.	1.00000	-.95800	.23932	-.30091	.08251	1.66450	-4.4
794.	62.	1.00000	-.86406	-.47795	-.27643	-.14470	1.62223	-4.2
1000.	62.	1.00000	-.11947	-.98019	-.04226	-.30914	1.26913	-2.1
158.	125.	1.00000	.93095	.35632	.13543	-.08326	.48482	6.3
200.	125.	1.00000	.89311	.44271	.14842	-.05698	.56114	5.0
251.	125.	1.00000	.83415	.54574	.15896	.00268	.63279	4.0
316.	125.	1.00000	.74322	.66428	.14449	.06632	.72011	2.9
398.	125.	1.00000	.60530	.79199	.13822	.07855	.89050	1.0
501.	125.	1.00000	.40175	.91227	.10637	.11815	1.06166	-.5
631.	125.	1.00000	.11489	.99017	.04195	.15335	1.24889	-1.9
794.	125.	1.00000	-.25751	.96298	-.03115	.15590	1.46811	-3.3
1000.	125.	1.00000	-.66895	.73902	-.08657	.13335	1.69433	-4.6
158.	250.	1.00000	.98252	.18183	.07909	.01114	.19611	14.1
200.	250.	1.00000	.97280	.22816	.07852	.01466	.23824	12.5
251.	250.	1.00000	.95747	.28575	.07755	.01912	.29242	10.7
316.	250.	1.00000	.93333	.35678	.07594	.02476	.36135	8.8
398.	250.	1.00000	.89549	.44329	.07277	.03292	.44703	7.0
501.	250.	1.00000	.83652	.54648	.06818	.04160	.55550	5.1
631.	250.	1.00000	.74557	.66523	.06080	.05179	.68969	3.2
794.	250.	1.00000	.60761	.79323	.05002	.06227	.85443	1.4
1000.	250.	1.00000	.40395	.91391	.03336	.07257	1.05071	-.4
158.	500.	1.00000	.99562	.09138	.02712	-.02938	.12480	18.1
200.	500.	1.00000	.99317	.11494	.03028	-.02611	.14586	16.7
251.	500.	1.00000	.98930	.14452	.03655	-.01621	.16753	15.5
316.	500.	1.00000	.98318	.18157	.03971	-.00465	.19461	14.2
398.	500.	1.00000	.97349	.22783	.03940	-.00683	.24374	12.3
501.	500.	1.00000	.95822	.28534	.03997	-.00115	.29793	10.5
631.	500.	1.00000	.93416	.35628	.03908	.00845	.36332	8.8
794.	500.	1.00000	.89645	.44270	.03691	.01537	.44982	6.9
1000.	500.	1.00000	.83767	.54581	.03655	.01622	.56570	4.9
158.	1000.	1.00000	.99890	.04575	.02000	.00005	.05033	26.0
200.	1000.	1.00000	.99829	.05758	.02000	.00024	.06131	24.2
251.	1000.	1.00000	.99732	.07247	.01999	.00049	.07547	22.4
316.	1000.	1.00000	.99578	.09118	.01998	.00083	.09354	20.6
398.	1000.	1.00000	.99335	.11470	.01993	.00160	.11618	18.7
501.	1000.	1.00000	.98950	.14421	.01987	.00227	.14515	16.8
631.	1000.	1.00000	.98340	.18118	.01975	.00317	.18168	14.8
794.	1000.	1.00000	.97376	.22735	.01957	.00409	.22791	12.8
1000.	1000.	1.00000	.95855	.28475	.01925	.00541	.28586	10.9

TABLE C.2

ATTENUATION DATA FOR Z = 10 FEET FOR CONCRETE

f(Hz)	r(ft)	A	B	C	D	E	F	-F(dB)
158.	31.	.98744	-.83692	.33511	-.21039	.75133	1.66678	-4.4
200.	31.	.98744	-.85171	-.29551	-.68735	.36921	1.32986	-2.5
251.	31.	.98744	-.29803	-.85084	-.61095	-.48529	.76720	2.3
316.	31.	.98744	.64419	-.63068	.37195	-.68587	.71732	2.9
398.	31.	.98744	.71689	.54664	.75598	.19304	1.08572	-.7
501.	31.	.98744	-.69266	.57703	-.41315	.66187	1.26979	-2.1
631.	31.	.98744	-.00442	-.90151	-.12156	-.77071	.88007	1.1
794.	31.	.98744	.26704	.86106	.27838	.72888	1.00749	-.1
1000.	31.	.98744	.12606	-.89267	-.01529	-.78008	.85355	1.4
158.	62.	.99682	.12512	.96430	.07770	.44716	1.08111	-.7
200.	62.	.99682	-.23518	.94352	-.08950	.44495	1.24654	-1.9
251.	62.	.99682	-.63696	.73473	-.28041	.35687	1.40512	-3.0
316.	62.	.99682	-.93847	.25458	-.43154	.14056	1.50806	-3.6
398.	62.	.99682	-.86252	-.44899	-.40964	-.19540	1.47171	-3.4
501.	62.	.99682	-.14833	-.96101	-.08305	-.44620	1.18029	-1.4
631.	62.	.99682	.83231	-.50279	.38298	-.24354	.60577	4.4
794.	62.	.99682	.57134	.78683	.27511	.36098	.81985	1.7
1000.	62.	.99682	-.92059	.31314	-.42749	.15243	1.49855	-3.5
158.	125.	.99920	.74029	.66165	.23244	-.04411	.85996	1.3
200.	125.	.99920	.60292	.78886	.23561	.02157	.99399	.1
251.	125.	.99920	.40017	.90866	.19615	.13229	1.11134	-.9
316.	125.	.99920	.11445	.98626	.09531	.21655	1.24618	-1.9
398.	125.	.99920	-.25647	.95918	.03306	.23427	1.47862	-3.4
501.	125.	.99920	-.66628	.73612	-.09592	.21627	1.65341	-4.4
631.	125.	.99920	-.96490	.23404	-.21887	.08984	1.75118	-4.9
794.	125.	.99920	-.86465	-.48805	-.21306	-.10286	1.69513	-4.6
1000.	125.	.99920	-.10943	-.98683	-.06318	-.22800	1.29181	-2.2
158.	250.	.99980	.93217	.35703	.11340	.03792	.36687	8.7
200.	250.	.99980	.89423	.44358	.10943	.04818	.45007	6.9
251.	250.	.99980	.83512	.54679	.10308	.06059	.55505	5.1
316.	250.	.99980	.74397	.66553	.09299	.07517	.68571	3.3
398.	250.	.99980	.60571	.79343	.07582	.09245	.84391	1.5
501.	250.	.99980	.40168	.91382	.05147	.10792	1.03511	-.3
631.	250.	.99980	.11419	.99165	.01640	.11844	1.25544	-2.0
794.	250.	.99980	-.25892	.96404	-.02833	.11616	1.49424	-3.5
1000.	250.	.99980	-.67090	.73913	-.07906	.08970	1.71903	-4.7
158.	500.	.99995	.98286	.18192	.04451	-.04015	.23046	12.7
200.	500.	.99995	.97313	.22827	.04959	-.03367	.27286	11.3
251.	500.	.99995	.95779	.28589	.05773	-.01614	.31812	9.9
316.	500.	.99995	.93364	.35695	.05982	.00396	.37485	8.5
398.	500.	.99995	.89577	.44351	.05984	.00349	.46959	6.6
501.	500.	.99995	.83676	.54674	.05792	.01544	.57547	4.8
631.	500.	.99995	.74576	.66554	.05024	.03271	.70225	3.1
794.	500.	.99995	.60771	.79359	.03942	.04516	.86399	1.3
1000.	500.	.99995	.40393	.91430	.03265	.05028	1.06853	-.6
158.	1000.	.99999	.99570	.09139	.02781	-.01124	.10753	19.4
200.	1000.	.99999	.99326	.11496	.02850	-.00934	.12920	17.8
251.	1000.	.99999	.98939	.14454	.02963	-.00464	.15450	16.2
316.	1000.	.99999	.98326	.18159	.02999	.00052	.18700	14.6
398.	1000.	.99999	.97358	.22786	.02999	.00049	.23426	12.6
501.	1000.	.99999	.95830	.28538	.02978	.00359	.29071	10.7
631.	1000.	.99999	.93424	.35633	.02878	.00843	.36051	8.9
794.	1000.	.99999	.89652	.44276	.02714	.01276	.44939	6.9
1000.	1000.	.99999	.83774	.54587	.02640	.01424	.56411	5.0

TABLE C.3

ATTENUATION DATA FOR Z = 20 FEET FOR CONCRETE

f(Hz)	r(ft)	A	B	C	D	E	F	-F(dB)
158.	31.	.90152	.14756	-.76680	-.27884	-.93491	.50399	6.0
200.	31.	.90152	.77604	-.08673	.83294	-.50797	1.04691	-.4
251.	31.	.90152	.06554	.77811	.37044	.90255	1.21282	-1.7
316.	31.	.90152	-.73163	-.27289	-.95941	-.17703	.68053	3.3
398.	31.	.90152	.75624	-.19458	.86982	-.44184	1.04479	-.4
501.	31.	.90152	-.76454	.15887	-.90622	.36135	.78635	2.1
631.	31.	.90152	.61319	.48348	.81585	.53498	1.10538	-.9
794.	31.	.90152	.66076	-.41612	.80208	-.55542	1.05210	-.4
1000.	31.	.90152	.69146	-.36282	.82111	-.52687	1.04414	-.4
158.	62.	.97239	-.86922	.32638	-.46075	.51316	1.39343	-2.9
200.	62.	.97239	-.86855	-.32816	-.68771	.05174	1.21419	-1.7
251.	62.	.97239	-.27667	-.88630	-.39396	-.56606	.91310	.8
316.	62.	.97239	.69090	-.62026	.42539	-.54283	.71110	3.0
398.	62.	.97239	.70661	.60231	.60924	.32318	.91847	.7
501.	62.	.97239	-.75238	.54405	-.48019	.49501	1.24554	-1.9
631.	62.	.97239	.07545	-.92541	-.00408	-.68964	.92346	.7
794.	62.	.97239	.17730	.91139	.16110	.67058	.98604	.1
1000.	62.	.97239	.25391	-.89309	.13006	-.67728	.87556	1.2
158.	125.	.99288	.12299	.97284	.21898	.31619	1.27155	-2.1
200.	125.	.99288	-.24109	.95048	.07185	.37784	1.42586	-3.1
251.	125.	.99288	-.64617	.73757	-.15473	.35212	1.53355	-3.7
316.	125.	.99288	-.94804	.25052	-.34914	.16134	1.59427	-4.1
398.	125.	.99288	-.86603	-.45992	-.37068	-.10260	1.53052	-3.7
501.	125.	.99288	-.13951	-.97061	-.12000	-.36542	1.17949	-1.4
631.	125.	.99288	.84587	-.49602	.31356	-.22273	.53554	5.4
794.	125.	.99288	.56303	.80283	.23436	.37496	.83009	1.6
1000.	125.	.99288	-.93468	.29649	-.35508	.14780	1.57949	-4.0
158.	250.	.99820	.74161	.66341	.19187	.04896	.76070	2.4
200.	250.	.99820	.60380	.79090	.17542	.09187	.90186	.9
251.	250.	.99820	.40042	.91091	.13051	.14893	1.05406	-.5
316.	250.	.99820	.11385	.98850	.05647	.18980	1.23413	-1.8
398.	250.	.99820	-.25807	.96099	-.00875	.19783	1.46244	-3.3
501.	250.	.99820	-.66874	.73681	-.10560	.16751	1.66190	-4.4
631.	250.	.99820	-.96740	.23289	-.18775	.06295	1.78596	-5.0
794.	250.	.99820	-.86547	-.49098	-.17633	-.09010	1.73431	-4.8
1000.	250.	.99820	-.10697	-.98927	-.03837	-.19427	1.33046	-2.5
158.	500.	.99955	.93266	.35727	.09910	-.01136	.40428	7.9
200.	500.	.99955	.89469	.44388	.09972	.00241	.48656	6.3
251.	500.	.99955	.83553	.54717	.09602	.02703	.58152	4.7
316.	500.	.99955	.74430	.66597	.08476	.05260	.70131	3.1
398.	500.	.99955	.60593	.79395	.07625	.06432	.86783	1.2
501.	500.	.99955	.40174	.91439	.05537	.08297	1.05731	-.5
631.	500.	.99955	.11404	.99222	.01998	.09773	1.27281	-2.1
794.	500.	.99955	-.25933	.96450	-.02167	.09737	1.51082	-3.6
1000.	500.	.99955	-.67152	.73930	-.06038	.07940	1.74063	-4.8
158.	1000.	.99989	.98299	.18195	.04778	-.01462	.20694	13.7
200.	1000.	.99989	.97327	.22831	.04891	-.01022	.25020	12.0
251.	1000.	.99989	.95792	.28594	.04996	-.00077	.30108	10.4
316.	1000.	.99989	.93376	.35701	.04906	.00947	.36614	8.7
398.	1000.	.99989	.89589	.44358	.04852	.01195	.45778	6.8
501.	1000.	.99989	.83687	.54684	.04594	.01965	.56709	4.9
631.	1000.	.99989	.74584	.66565	.04004	.02990	.70048	3.1
794.	1000.	.99989	.60777	.79372	.03208	.03831	.86637	1.2
1000.	1000.	.99989	.40395	.91444	.02410	.04377	1.06888	-.6

TABLE C.4

ATTENUATION DATA FOR Z = 30 FEET FOR CONCRETE

f(Hz)	r(ft)	A	B	C	D	E	F	-F(dB)
158.	31.	.78087	.66564	.02251	.89635	-.42875	1.10767	-.9
200.	31.	.78087	-.06559	.66278	.32920	.93749	1.20732	-1.6
251.	31.	.78087	-.55454	-.36887	-.95449	-.27606	.39206	8.1
316.	31.	.78087	.66554	.02509	.98432	-.13555	1.11132	-.9
398.	31.	.78087	-.65755	-.10584	-.99191	.05816	.47568	6.5
501.	31.	.78087	.28626	.60136	.57636	.80937	1.09099	-.8
631.	31.	.78087	.66593	.01042	.99107	-.07110	1.10900	-.9
794.	31.	.78087	.64628	.16091	.97373	.19778	1.10893	-.9
1000.	31.	.78087	-.36922	.55431	-.47666	.87182	.74453	2.6
158.	62.	.92848	-.60096	-.63254	-.80633	-.27711	.80574	1.9
200.	62.	.92848	.22736	-.84236	-.14652	-.83993	.55460	5.1
251.	62.	.92848	.87235	-.01637	.80820	-.27159	.90123	.9
316.	62.	.92848	-.02832	.87205	.12072	.84403	1.07788	-.7
398.	62.	.92848	-.76416	-.42111	-.81810	-.24013	.89306	1.0
501.	62.	.92848	.87054	-.05858	.82783	-.20410	.89764	.9
631.	62.	.92848	-.87217	-.02405	-.85110	.05087	.95250	.4
794.	62.	.92848	.50018	.71490	.51879	.67662	.94786	.5
1000.	62.	.92848	.85620	-.16787	.81921	-.23634	.89411	1.0
158.	125.	.98058	-.51463	.81391	-.04349	.51746	1.48167	-3.4
200.	125.	.98058	-.86530	.42255	-.32660	.40372	1.51940	-3.6
251.	125.	.98058	-.93501	-.23035	-.51823	.03315	1.42199	-3.1
316.	125.	.98058	-.42168	-.86573	-.30501	-.42027	1.18423	-1.5
398.	125.	.98058	.58241	-.76687	.21712	-.47172	.68242	3.3
501.	125.	.98058	.85982	.43360	.49723	.14975	.68005	3.3
631.	125.	.98058	-.57823	.77003	-.27444	.44084	1.32589	-2.5
794.	125.	.98058	-.28194	-.92077	-.17355	-.48943	1.17128	-1.4
1000.	125.	.98058	.59695	.75561	.35620	.37786	.83069	1.6
158.	250.	.99504	.45770	.87823	.22503	.15741	1.04918	-.4
200.	250.	.99504	.19491	.97097	.16277	.22118	1.22039	-1.7
251.	250.	.99504	-.15516	.97811	.04053	.27161	1.38454	-2.8
316.	250.	.99504	-.56308	.81469	-.11454	.24959	1.55024	-3.8
398.	250.	.99504	-.91111	.38813	-.22336	.15976	1.69821	-4.6
501.	250.	.99504	-.94420	-.29876	-.27223	-.03612	1.68757	-4.5
631.	250.	.99504	-.35956	-.92276	-.12163	-.24621	1.40639	-3.0
794.	250.	.99504	.67678	-.72301	.17875	-.20848	.71536	2.9
1000.	250.	.99504	.81928	.55638	.23977	.13389	.59258	4.5
158.	500.	.99875	.85139	.51987	.13899	.00950	.58522	4.7
200.	500.	.99875	.76928	.63508	.13485	.03498	.70204	3.1
251.	500.	.99875	.64415	.76170	.11779	.07440	.83398	1.6
316.	500.	.99875	.45801	.88620	.08448	.11078	.99609	.0
398.	500.	.99875	.19213	.97888	.05579	.12766	1.21175	-1.7
501.	500.	.99875	-.16161	.98438	.00164	.13931	1.43681	-3.1
631.	500.	.99875	-.57276	.81674	-.06974	.12060	1.65527	-4.4
794.	500.	.99875	-.92107	.38308	-.12618	.05906	1.82268	-5.2
1000.	500.	.99875	-.94778	-.31118	-.13565	-.03176	1.83232	-5.3
158.	1000.	.99969	.96198	.27087	.06844	-.01427	.30426	10.3
200.	1000.	.99969	.94032	.33850	.06963	-.00634	.36818	8.7
251.	1000.	.99969	.90631	.42116	.06933	.00903	.44308	7.1
316.	1000.	.99969	.85323	.52036	.06510	.02548	.53820	5.4
398.	1000.	.99969	.77113	.63572	.06229	.03174	.67036	3.5
501.	1000.	.99969	.64599	.76255	.05377	.04469	.82544	1.7
631.	1000.	.99969	.45981	.88733	.03745	.05904	1.00965	-.1
794.	1000.	.99969	.19381	.98041	.01654	.06793	1.22841	-1.8
1000.	1000.	.99969	-.16022	.98646	-.00515	.06972	1.47441	-3.4

TABLE C.5

ATTENUATION DATA FOR Z = 5 FEET FOR ASPHALT

f(Hz)	r(ft)	A	B	C	D	E	F	-F(dB)
158.	31.	1.00000	.13474	.94285	.19024	.54850	1.12676	-1.0
200.	31.	1.00000	-.21529	.92777	-.05865	.57758	1.20849	-1.6
251.	31.	1.00000	-.60902	.73226	-.33285	.47566	1.30171	-2.3
316.	31.	1.00000	-.91247	.27295	-.54923	.18812	1.36588	-2.7
398.	31.	1.00000	-.85863	-.41214	-.52473	-.24839	1.34392	-2.6
501.	31.	1.00000	-.18359	-.93456	-.10555	-.57088	1.13773	-1.1
631.	31.	1.00000	.78884	-.53371	.49509	-.30320	.74291	2.6
794.	31.	1.00000	.60829	.73287	.35417	.46000	.79423	2.0
1000.	31.	1.00000	-.87374	.37908	-.53744	.21955	1.34579	-2.6
158.	62.	1.00000	.73737	.65676	.26813	.15956	.72726	2.8
200.	62.	1.00000	.60131	.78324	.23686	.20309	.86052	1.3
251.	62.	1.00000	.40044	.90260	.18539	.25097	1.02018	-.2
316.	62.	1.00000	.11719	.98046	.10733	.29297	1.20541	-1.6
398.	62.	1.00000	-.25094	.95502	.00481	.31198	1.41083	-3.0
501.	62.	1.00000	-.65865	.73568	-.11795	.28886	1.60418	-4.1
631.	62.	1.00000	-.95800	.23932	-.21987	.22138	1.73822	-4.8
794.	62.	1.00000	-.86406	-.47795	-.30363	.07184	1.65445	-4.4
1000.	62.	1.00000	-.11947	-.98019	-.27233	-.15228	1.18451	-1.5
158.	125.	1.00000	.93095	.35632	.15643	-.01324	.43396	7.3
200.	125.	1.00000	.89311	.44271	.15696	.02527	.49384	6.1
251.	125.	1.00000	.83415	.54574	.14774	.05872	.57925	4.7
316.	125.	1.00000	.74322	.66428	.12841	.09373	.68840	3.2
398.	125.	1.00000	.60530	.79199	.09873	.12461	.82998	1.6
501.	125.	1.00000	.40175	.91227	.05941	.14746	1.00869	-.1
631.	125.	1.00000	.11489	.99017	-.01417	.15835	1.20435	-1.6
794.	125.	1.00000	-.25751	.96298	-.07255	.14146	1.44188	-3.2
1000.	125.	1.00000	-.66895	.73902	-.12263	.10118	1.67271	-4.5
158.	250.	1.00000	.98252	.18183	.07985	-.00168	.20773	13.7
200.	250.	1.00000	.97280	.22816	.07987	.00068	.25142	12.0
251.	250.	1.00000	.95747	.28575	.07975	.00443	.30674	10.3
316.	250.	1.00000	.93333	.35678	.07934	.00919	.37701	8.5
398.	250.	1.00000	.89549	.44329	.07881	.01297	.46774	6.6
501.	250.	1.00000	.83652	.54648	.07832	.01569	.58327	4.7
631.	250.	1.00000	.74557	.66523	.07958	.00684	.73827	2.6
794.	250.	1.00000	.60761	.79323	.07987	.00033	.92289	.7
1000.	250.	1.00000	.40395	.91391	.07981	-.00314	1.13920	-1.1
158.	500.	1.00000	.99562	.09138	.03744	-.01404	.11341	18.9
200.	500.	1.00000	.99317	.11494	.03929	-.00741	.13076	17.7
251.	500.	1.00000	.98930	.14452	.03992	-.00227	.15527	16.2
316.	500.	1.00000	.98318	.18157	.03985	.00333	.18703	14.6
398.	500.	1.00000	.97349	.22783	.03909	.00843	.22900	12.8
501.	500.	1.00000	.95822	.28534	.03794	.01263	.28413	10.9
631.	500.	1.00000	.93416	.35628	.03364	.02161	.34914	9.1
794.	500.	1.00000	.89645	.44270	.03124	.02496	.43895	7.2
1000.	500.	1.00000	.83767	.54581	.02993	.02651	.55374	5.1
158.	1000.	1.00000	.99890	.04575	.01975	-.00315	.05316	25.5
200.	1000.	1.00000	.99829	.05758	.01973	-.00327	.06452	23.8
251.	1000.	1.00000	.99732	.07247	.01974	-.00323	.07894	22.1
316.	1000.	1.00000	.99578	.09118	.01975	-.00316	.09734	20.2
398.	1000.	1.00000	.99335	.11470	.01967	-.00361	.12120	18.3
501.	1000.	1.00000	.98950	.14421	.01944	-.00468	.15188	16.4
631.	1000.	1.00000	.98340	.18118	.01791	-.00889	.19318	14.3
794.	1000.	1.00000	.97376	.22735	.01550	-.01264	.24359	12.3
1000.	1000.	1.00000	.95855	.28475	.01234	-.01574	.30527	10.3

TABLE C.6

ATTENUATION DATA FOR Z = 10 FEET FOR ASPHALT

f(Hz)	r(ft)	A	B	C	D	E	F	-F(dB)
158.	31.	.98744	-.83692	.33511	-.52582	.57644	1.32078	-2.4
200.	31.	.98744	-.85171	-.29551	-.77983	-.02519	1.09327	-.8
251.	31.	.98744	-.29803	-.85084	-.40028	-.66973	.90353	.9
316.	31.	.98744	.64419	-.63068	.50071	-.59837	.84458	1.5
398.	31.	.98744	.71689	.54664	.62864	.46215	.90315	.9
501.	31.	.98744	-.69266	.57703	-.61515	.47996	1.06937	-.6
631.	31.	.98744	-.00442	-.90151	.15642	-.76439	1.15643	-1.3
794.	31.	.98744	.26704	.86106	.06654	.77739	.79137	2.0
1000.	31.	.98744	.12606	-.89267	.22147	-.74814	1.09246	-.8
158.	62.	.99682	.12512	.96430	.14840	.42891	1.15206	-1.2
200.	62.	.99682	-.23518	.94352	-.01014	.45374	1.31636	-2.4
251.	62.	.99682	-.63696	.73473	-.20946	.40263	1.46252	-3.3
316.	62.	.99682	-.93847	.25458	-.39505	.22344	1.54055	-3.8
398.	62.	.99682	-.86252	-.44899	-.44625	-.08274	1.45978	-3.3
501.	62.	.99682	-.14833	-.96101	-.23109	-.39062	1.07742	-.6
631.	62.	.99682	.83231	-.50279	.17015	]42075	.34457	9.3
794.	62.	.99682	.57134	.78683	.45366	.01328	1.17101	-1.4
1000.	62.	.99682	-.92059	.31314	-.02187	.45333	1.90071	-5.6
158.	125.	.99920	.74029	.66165	.22745	.06514	.76965	2.3
200.	125.	.99920	.60292	.78886	.19303	.13680	.87890	1.1
251.	125.	.99920	.40017	.90866	.13682	.19302	1.02646	-.2
316.	125.	.99920	.11445	.98626	.05042	.23116	1.20196	-1.6
398.	125.	.99920	-.25647	.95918	-.05710	.22960	1.40316	-2.9
501.	125.	.99920	-.66628	.73612	-.16430	.17024	1.60430	-4.1
631.	125.	.99920	-.96490	.23404	-.23648	.00738	1.74243	-4.8
794.	125.	.99920	-.86465	-.48805	-.17643	-.15764	1.71946	-4.7
1000.	125.	.99920	-.10943	-.98683	.00877	-.23643	1.34599	-2.6
158.	250.	.99980	.93217	.35703	.11801	.01925	.38543	8.3
200.	250.	.99982	.89423	.44358	.11618	.02825	.47081	6.5
251.	250.	.99980	.83512	.54679	.11252	.04046	.57725	4.8
316.	250.	.99980	.74397	.66553	.10606	.05521	.70954	3.0
398.	250.	.99980	.60571	.79343	.09717	.06968	.87472	1.2
501.	250.	.99980	.40168	.91382	.08537	.08372	1.07529	-.6
631.	250.	.99980	.11419	.99165	.08218	.08686	1.32487	-2.4
794.	250.	.99980	-.25892	.96404	.07247	.09511	1.58969	-4.0
1000.	250.	.99980	-.67090	.73913	.05283	.10726	1.83571	-5.3
158.	500.	.99995	.98286	.18192	.05782	-.01584	.21147	13.5
200.	500.	.99995	.97313	.22827	.05979	-.00427	.24815	12.1
251.	500.	.99995	.95779	.28589	.05971	.00529	.29852	10.5
316.	500.	.99995	.93364	.35695	.05784	.01576	.36308	8.8
398.	500.	.99995	.89577	.44351	.05418	.02565	.44685	7.0
501.	500.	.99995	.83676	.54674	.04911	.03438	.55461	5.1
631.	500.	.99995	.74576	.66554	.03558	.04825	.68193	3.3
794.	500.	.99995	.60771	.79359	.02543	.05428	.84914	1.4
1000.	500.	.99995	.40393	.91430	.01590	.05780	1.05263	-.4
158.	1000.	.99999	.99570	.09139	.02980	-.00337	.10070	19.9
200.	1000.	.99999	.99326	.11496	.02982	-.00319	.12368	18.2
251.	1000.	.99999	.98939	.14454	.02987	-.00268	.15268	16.3
316.	1000.	.99999	.98326	.18159	.02993	-.00201	.18944	14.5
398.	1000.	.99999	.97358	.22786	.02993	-.00200	.23666	12.5
501.	1000.	.99999	.95830	.28538	.02987	-.00274	.29688	10.5
631.	1000.	.99999	.93424	.35633	.02884	-.00825	.37665	8.5
794.	1000.	.99999	.89652	.44276	.02695	-.01317	.47422	6.5
1000.	1000.	.99999	.83774	.54587	.02446	-.01736	.59337	4.5

TABLE C.7

ATTENUATION DATA FOR Z = 20 FEET FOR ASPHALT

f(Hz)	r(ft)	A	B	C	D	E	F	-F(dB)
158.	31.	.90152	.14756	-.76680	-.25111	-.94274	.53274	5.5
200.	31.	.90152	.77604	-.08673	.89359	-.39154	1.06369	-.5
251.	31.	.90152	.06554	.77811	.27506	.93603	1.12221	-1.0
316.	31.	.90152	-.73163	-.27289	-.94337	-.24872	.69021	3.2
398.	31.	.90152	.75624	-.19458	.94043	-.25963	1.08766	-.7
501.	31.	.90152	-.76454	.15887	-.96107	.16782	.70505	3.0
631.	31.	.90152	.61319	.48348	.62581	.74845	.95177	.4
794.	31.	.90152	.66076	-.41612	.91757	-.33148	1.16142	-1.3
1000.	31.	.90152	.69146	-.36282	.92115	-.32139	1.13197	-1.1
158.	62.	.97239	-.86922	.32638	-.58312	.36824	1.25919	-2.0
200.	62.	.97239	-.86855	-.32816	-.68297	-.09577	1.18105	-1.4
251.	62.	.97239	-.27667	-.88630	-.35288	-.59254	.94310	.5
316.	62.	.97239	.69090	-.62026	.38334	-.57330	.66648	3.5
398.	62.	.97239	.70661	.60231	.63270	.27443	.95644	.4
501.	62.	.97239	-.75238	.54405	-.36847	.58297	1.35686	-2.7
631.	62.	.97239	.07545	-.92541	-.36734	-.58368	.63027	4.0
794.	62.	.97239	.17730	.91139	.61637	.30937	1.53449	-3.7
1000.	62.	.97239	.25391	-.89309	-.54774	-.41905	.50385	6.0
158.	125.	.99288	.12299	.97284	.20955	.32252	1.26020	-2.0
200.	125.	.99288	-.24109	.95048	.02048	.38407	1.37639	-2.8
251.	125.	.99288	-.64617	.73757	-.19033	.33422	1.50382	-3.5
316.	125.	.99288	-.94804	.25052	-.36029	.13462	1.58487	-4.0
398.	125.	.99288	-.86603	-.45992	-.34280	-.17441	1.54276	-3.8
501.	125.	.99288	-.13951	-.97061	-.04251	-.38226	1.23854	-1.9
631.	125.	.99288	.84587	-.49602	.36465	-.12231	.63360	4.0
794.	125.	.99288	.56303	.80283	.14845	.35481	.73154	2.7
1000.	125.	.99288	-.93468	.29649	-.37972	.06114	1.56563	-3.9
158.	250.	.99820	.74161	.66341	.17128	.09937	.70796	3.0
200.	250.	.99820	.60380	.79090	.15186	.12709	.85968	1.3
251.	250.	.99820	.40042	.91091	.11963	.15780	1.04014	-.3
316.	250.	.99820	.11385	.98850	.07059	.18501	1.24801	-1.9
398.	250.	.99820	-.25807	.96099	.00678	.19790	1.47568	-3.4
501.	250.	.99820	-.66874	.73681	-.06900	.18561	1.69034	-4.6
631.	250.	.99820	-.96740	.23289	-.12627	.15253	1.84109	-5.3
794.	250.	.99820	-.86547	-.49098	-.18258	.07665	1.77433	-5.0
1000.	250.	.99820	-.10697	-.98927	-.19093	-.05251	1.30896	-2.3
158.	500.	.99955	.93266	.35727	.09939	-.00843	.40173	7.9
200.	500.	.99955	.89469	.44388	.09849	.01578	.47394	6.5
251.	500.	.99955	.83553	.54717	.09271	.03682	.57128	4.9
316.	500.	.99955	.74430	.66597	.08056	.05882	.69383	3.2
398.	500.	.99955	.60593	.79395	.06190	.07822	.84838	1.4
501.	500.	.99955	.40174	.91439	.03718	.09256	1.03857	-.3
631.	500.	.99955	.11404	.99222	-.00920	.09933	1.25108	-1.9
794.	500.	.99955	-.25933	.96450	-.04589	.08857	1.49620	-3.5
1000.	500.	.99955	-.67152	.73930	-.07719	.06318	1.73136	-4.8
158.	1000.	.99989	.98299	.18195	.04996	-.00105	.19483	14.2
200.	1000.	.99989	.97327	.22831	.04997	.00042	.24041	12.4
251.	1000.	.99989	.95792	.28594	.04989	.00277	.29769	10.5
316.	1000.	.99989	.93376	.35701	.04964	.00575	.36985	8.6
398.	1000.	.99989	.89589	.44358	.04931	.00811	.46167	6.7
501.	1000.	.99989	.83687	.54684	.04900	.00982	.57736	4.8
631.	1000.	.99989	.74584	.66565	.04979	.00427	.72783	2.8
794.	1000.	.99989	.60777	.79372	.04997	.00019	.90837	.8
1000.	1000.	.99989	.40395	.91444	.04993	-.00199	1.12116	-1.0

TABLE C.8

ATTENUATION DATA FOR Z = 30 FEET FOR ASPHALT

f(Hz)	r(ft)	A	B	C	D	E	F	-F(dB)
158.	31.	.78087	.66564	.02251	.90862	-.40210	1.10840	-.9
200.	31.	.78087	-.06559	.66278	.20036	.97320	1.09187	-.8
251.	31.	.78087	-.55454	-.36887	-.92081	-.37334	.41463	7.6
316.	31.	.78087	.66554	.02509	.99173	-.06111	1.11041	-.9
398.	31.	.78087	-.65755	-.10584	-.98360	-.14068	.45615	6.8
501.	31.	.78087	.28626	.60136	.39813	.91036	.94471	.5
631.	31.	.78087	.66593	.01042	.96914	.21915	1.10399	-.9
794.	31.	.78087	.64628	.16091	.89061	.44055	1.06265	-.5
1000.	31.	.78087	-.36922	.55431	-.66640	.73701	.51704	5.7
158.	62.	.92848	-.60096	-.63254	-.70034	-.48629	.84190	1.5
200.	62.	.92848	.22736	-.84236	.03554	-.85188	.73672	2.7
251.	62.	.92848	.87235	-.01637	.82541	-.21367	.90335	.9
316.	62.	.92848	-.02832	.87205	.18389	.83255	1.14137	-1.1
398.	62.	.92848	-.76416	-.42111	-.83441	-.17527	.89274	1.0
501.	62.	.92848	.87054	-.05858	.76838	-.36953	.88289	1.1
631.	62.	.92848	-.87217	-.02405	-.69615	.49228	1.21923	-1.7
794.	62.	.92848	.50018	.71490	.85168	.03991	1.44705	-3.2
1000.	62.	.92848	.85620	-.16787	.15471	-.83846	.70797	3.0
158.	125.	.98058	-.51463	.81391	-.00517	.51926	1.51889	-3.6
200.	125.	.98058	-.86530	.42255	-.21587	.47229	1.63077	-4.2
251.	125.	.98058	-.93501	-.23035	-.51092	-.09286	1.41138	-3.0
316.	125.	.98058	-.42168	-.86573	-.11434	-.50654	1.33707	-2.5
398.	125.	.98058	.58241	-.76687	.34588	-.38734	.83526	1.6
501.	125.	.98058	.85982	.43360	.45739	.24588	.60786	4.3
631.	125.	.98058	-.57823	.77003	-.28404	.43472	1.31813	-2.4
794.	125.	.98058	-.28194	-.92077	-.24658	-.45701	1.11678	-1.0
1000.	125.	.98058	.59695	.75561	.44788	.26280	.96657	.3
158.	250.	.99504	.45770	.87823	.19804	.19025	1.00702	-.1
200.	250.	.99504	.19491	.97097	.12022	.24690	1.17103	-1.4
251.	250.	.99504	-.15516	.97811	.02124	.27379	1.36686	-2.7
316.	250.	.99504	-.56308	.81469	-.11362	.25001	1.55095	-3.8
398.	250.	.99504	-.91111	.38813	-.23236	.14637	1.69116	-4.6
501.	250.	.99504	-.94420	-.29876	-.27230	-.03558	1.68759	-4.5
631.	250.	.99504	-.35956	-.92276	-.15307	-.22800	1.38794	-2.8
794.	250.	.99504	.67678	-.72301	.10740	-.25275	.63429	4.0
1000.	250.	.99504	.81928	.55638	.27392	.01960	.70024	3.1
158.	500.	.99875	.85139	.51987	.13593	.03053	.56543	5.0
200.	500.	.99875	.76928	.63508	.12674	.05786	.67829	3.4
251.	500.	.99875	.64415	.76170	.11084	.08440	.82181	1.7
316.	500.	.99875	.45801	.88620	.08448	.11078	.99608	.0
398.	500.	.99875	.19213	.97888	.04788	.13083	1.20390	-1.6
501.	500.	.99875	-.16161	.98438	.00164	.13931	1.43681	-3.1
631.	500.	.99875	-.57276	.81674	-.05341	.12867	1.66676	-4.4
794.	500.	.99875	-.92107	.38308	-.10258	.09427	1.84005	-5.3
1000.	500.	.99875	-.94778	-.31118	-.13636	.02854	1.84177	-5.3
158.	1000.	.99969	.96198	.27087	.06982	-.00369	.29487	10.6
200.	1000.	.99969	.94032	.33850	.06967	.00585	.35680	9.0
251.	1000.	.99969	.90631	.42116	.06828	.01504	.43711	7.2
316.	1000.	.99969	.85323	.52036	.06510	.02548	.53820	5.4
398.	1000.	.99969	.77113	.63572	.06024	.03549	.66610	3.5
501.	1000.	.99969	.64599	.76255	.05377	.04469	.82544	1.7
631.	1000.	.99969	.45981	.88733	.04484	.05364	1.01830	-.2
794.	1000.	.99969	.19381	.98041	.03620	.05981	1.24764	-1.9
1000.	1000.	.99969	-.16022	.98646	.02480	.06537	1.50065	-3.5

TABLE C.9

ATTENUATION DATA FOR Z = 5 FEET FOR GRASS

f(Hz)	r(ft)	A	B	C	D	E	F	-F(dB)
158.	31.	1.00000	.13474	.94285	.21232	.54033	1.15030	-1.2
200.	31.	1.00000	-.21529	.92777	-.01767	.58028	1.24702	-1.9
251.	31.	1.00000	-.60902	.73226	-.30203	.49580	1.32821	-2.5
316.	31.	1.00000	-.91247	.27295	-.53028	.23631	1.38268	-2.8
398.	31.	1.00000	-.85863	-.41214	-.55299	-.17677	1.32669	-2.5
501.	31.	1.00000	-.18359	-.93456	-.18316	-.55090	1.07147	-.6
631.	31.	1.00000	.78884	-.53371	.43170	-.38817	.65913	3.6
794.	31.	1.00000	.60829	.73287	.43589	.38345	.89835	.9
1000.	31.	1.00000	-.87374	.37908	-.46905	.34211	1.40518	-3.0
158.	62.	1.00000	.73737	.65676	.26058	.17160	.71353	2.9
200.	62.	1.00000	.60131	.78324	.23411	.20627	.85634	1.3
251.	62.	1.00000	.40044	.90260	.18637	.25024	1.02140	-.2
316.	62.	1.00000	.11719	.98046	.10063	.29534	1.19856	-1.6
398.	62.	1.00000	-.25094	.95502	-.00704	.31193	1.40031	-2.9
501.	62.	1.00000	-.65865	.73568	-.13523	.28119	1.58977	-4.0
631.	62.	1.00000	-.95800	.23932	-.27035	.15577	1.68972	-4.6
794.	62.	1.00000	-.86406	-.47795	-.29771	-.09338	1.61287	-4.2
1000.	62.	1.00000	-.11947	-.98019	-.06809	-.30449	1.24978	-1.9
158.	125.	1.00000	.93095	.35632	.12233	-.10154	.49625	6.1
200.	125.	1.00000	.89311	.44271	.14812	-.05776	.56169	5.0
251.	125.	1.00000	.83415	.54574	.15887	.00589	.62999	4.0
316.	125.	1.00000	.74322	.66428	.15183	.04714	.74015	2.6
398.	125.	1.00000	.60530	.79199	.14706	.06040	.91035	.8
501.	125.	1.00000	.40175	.91227	.13499	.08398	1.10622	-.9
631.	125.	1.00000	.11489	.99017	.12722	.09535	1.35111	-2.6
794.	125.	1.00000	-.25751	.96298	.11498	.10979	1.61606	-4.2
1000.	125.	1.00000	-.66895	.73902	.08242	.13595	1.85230	-5.4
158.	250.	1.00000	.98252	.18183	.07985	.00180	.20466	13.8
200.	250.	1.00000	.97280	.22816	.07986	.00140	.25076	12.0
251.	250.	1.00000	.95747	.28575	.07978	.00386	.30728	10.2
316.	250.	1.00000	.93333	.35678	.07909	.01114	.37511	8.5
398.	250.	1.00000	.89549	.44329	.07821	.01620	.46454	6.7
501.	250.	1.00000	.83652	.54648	.07711	.02084	.57808	4.8
631.	250.	1.00000	.74557	.66523	.07326	.03181	.71316	2.9
794.	250.	1.00000	.60761	.79323	.06198	.05038	.87079	1.2
1000.	250.	1.00000	.40395	.91391	.04022	.06900	1.05769	-.5
158.	500.	1.00000	.99562	.09138	.02261	-.03298	.12725	17.9
200.	500.	1.00000	.99317	.11494	.03008	-.02634	.14602	16.7
251.	500.	1.00000	.98930	.14452	.03685	-.01552	.16695	15.5
316.	500.	1.00000	.98318	.18157	.03877	-.00977	.19925	14.0
398.	500.	1.00000	.97349	.22783	.03820	-.01182	.24823	12.1
501.	500.	1.00000	.95822	.28534	.03805	-.01228	.30814	10.2
631.	500.	1.00000	.93416	.35628	.03598	-.01743	.38734	8.2
794.	500.	1.00000	.89645	.44270	.03264	-.02309	.48530	6.3
1000.	500.	1.00000	.83767	.54581	.03040	-.02598	.60339	4.4
158.	1000.	1.00000	.99890	.04575	.01987	-.00229	.05241	25.6
200.	1000.	1.00000	.99829	.05758	.01976	-.00309	.06436	23.8
251.	1000.	1.00000	.99732	.07247	.01971	-.00337	.07907	22.0
316.	1000.	1.00000	.99578	.09118	.01982	-.00267	.09688	20.3
398.	1000.	1.00000	.99335	.11470	.01980	-.00280	.12044	18.4
501.	1000.	1.00000	.98950	.14421	.01971	-.00338	.15066	16.4
631.	1000.	1.00000	.98340	.18118	.01981	-.00273	.18748	14.5
794.	1000.	1.00000	.97376	.22735	.02000	-.00010	.23211	12.7
1000.	1000.	1.00000	.95855	.28475	.01968	.00352	.28780	10.8

TABLE C.10

ATTENUATION DATA FOR Z = 10 FEET FOR GRASS

f(Hz)	r(ft)	A	B	C	D	E	F	-F(dB)
158.	31.	.98744	-.83692	.33511	-.10011	.77378	1.77918	-5.0
200.	31.	.98744	-.85171	-.29551	-.68459	.37431	1.33480	-2.5
251.	31.	.98744	-.29803	-.85084	-.60167	-.49675	.77004	2.3
316.	31.	.98744	.64419	-.63068	.27971	-.72837	.63057	4.0
398.	31.	.98744	.71689	.54664	.77448	.09457	1.13862	-1.1
501.	31.	.98744	-.69266	.57703	-.21162	.75099	1.47875	-3.4
631.	31.	.98744	-.00442	-.90151	-.57069	-.53205	.56025	5.0
794.	31.	.98744	.26704	.86106	.76534	.15170	1.64640	-4.3
1000.	31.	.98744	.12606	-.89267	-.71037	-.32272	.58962	4.6
158.	62.	.99682	.12512	.96430	.12956	.43497	1.13256	-1.1
200.	62.	.99682	-.23518	.94352	-.01425	.45363	1.31259	-2.4
251.	62.	.99682	-.63696	.73473	-.20658	.40412	1.46499	-3.3
316.	62.	.99682	-.93847	.25458	-.40044	.21362	1.53539	-3.7
398.	62.	.99682	-.86252	-.44899	-.44247	-.10104	1.45897	-3.3
501.	62.	.99682	-.14833	-.96101	-.20469	-.40508	1.09248	-.8
631.	62.	.99682	.83231	-.50279	.29530	-.34465	.48624	6.3
794.	62.	.99682	.57134	.78683	.34474	.29520	.91374	.8
1000.	62.	.99682	-.92059	.31314	-.41073	.19310	1.51145	-3.6
158.	125.	.99920	.74029	.66165	.22368	-.07709	.88240	1.1
200.	125.	.99920	.60292	.78886	.23576	.01982	.99544	.0
251.	125.	.99920	.40017	.90866	.19362	.13597	1.10695	-.9
316.	125.	.99920	.11445	.98626	.12263	.20233	1.27646	-2.1
398.	125.	.99920	-.25647	.95918	.06281	.22810	1.50760	-3.6
501.	125.	.99920	-.66628	.73612	-.03163	.23447	1.70913	-4.7
631.	125.	.99920	-.96490	.23404	-.11701	.20563	1.84731	-5.3
794.	125.	.99920	-.86465	-.48805	-.20039	.12578	1.77310	-5.0
1000.	125.	.99920	-.10943	-.98683	-.23295	-.04135	1.28869	-2.2
158.	250.	.99980	.93217	.35703	.11706	.02438	.38048	8.4
200.	250.	.99980	.89423	.44358	.11592	.02930	.46977	6.6
251.	250.	.99980	.83512	.54679	.11280	.03965	.57809	4.8
316.	250.	.99980	.74397	.66553	.10466	.05781	.70659	3.0
398.	250.	.99980	.60571	.79343	.09421	.07362	.86981	1.2
501.	250.	.99980	.40168	.91382	.07964	.08919	1.06742	-.6
631.	250.	.99980	.11419	.99165	.05023	.10851	1.28676	-2.2
794.	250.	.99980	-.25892	.96404	-.00332	.11952	1.51302	-3.6
1000.	250.	.99980	-.67090	.73913	-.07000	.09693	1.72471	-4.7
158.	500.	.99995	.98286	.18192	.03828	-.04614	.23468	12.6
200.	500.	.99995	.97313	.22827	.04934	-.03404	.27315	11.3
251.	500.	.99995	.95779	.28589	.05803	-.01504	.31717	10.0
316.	500.	.99995	.93364	.35695	.05982	-.00384	.38221	8.4
398.	500.	.99995	.89577	.44351	.05980	-.00421	.47680	6.4
501.	500.	.99995	.83676	.54674	.05993	-.00137	.59178	4.6
631.	500.	.99995	.74576	.66554	.05972	-.00520	.74057	2.6
794.	500.	.99995	.60771	.79359	.05921	-.00938	.92118	.7
1000.	500.	.99995	.40393	.91430	.05944	-.00776	1.13129	-1.1
158.	1000.	.99999	.99570	.09139	.02992	-.00207	.09952	20.0
200.	1000.	.99999	.99326	.11496	.02985	-.00292	.12343	18.2
251.	1000.	.99999	.98939	.14454	.02985	-.00289	.15288	16.3
316.	1000.	.99999	.98326	.18159	.02997	-.00128	.18873	14.5
398.	1000.	.99999	.97358	.22786	.02998	-.00077	.23548	12.6
501.	1000.	.99999	.95830	.28538	.02998	-.00076	.29498	10.6
631.	1000.	.99999	.93424	.35633	.02996	.00136	.36764	8.7
794.	1000.	.99999	.89652	.44276	.02924	.00667	.45584	6.8
1000.	1000.	.99999	.83774	.54587	.02680	.01347	.56497	5.0

TABLE C.11

ATTENUATION DATA FOR Z = 20 FEET FOR GRASS

f(Hz)	r(ft)	A	B	C	D	E	F	-F(dB)
158.	31.	.90152	.14756	-.76680	-.74641	-.62824	.13877	17.2
200.	31.	.90152	.77604	-.08673	.57097	-.79108	.99053	.1
251.	31.	.90152	.06554	.77811	.57299	.78961	1.40902	-3.0
316.	31.	.90152	-.73163	-.27289	-.97306	.07051	.74408	2.6
398.	31.	.90152	.75624	-.19458	.69235	-.68737	.97184	.2
501.	31.	.90152	-.76454	.15887	-.67519	.70422	1.13103	-1.1
631.	31.	.90152	.61319	.48348	.96496	-.14373	1.40148	-2.9
794.	31.	.90152	.66076	-.41612	-.06397	-.97351	.58476	4.7
1000.	31.	.90152	.69146	-.36282	-.19104	-.95672	.59421	4.5
158.	62.	.97239	-.86922	.32638	-.59861	.34247	1.24310	-1.9
200.	62.	.97239	-.86855	-.32816	-.68208	-.10195	1.18073	-1.4
251.	62.	.97239	-.27667	-.88630	-.35710	-.59000	.93988	.5
316.	62.	.97239	.69090	-.62026	.39738	-.56366	.68122	3.3
398.	62.	.97239	.70661	.60231	.62087	.30025	.93669	.6
501.	62.	.97239	-.75238	.54405	-.40630	.55726	1.31854	-2.4
631.	62.	.97239	.07545	-.92541	-.16231	-.67028	.77766	2.2
794.	62.	.97239	.17730	.91139	.28545	.62781	1.11713	-1.0
1000.	62.	.97239	.25391	-.89309	.11355	-.68024	.85882	1.3
158.	125.	.99288	.12299	.97284	.35664	.14401	1.48031	-3.4
200.	125.	.99288	-.24109	.95048	.21268	.32046	1.57788	-4.0
251.	125.	.99288	-.64617	.73757	-.06724	.37869	1.61225	-4.1
316.	125.	.99288	-.94804	.25052	-.29720	.24414	1.64373	-4.3
398.	125.	.99288	-.86603	-.45992	-.38428	.01606	1.54954	-3.8
501.	125.	.99288	-.13951	-.97061	-.26056	-.28291	1.11041	-.9
631.	125.	.99288	.84587	-.49602	.08578	-.37493	.26239	11.6
794.	125.	.99288	.56303	.80283	.38207	-.04421	1.17332	-1.4
1000.	125.	.99288	-.93468	.29649	.00809	.38453	1.93765	-5.7
158.	250.	.99820	.74161	.66341	.16678	.10675	.69937	3.1
200.	250.	.99820	.60380	.79090	.15070	.12846	.85789	1.3
251.	250.	.99820	.40042	.91091	.12076	.15694	1.04153	-.4
316.	250.	.99820	.11385	.98850	.06600	.18670	1.24341	-1.9
398.	250.	.99820	-.25807	.96099	-.00137	.19802	1.46865	-3.3
501.	250.	.99820	-.66874	.73681	-.08115	.18063	1.68050	-4.5
631.	250.	.99820	-.96740	.23289	-.16828	.10438	1.80192	-5.1
794.	250.	.99820	-.86547	-.49098	-.19023	-.05500	1.72930	-4.8
1000.	250.	.99820	-.10697	-.98927	-.04308	-.19328	1.32727	-2.5
158.	500.	.99955	.93266	.35727	.07659	-.06391	.44495	7.0
200.	500.	.99955	.89469	.44388	.09286	-.03642	.51941	5.7
251.	500.	.99955	.83553	.54717	.09969	.00360	.60416	4.4
316.	500.	.99955	.74430	.66597	.09528	.02953	.72658	2.8
398.	500.	.99955	.60593	.79395	.09230	.03783	.89879	.9
501.	500.	.99955	.40174	.91439	.08476	.05259	1.09937	-.8
631.	500.	.99955	.11404	.99222	.07996	.05964	1.34233	-2.6
794.	500.	.99955	-.25933	.96450	.07237	.06865	1.60460	-4.1
1000.	500.	.99955	-.67152	.73930	.05191	.08518	1.84297	-5.3
158.	1000.	.99989	.98299	.18195	.04556	-.02053	.21189	13.5
200.	1000.	.99989	.97327	.22831	.04791	-.01418	.25369	11.9
251.	1000.	.99989	.95792	.28594	.04975	-.00470	.30477	10.3
316.	1000.	.99989	.93376	.35701	.04991	.00241	.37311	8.6
398.	1000.	.99989	.89589	.44358	.04982	.00383	.46588	6.6
501.	1000.	.99989	.83687	.54684	.04952	.00666	.58049	4.7
631.	1000.	.99989	.74584	.66565	.04923	.00859	.72368	2.8
794.	1000.	.99989	.60777	.79372	.04813	.01341	.89594	1.0
1000.	1000.	.99989	.40395	.91444	.04473	.02227	1.09837	-.8

TABLE C.12

ATTENUATION DATA FOR Z = 30 FEET FOR GRASS

f(Hz)	r(ft)	A	B	C	D	E	F	-F(dB)
158.	31.	.78087	.66564	.02251	.83270	-.54211	1.10334	-.9
200.	31.	.78087	-.06559	.66278	.40970	.90522	1.27933	-2.1
251.	31.	.78087	-.55454	-.36887	-.97493	-.19175	.40164	7.9
316.	31.	.78087	.66554	.02509	.95222	-.28380	1.11134	-.9
398.	31.	.78087	-.65755	-.10584	-.96672	.22960	.57881	4.7
501.	31.	.78087	.28626	.60136	.77989	.61566	1.27458	-2.1
631.	31.	.78087	.66593	.01042	.84620	-.52077	1.09816	-.8
794.	31.	.78087	.64628	.16091	.91104	-.39657	1.18496	-1.5
1000.	31.	.78087	-.36922	.55431	.10965	.98754	1.33215	-2.5
158.	62.	.92848	-.60096	-.63254	-.83560	-.16950	.83416	1.6
200.	62.	.92848	.22736	-.84236	-.21917	-.82397	.48230	6.3
251.	62.	.92848	.87235	-.01637	.78146	-.34100	.89829	.9
316.	62.	.92848	-.02832	.87205	.24771	.81584	1.20582	-1.6
398.	62.	.92848	-.76416	-.42111	-.84737	-.09442	.90619	.9
501.	62.	.92848	.87054	-.05858	.73764	-.42760	.87700	1.1
631.	62.	.92848	-.87217	-.02405	-.73145	.43812	1.16482	-1.3
794.	62.	.92848	.50018	.71490	.81306	.25669	1.32322	-2.4
1000.	62.	.92848	.85620	-.16787	.53550	-.66348	.78422	2.1
158.	125.	.98058	-.51463	.81391	.02442	.51871	1.54804	-3.8
200.	125.	.98058	-.86530	.42255	-.29017	.43065	1.55573	-3.8
251.	125.	.98058	-.93501	-.23035	-.51337	.07819	1.43576	-3.1
316.	125.	.98058	-.42168	-.86573	-.36539	-.36898	1.14972	-1.2
398.	125.	.98058	.58241	-.76687	.13191	-.50225	.59246	4.5
501.	125.	.98058	.85982	.43360	.51927	.00463	.77048	2.3
631.	125.	.98058	-.57823	.77003	-.03987	.51775	1.53975	-3.7
794.	125.	.98058	-.28194	-.92077	-.42289	-.30137	1.04338	-.4
1000.	125.	.98058	.59695	.75561	.50852	.10522	1.10405	-.9
158.	250.	.99504	.45770	.87823	.24365	.12669	1.08386	-.7
200.	250.	.99504	.19491	.97097	.18143	.20615	1.24435	-1.9
251.	250.	.99504	-.15516	.97811	.06404	.26705	1.40712	-3.0
316.	250.	.99504	-.56308	.81469	-.07524	.26411	1.58179	-4.0
398.	250.	.99504	-.91111	.38813	-.19223	.19612	1.72464	-4.7
501.	250.	.99504	-.94420	-.29876	-.27146	.04150	1.70213	-4.6
631.	250.	.99504	-.35956	-.92276	-.22157	-.16223	1.36461	-2.7
794.	250.	.99504	.67678	-.72301	.02684	-.27330	.56685	4.9
1000.	250.	.99504	.81928	.55638	.27320	-.02784	.73680	2.7
158.	500.	.99875	.85139	.51987	.13904	-.00873	.60120	4.4
200.	500.	.99875	.76928	.63508	.13739	.02309	.71352	2.9
251.	500.	.99875	.64415	.76170	.12382	.06385	.84610	1.5
316.	500.	.99875	.45801	.88620	.10035	.09664	1.01706	-.1
398.	500.	.99875	.19213	.97888	.07711	.11603	1.23511	-1.8
501.	500.	.99875	-.16161	.98438	.04056	.13328	1.47194	-3.4
631.	500.	.99875	-.57276	.81674	-.00618	.13918	1.70569	-4.6
794.	500.	.99875	-.92107	.38308	-.06948	.12075	1.86884	-5.4
1000.	500.	.99875	-.94778	-.31118	-.12933	.05179	1.85310	-5.4
158.	1000.	.99969	.96198	.27087	.06600	-.02308	.31171	10.1
200.	1000.	.99969	.94032	.33850	.06881	-.01238	.37356	8.6
251.	1000.	.99969	.90631	.42116	.06985	.00296	.44893	7.0
316.	1000.	.99969	.85323	.52036	.06822	.01528	.54881	5.2
398.	1000.	.99969	.77113	.63572	.06686	.02044	.68252	3.3
501.	1000.	.99969	.64599	.76255	.06413	.02786	.84519	1.5
631.	1000.	.99969	.45981	.88733	.06048	.03507	1.04249	-.4
794.	1000.	.99969	.19381	.98041	.05251	.04616	1.26872	-2.1
1000.	1000.	.99969	-.16022	.98646	.03577	.06007	1.51257	-3.6

APPENDIX D: EXPERIMENTAL PRESSURE FIELD DATA

Experimental data is presented in graphical form in Figures D.1 through D.19. In all cases, one vertical division corresponds to 1 dB.

Since the data presented here represents the pressure field less 6 dB per double r, excess attenuation is counted downward from the 0 dB level, i.e., in the negative sense.

As noted in the conclusions of Section 4.1, theoretical and experimental data do agree favorably.

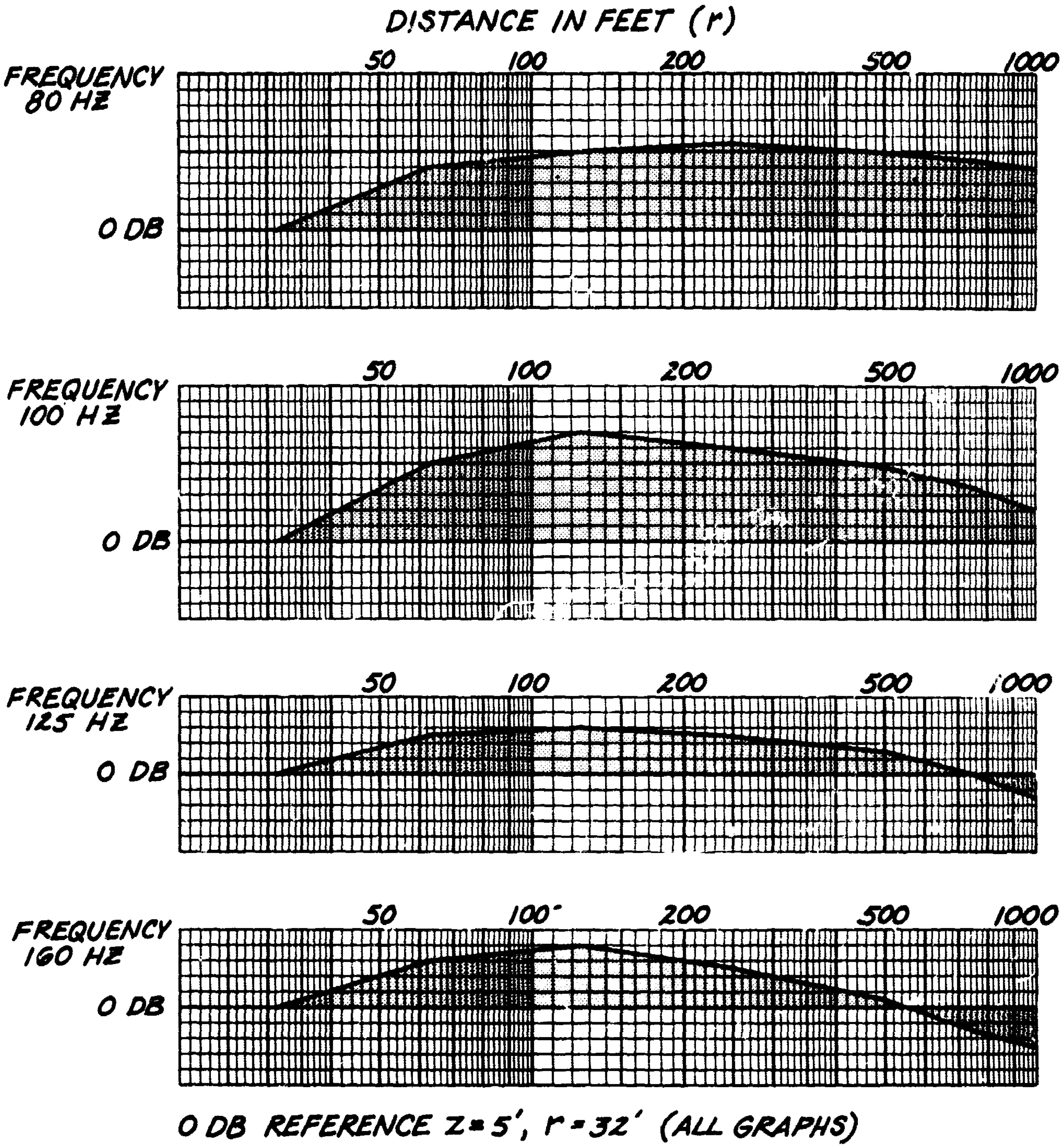

FIGURE D.1. ATTENUATION VERSUS DISTANCE - CONCRETE.

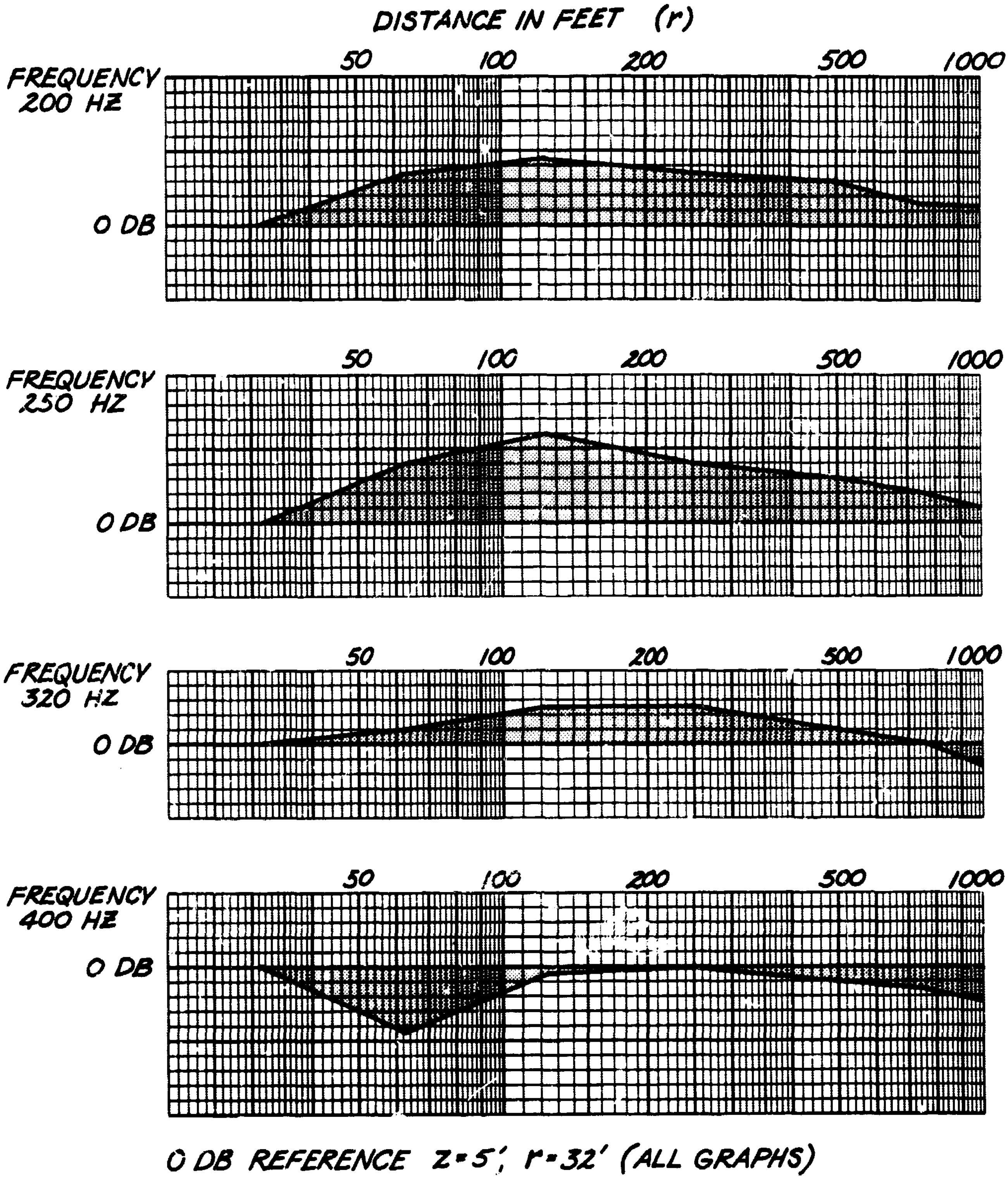

FIGURE D.2. ATTENUATION VERSUS DISTANCE - CONCRETE. (Continued)

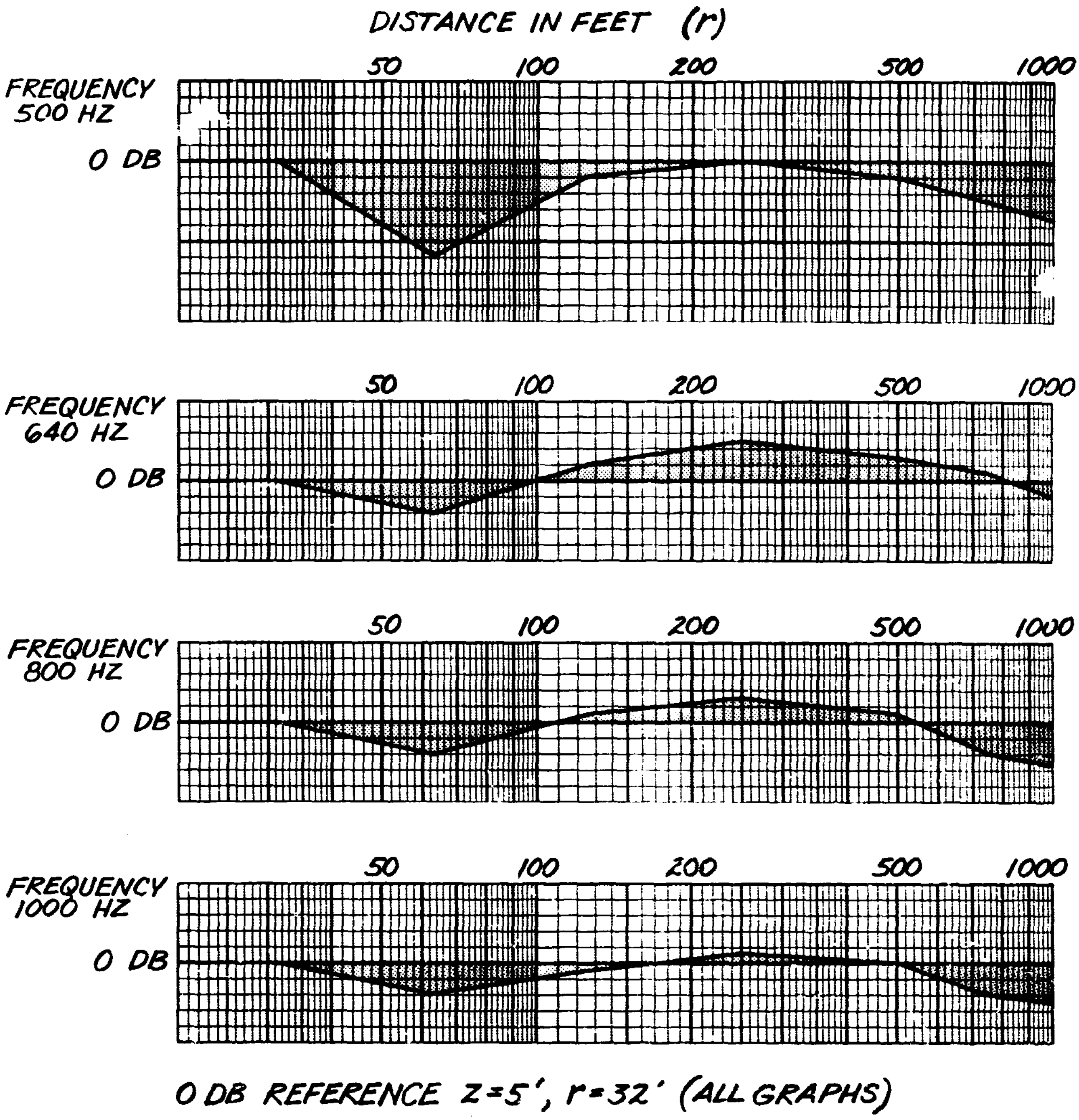

FIGURE D.3. ATTENUATION VERSUS DISTANCE - CONCRETE. (Continued)

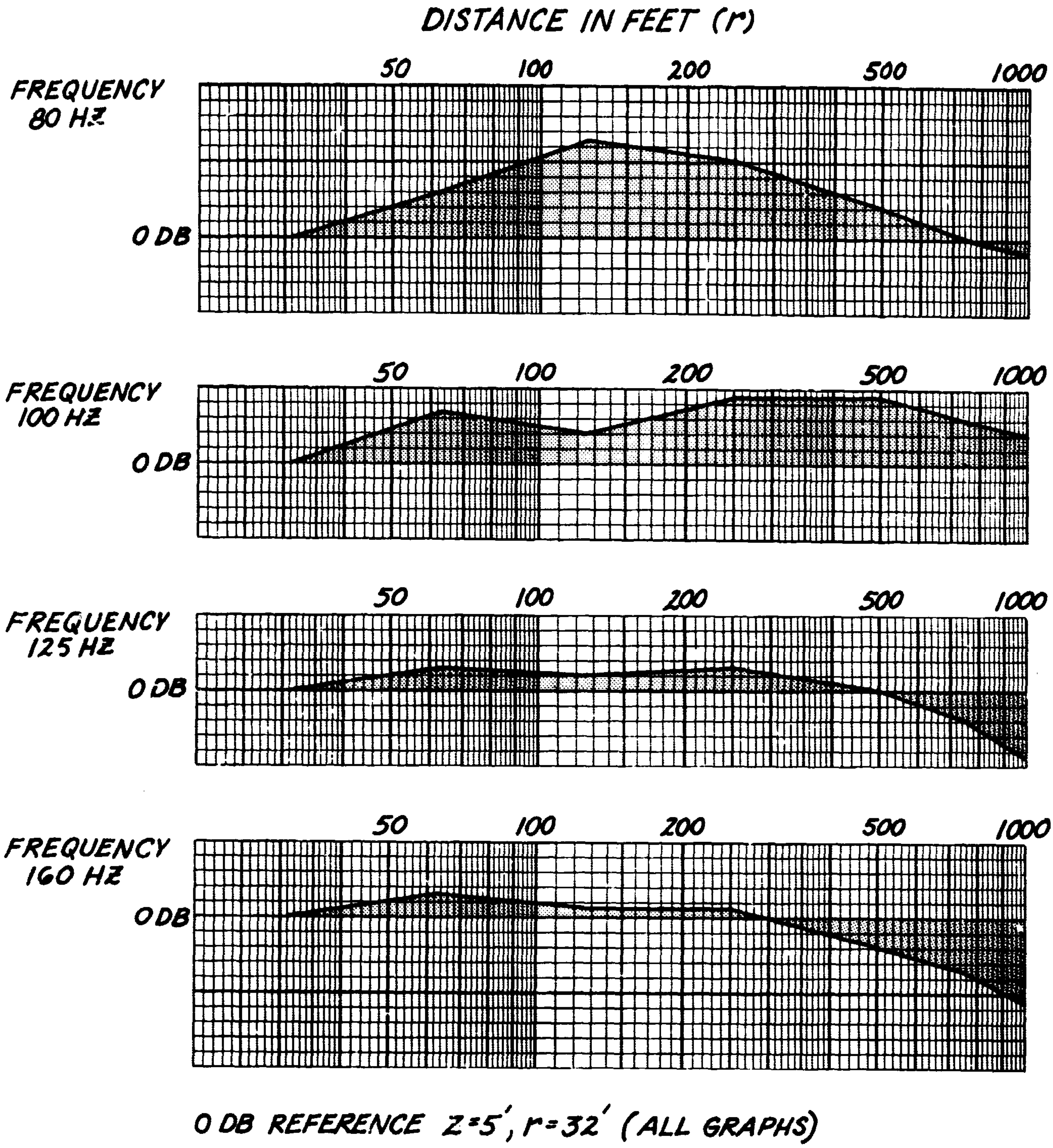

FIGURE D.4. ATTENUATION VERSUS DISTANCE - ASPHALT.

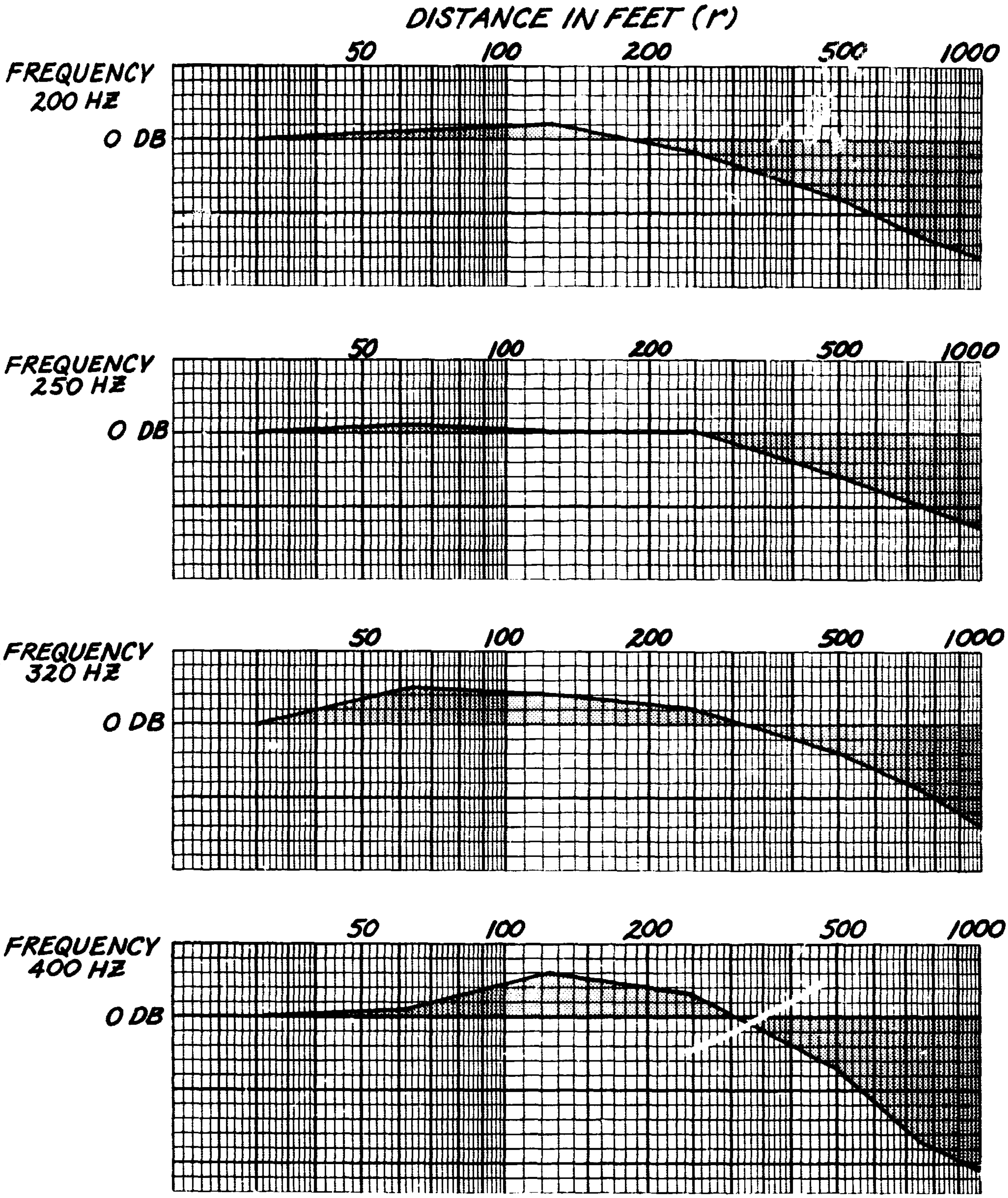

0 DB REFERENCE Z=5', r=32' (ALL GRAPHS)

FIGURE D.5. ATTENUATION VERSUS DISTANCE - ASPHALT. (Continued)

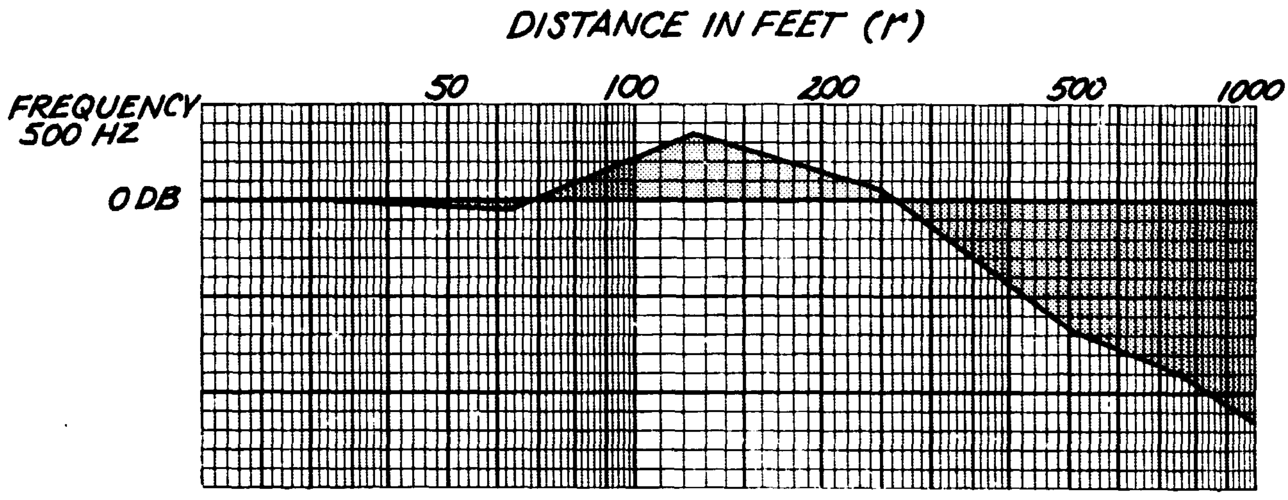

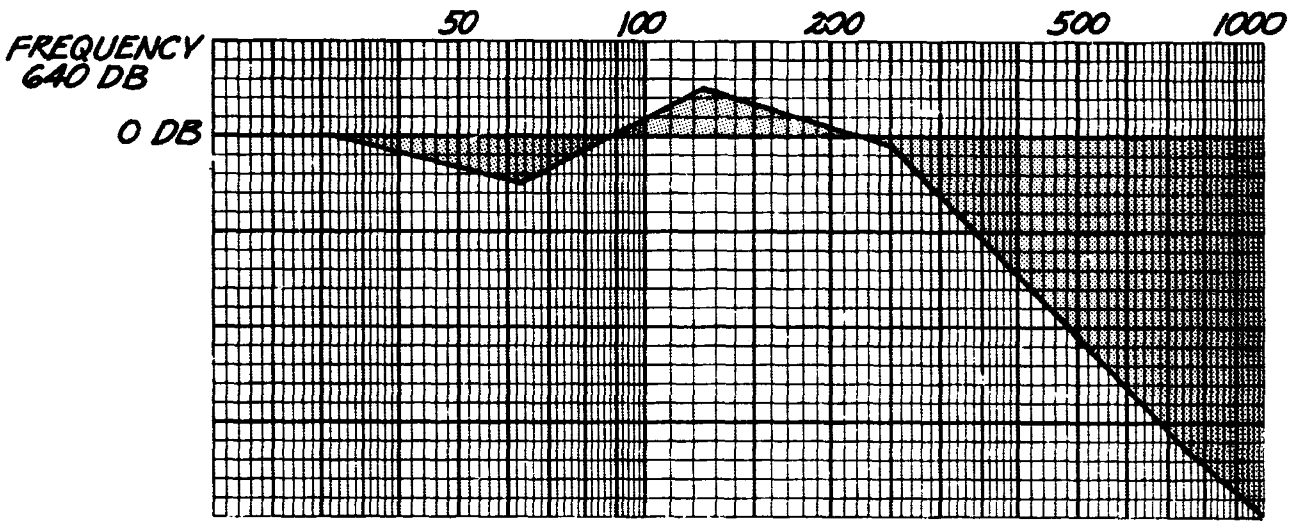

0 DB REFERENCE Z=5', r=32' (ALL GRAPHS)

FIGURE D.6. ATTENUATION VERSUS DISTANCE - ASPHALT. (Continued)

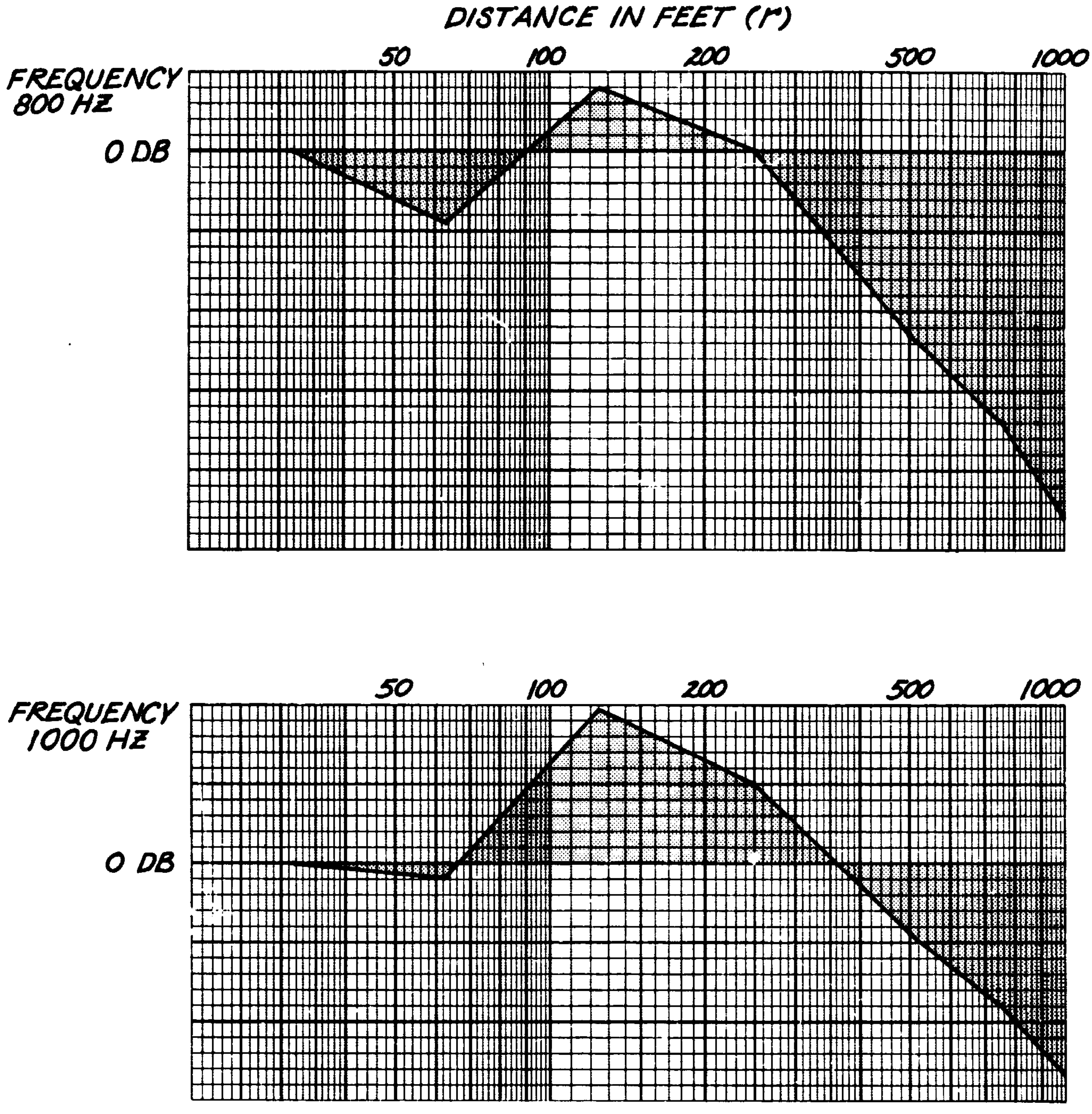

0 DB REFERENCE Z=5', r=32'

FIGURE D.7. ATTENUATION VERSUS DISTANCE - ASPHALT. (Continued)

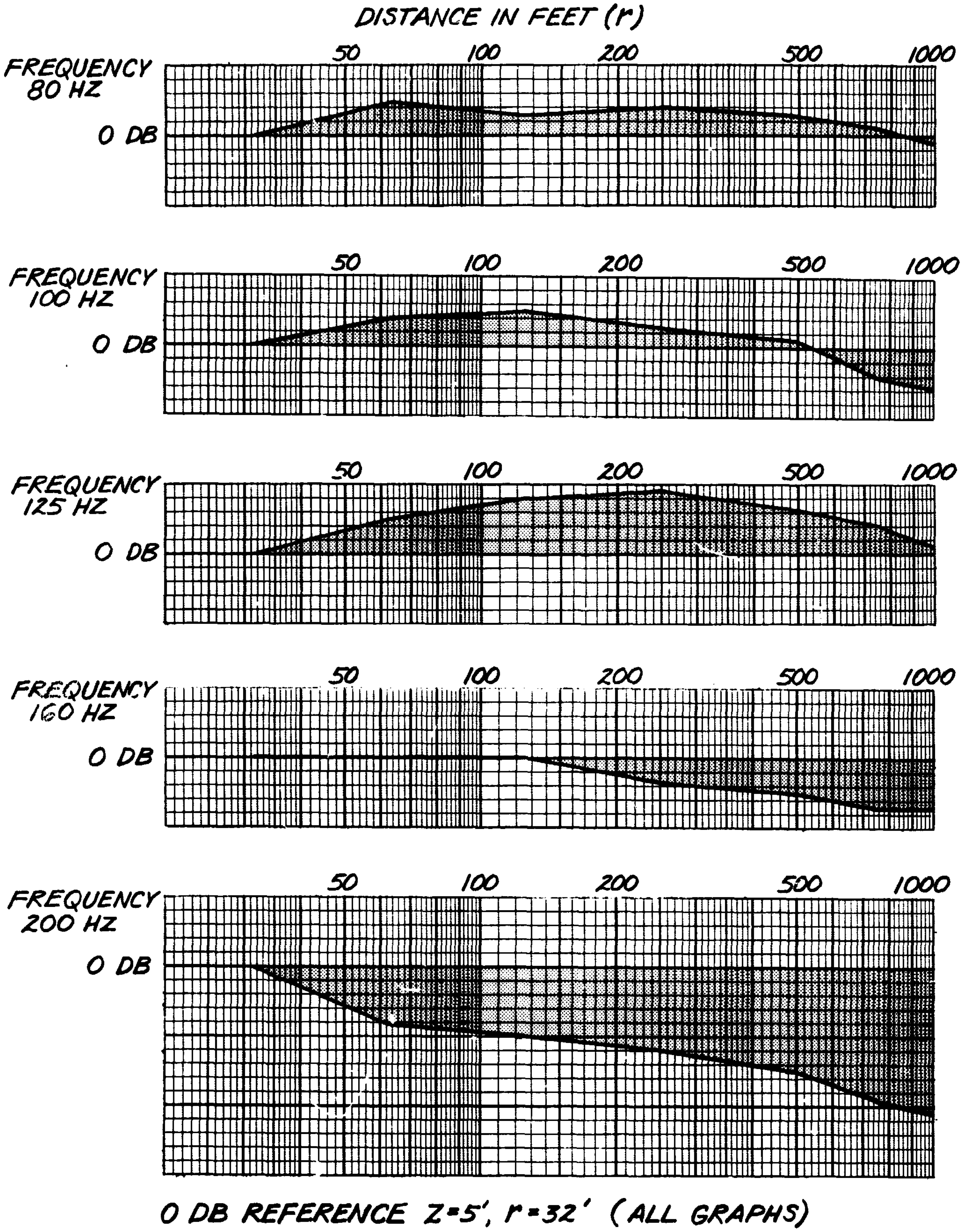

FIGURE D.8. ATTENUATION VERSUS DISTANCE - GRASS.

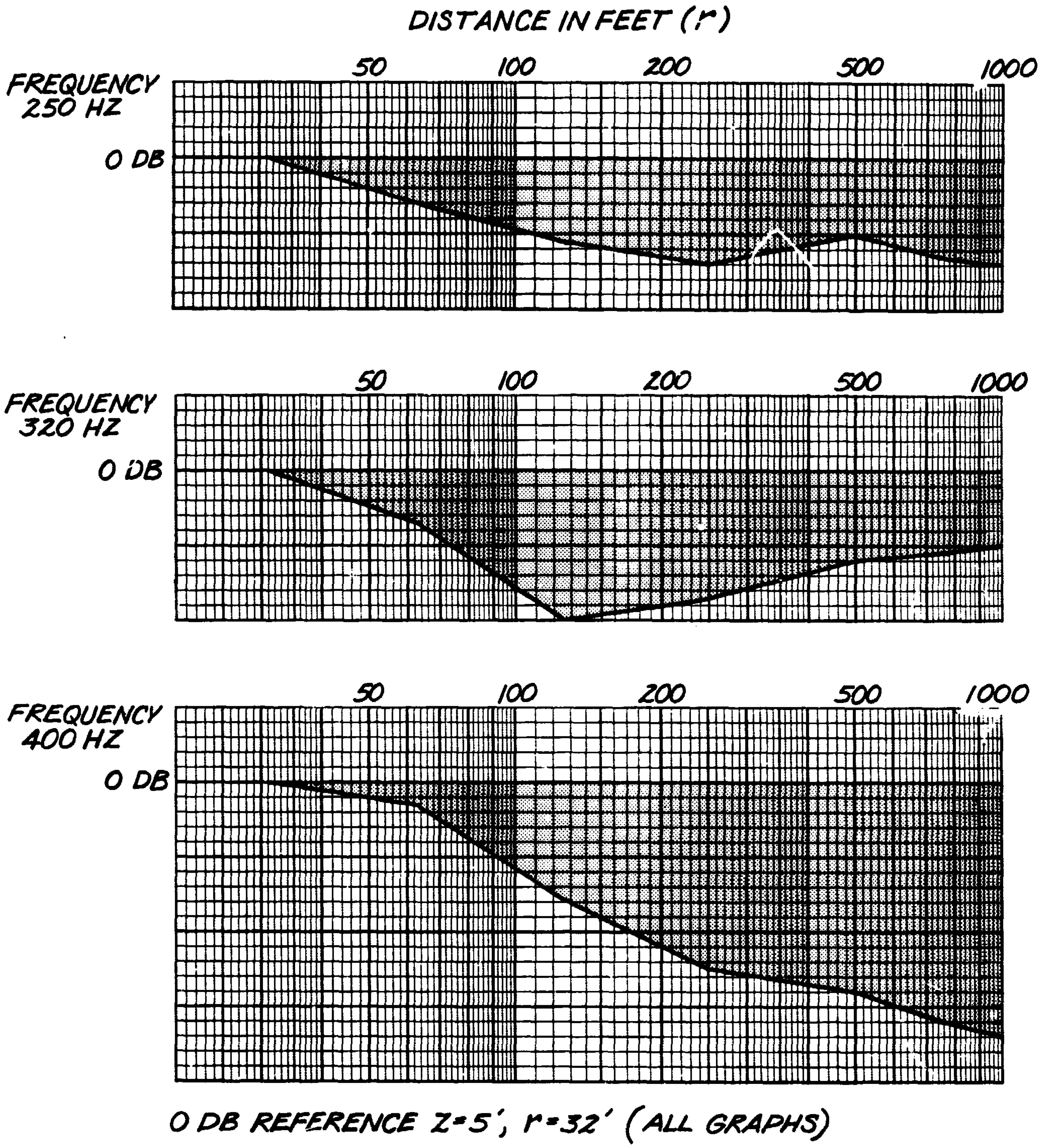

FIGURE D.9. ATTENUATION VERSUS DISTANCE - GRASS. (Continued)

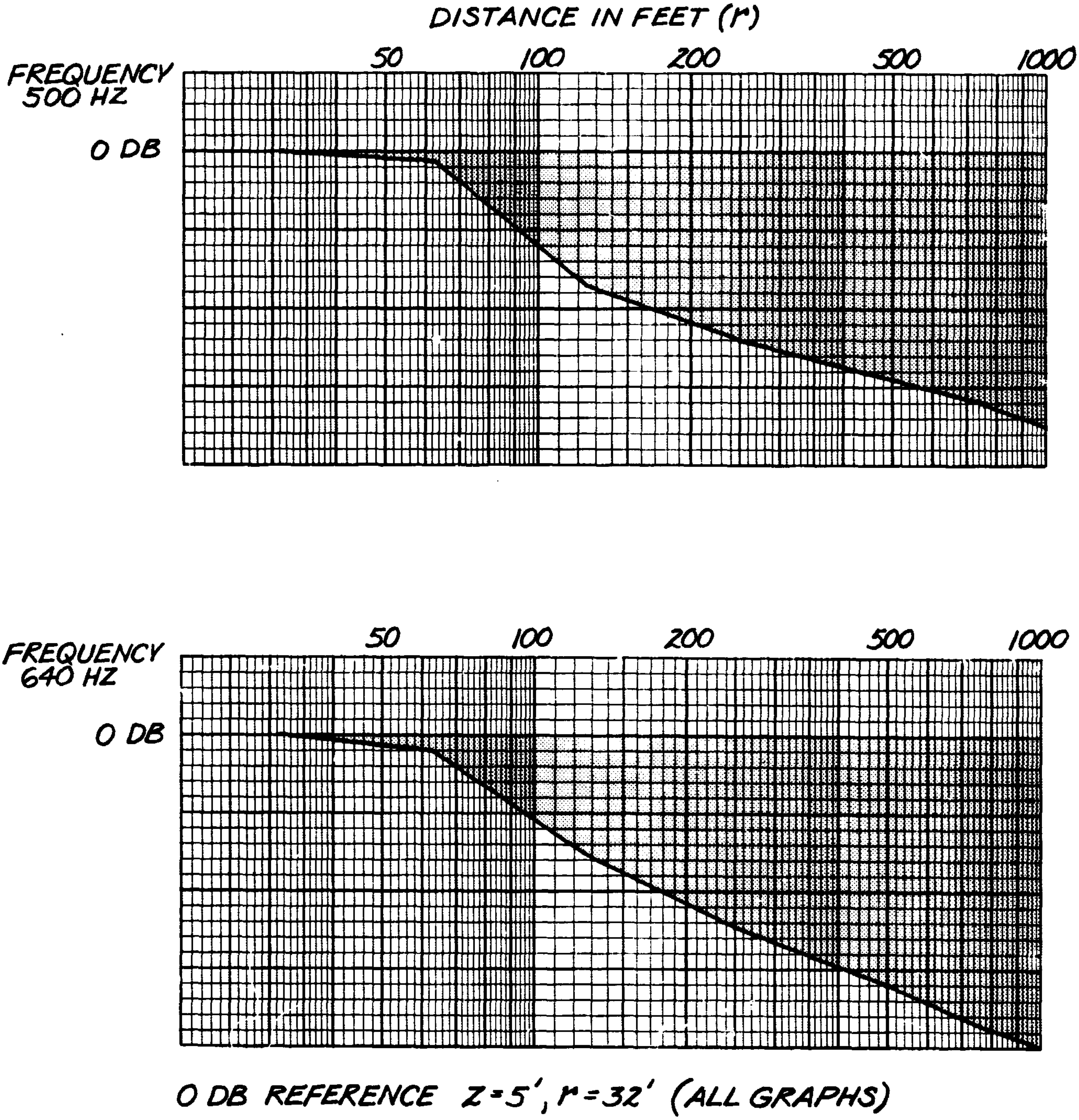

FIGURE D.10. ATTENUATION VERSUS DISTANCE - GRASS. (Continued)

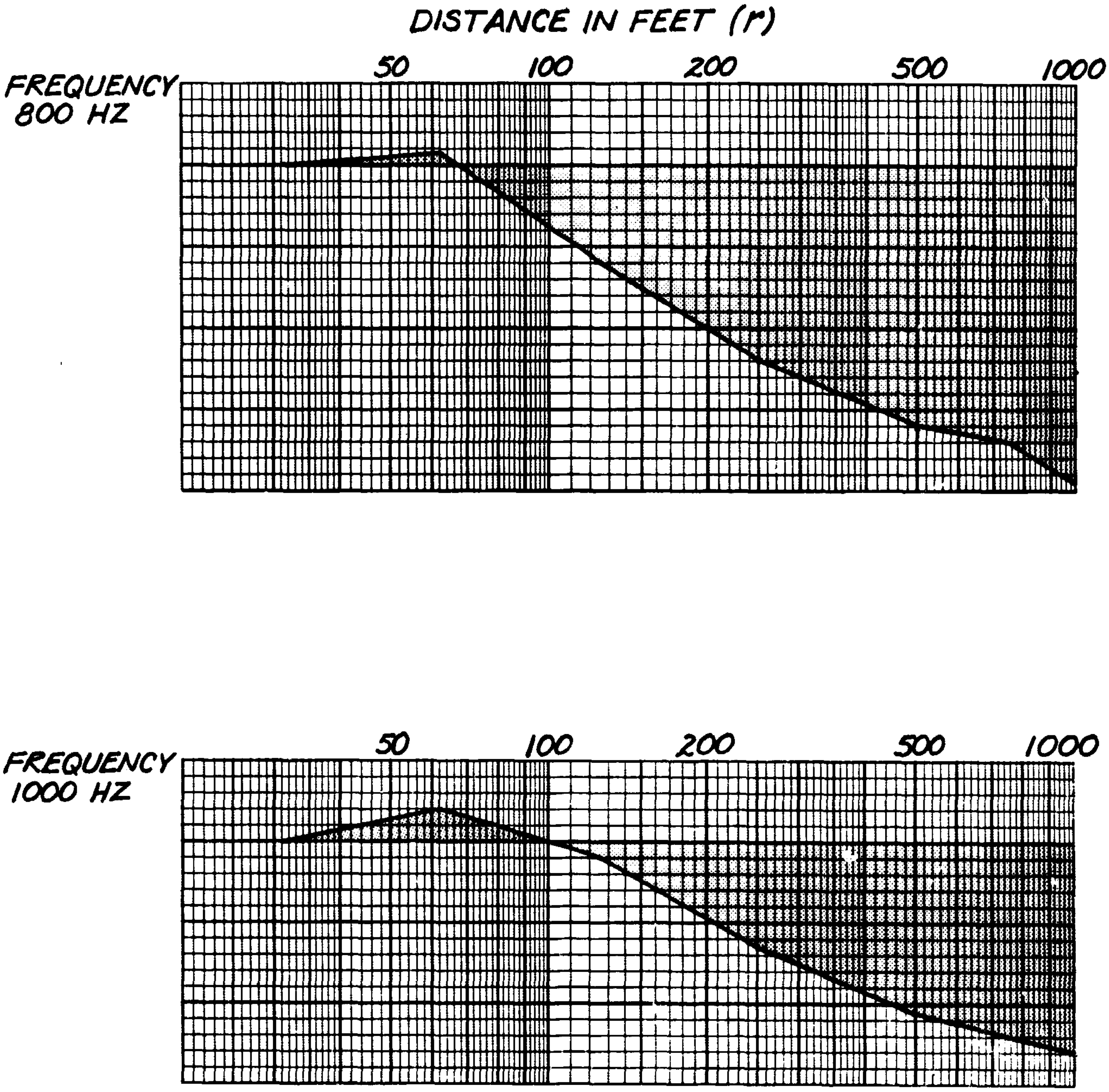

FIGURE D.11. ATTENUATION VERSUS DISTANCE - GRASS. (Continued)

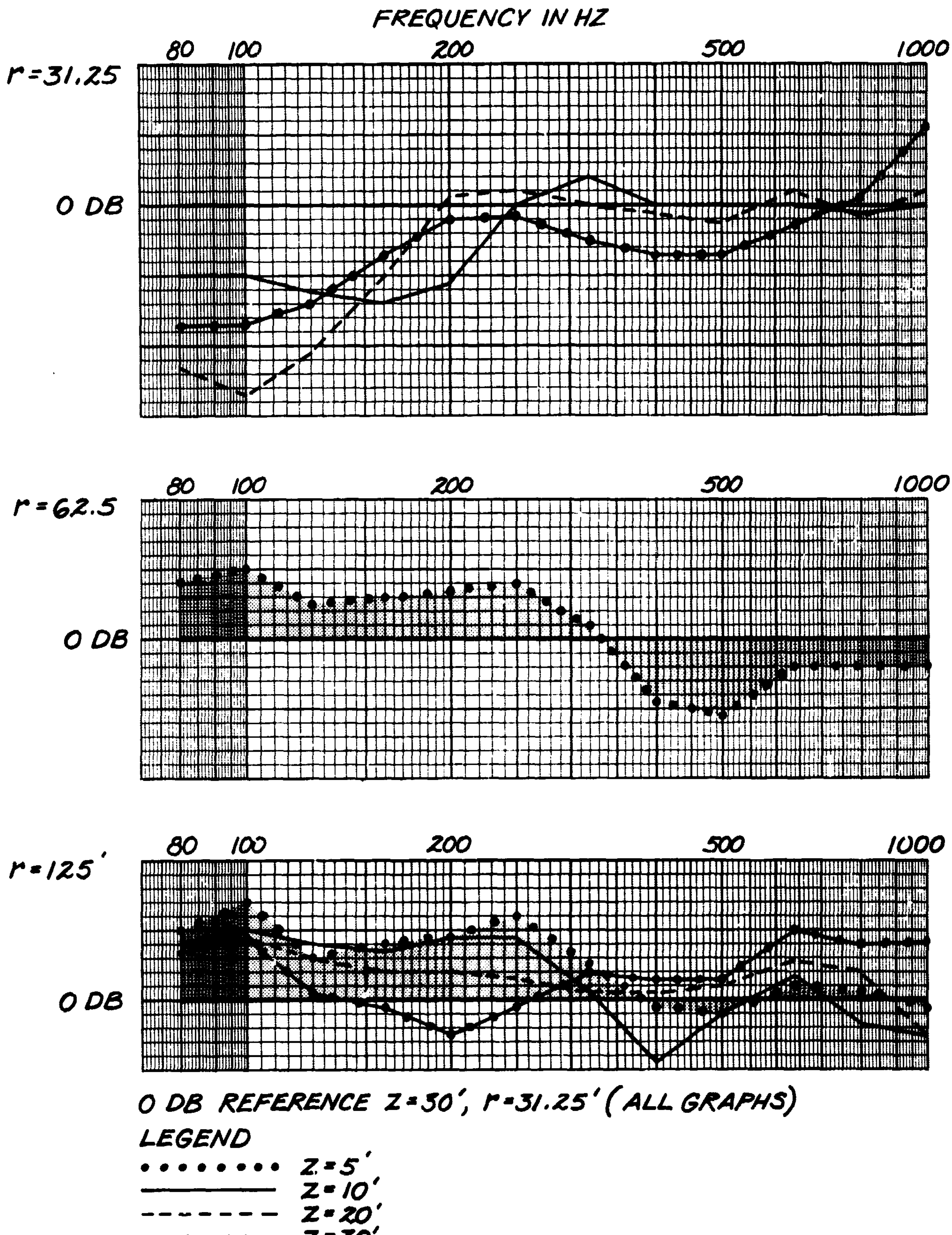

FIGURE D.12. ATTENUATION VERSUS FREQUENCY AT FIXED RADIUS, r - CONCRETE.

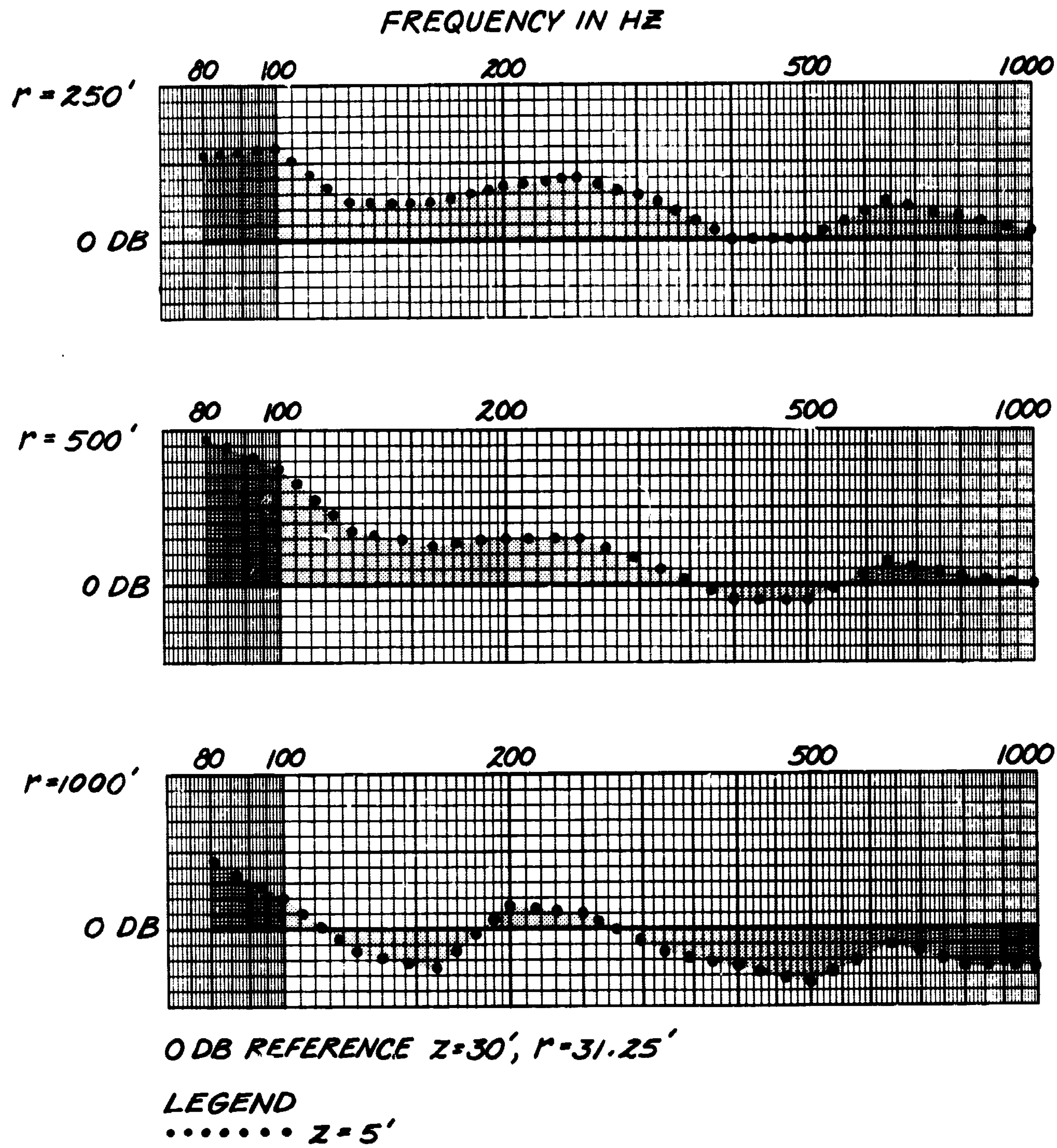

FIGURE D.13. ATTENUATION VERSUS FREQUENCY AT FIXED RADIUS, r - CONCRETE. (Continued)

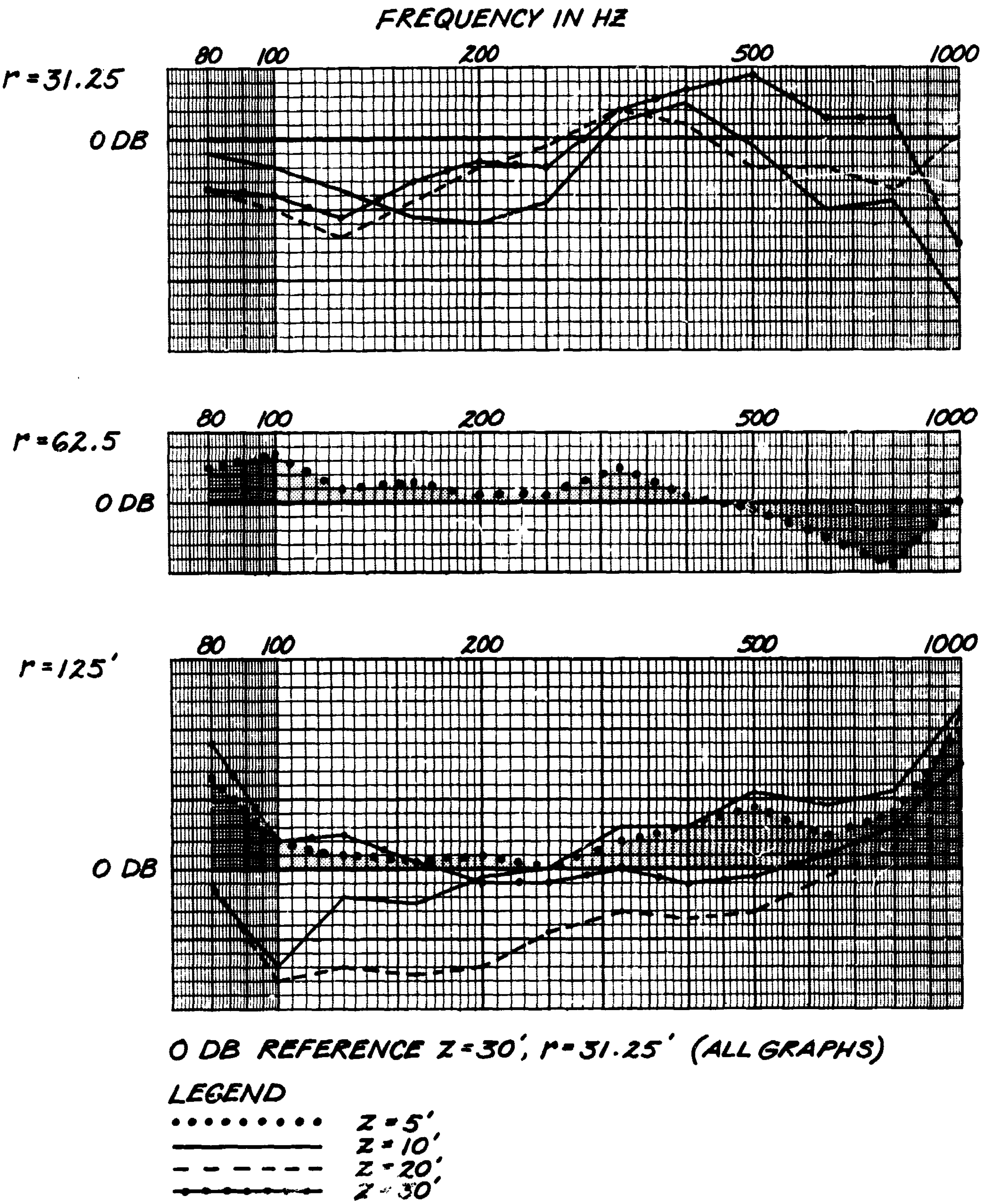

FIGURE D.14. ATTENUATION VERSUS FREQUENCY AT FIXED RADIUS, r - ASPHALT.

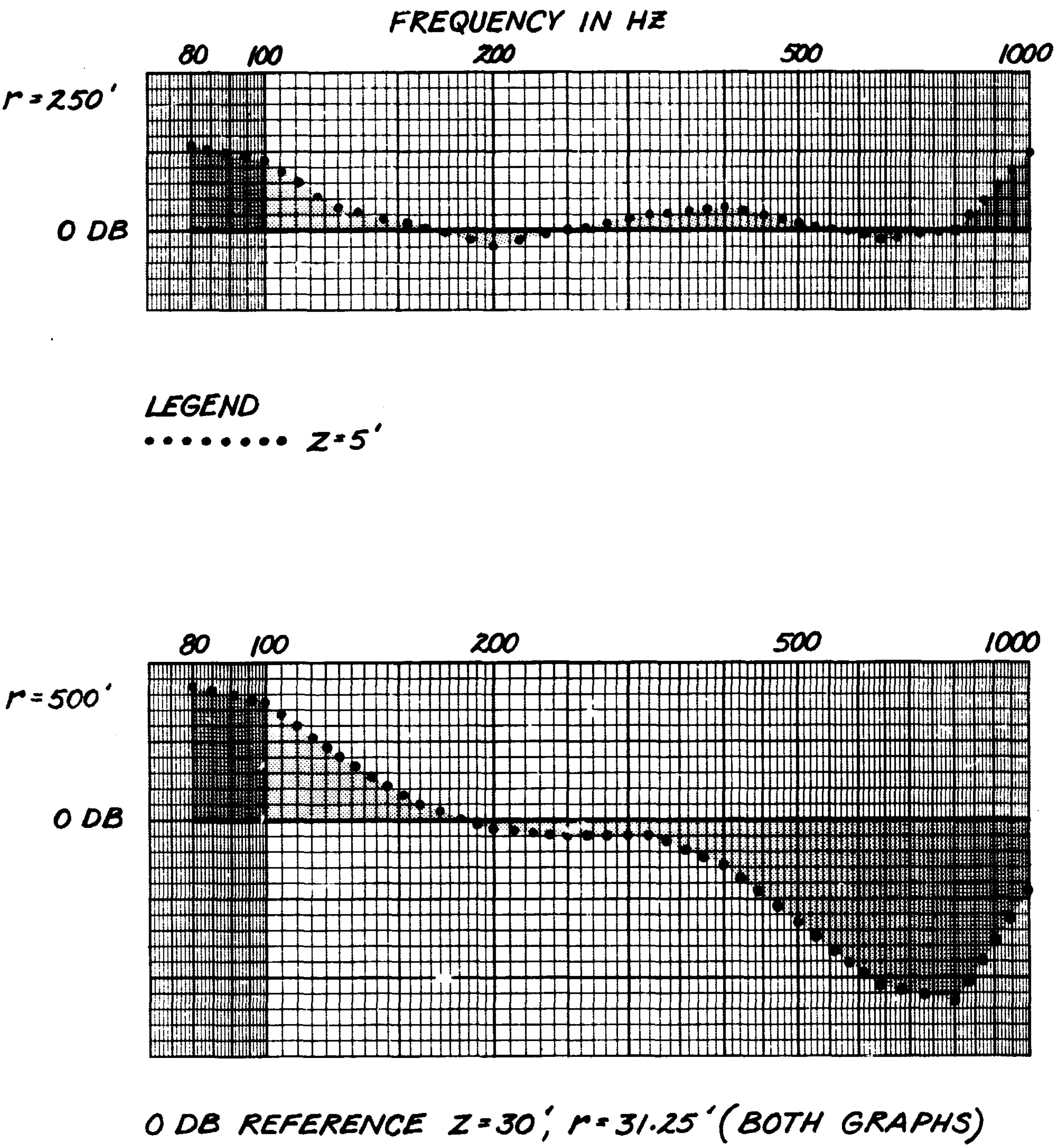

FIGURE D.15. ATTENUATION VERSUS FREQUENCY AT FIXED RADIUS, r - ASPHALT. (Continued)

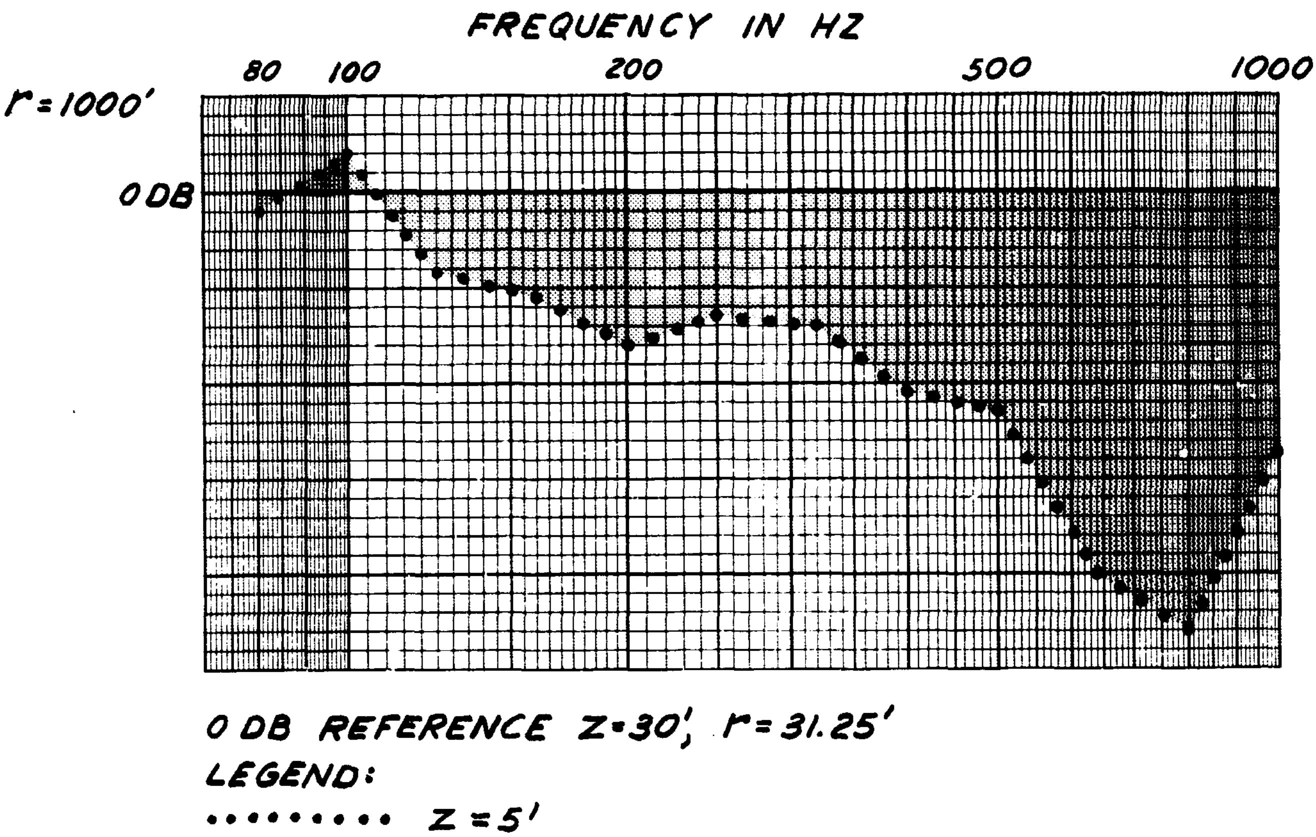

FIGURE D.16. ATTENUATION VERSUS FREQUENCY AT FIXED RADIUS, r - ASPHALT. (Continued)

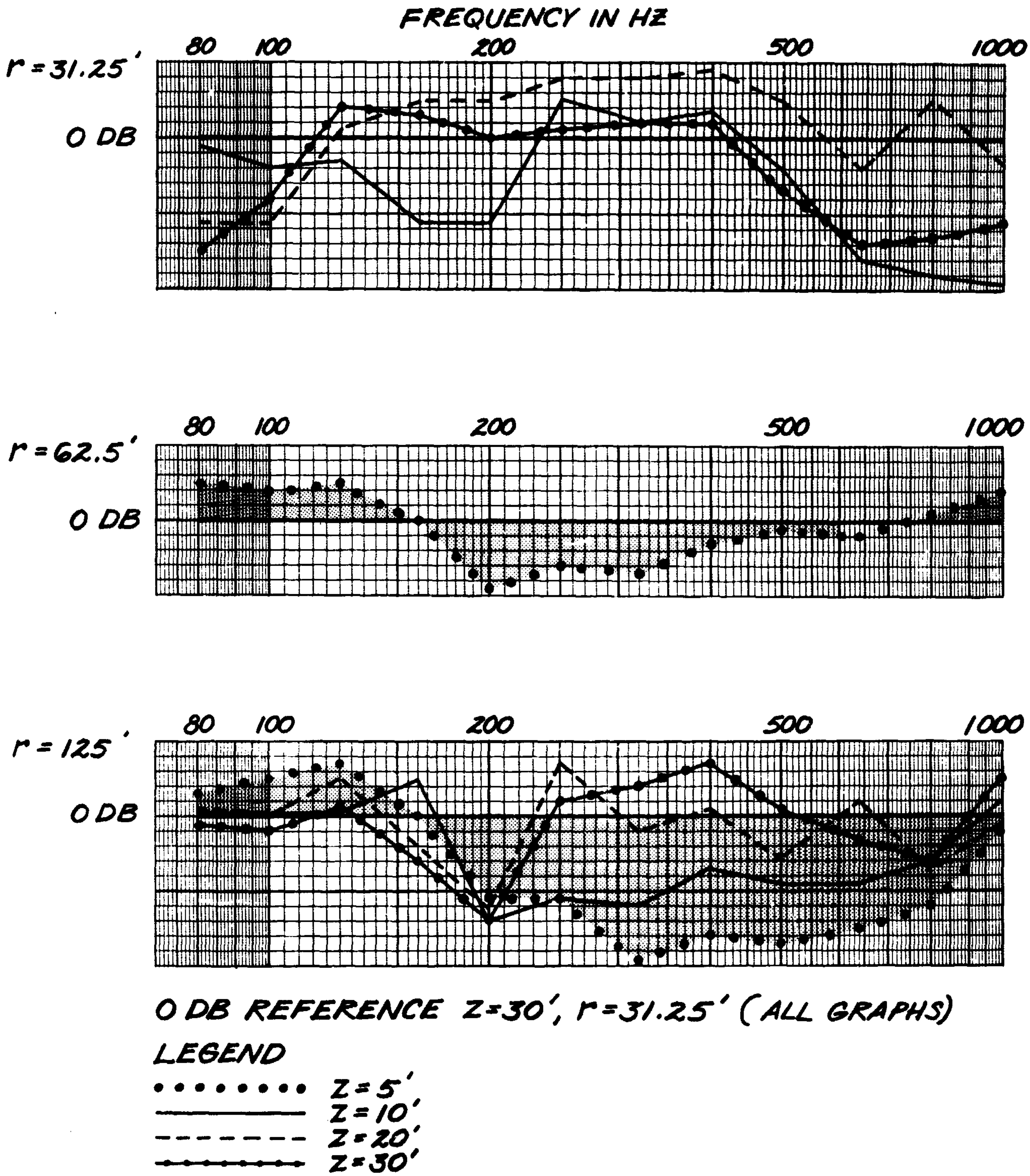

FIGURE D.17. ATTENUATION VERSUS FREQUENCY AT FIXED RADIUS, r - GRASS.

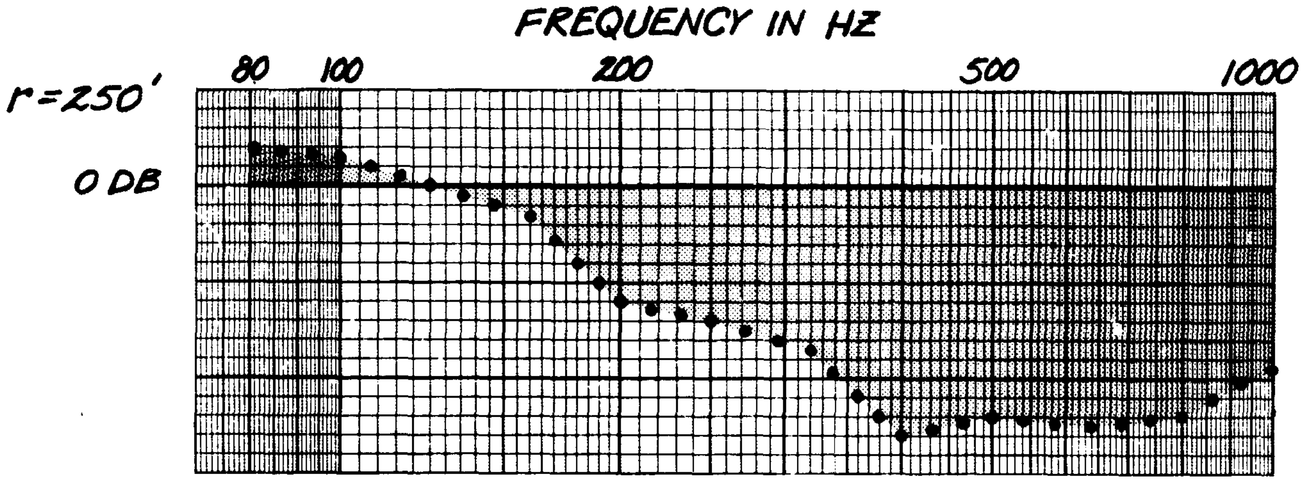

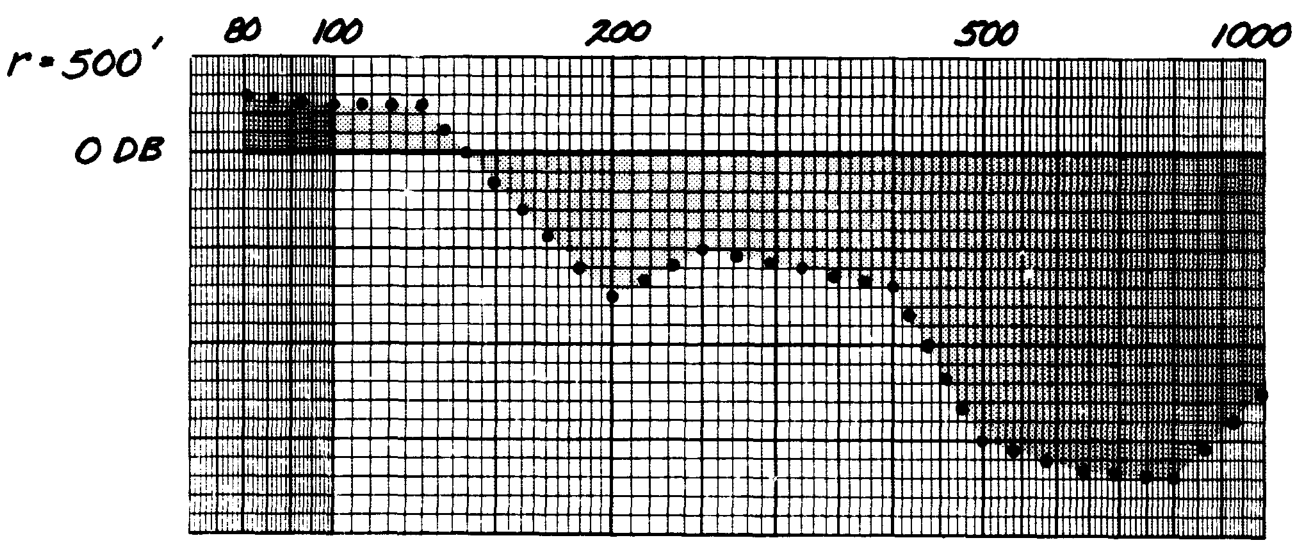

0 DB REFERENCE Z=30', r=31.25' (BOTH GRAPHS)

LEGEND

.... Z=5'

FIGURE D.18. ATTENUATION VERSUS FREQUENCY AT FIXED RADIUS, r - GRASS. (Continued)

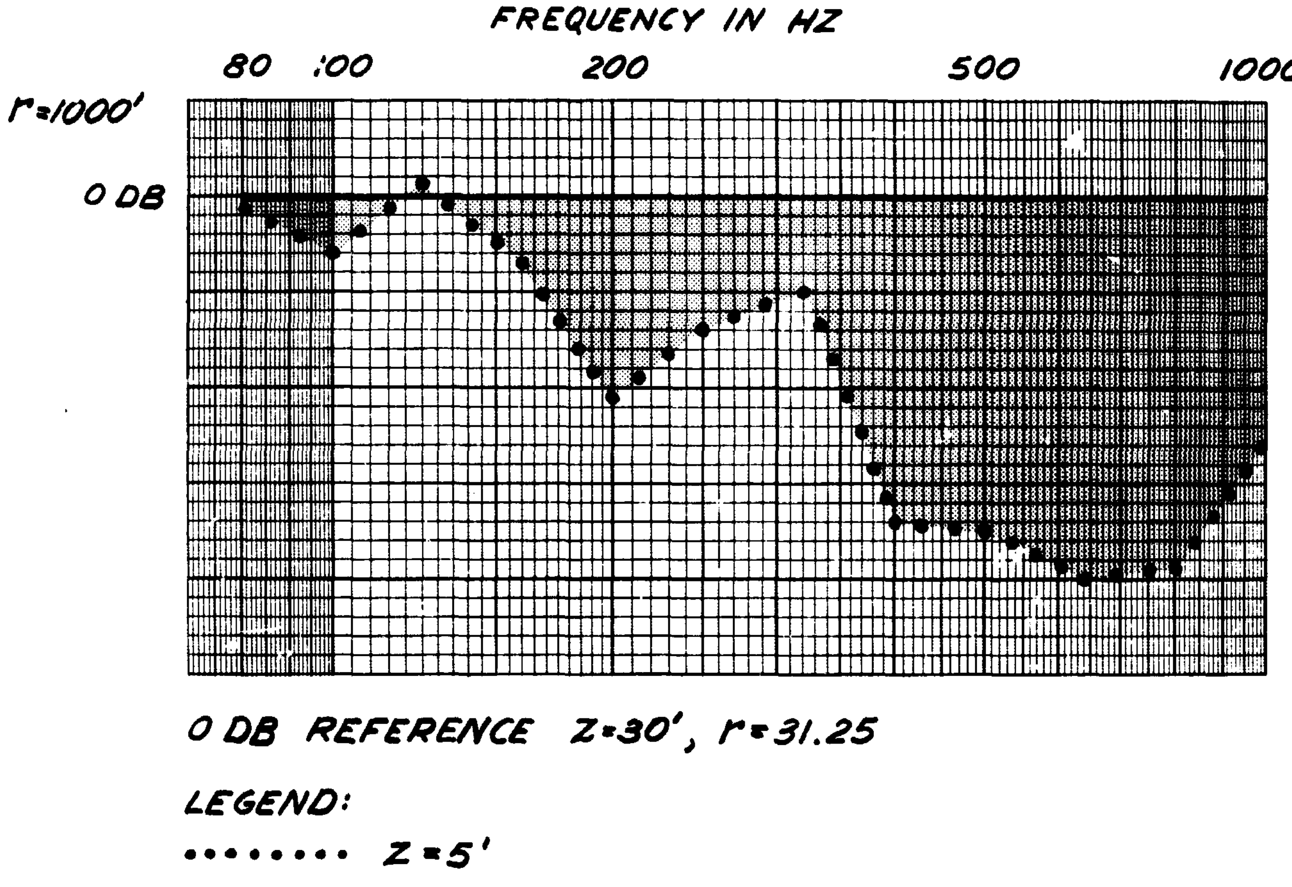

FIGURE D.19. ATTENUATION VERSUS FREQUENCY AT FIXED RADIUS, r - GRASS. (Continued)